UNIVERSITY OF SOUTHAMPTON

FACULTY OF SCIENCE

School of Ocean and Earth Science

Decadal variability of the subtropical gyre and deep meridional overturning circulation of the Indian Ocean

by

Matthew D. Palmer

Thesis for the degree of Doctor of Philosophy

June 2005

GRADUATE SCHOOL OF THE

SOUTHAMPTON OCEANOGRAPHY CENTRE

This PhD dissertation by

Matthew D. Palmer

has been produced under the supervision of the following persons

Supervisor

Jochem Marotzke

Chair of Advisory Panel

Martin Palmer

Member/s of Advisory Panel

Harry Bryden

Abstract

The work presented in this Thesis concerns the large-scale circulation of the Indian Ocean and follows three lines of investigation: (i) decadal variability of the subtropical gyre circulation; (ii) decadal variability of the deep meridional overturning circulation (MOC); and (iii) the influence of diapycnal diffusivity on quasi-steady MOC states.

The decadal variability of the subtropical gyre transport over the ocean interior (away from boundary currents) is investigated using hydrographic data from 32°S. Estimates of the relative gyre transports are: 41 ± 5.1 Sv (1 Sv = 10^6 m^3s^{-1}) for 1987, 42 ± 7.0 Sv for 1995 and 58 ± 7.0 Sv for 2002. This represents a 40% increase from 1987 to 2002. The main areas of change in the geostrophic transports are just east of Madagascar Ridge and around Broken Plateau, which is consistent with differences observed in the isopycnal depths in these areas. Maps of contoured velocity suggest that most of the change happened between 1995 and 2002, which supports the transport estimates.

The 1987 and 2002 hydrographic data are then combined with a regional model of the Indian Ocean to investigate the impact that changes in conditions near 32°S might have on the deep MOC. The model has lateral open boundaries at 35°S for the Southern Ocean and 122°E for the Indonesian Throughflow. The meridional velocity field dominates over density at the southern boundary (SB) in determining the basin-wide deep circulation on decadal timescales. The initial adjustment of the deep MOC to the first 5-6 years of model integration and shows a large sensitivity to the SB conditions. With 'best' estimates of the flow field near 32°S the model shows a 6 Sv and 16 Sv deep MOC for 1987 and 2002, respectively. There are also changes in the zonal structure of the deep circulation. The results suggest that the Indian Ocean exhibits decadal variability in the size and structure of the deep MOC. Furthermore, the apparent inconsistency between previous non-GCM and regional GCM studies may be a result of the lateral boundary conditions, rather than a conflict in the model dynamics.

200-year model integrations suggest that quasi-steady MOC states in the Indian Ocean are reached on century time scales. The size, structure and adjustment time of the quasi-steady deep MOC are controlled by the distribution of diapycnal diffusivity (K_d). The zonal mean distribution of K_d required to support the prescribed deep inflow at the model SB can be estimated using a one-dimensional (1-D) advective-diffusive balance in isopycnal layers. The 18 Sv overturning circulation put forward by Ferron and Marotzke [2003] (FM) collapses when their model configuration is integrated to quasi-steady state under a number of different K_d regimes. With a diagnosed K_d field only 70% of the FM circulation can be supported in quasi-steady state, and the K_d values are an order of magnitude larger than recent observations suggest. The results imply that one can get a good a priori estimate of the K_d-field required to support a quasi-steady model MOC by applying a 1-D advective-diffusive balance in isopycnal layers to the SB conditions. Overall, the research highlights the need to implement improved estimates of (non-uniform) K_d in ocean GCMs when investigating quasi-equilibrium model states.

Chapter 1: Introduction

Chapter 2: Description of the Indian Ocean model

Chapter 3: The gyre circulation of the subtropical Indian Ocean

Chapter 4: Deacadal variability in the deep circulation?

Chapter 6: Summary and discussion

Acknowledgements

Firstly, I would like to acknowledge my supervisors: Jochem Marotzke and Harry Bryden. Jochem has provided excellent teaching and guidance throughout my research and I thank him for introducing me to the world of ocean modelling. Harry has taught me a lot about physical oceanography from a hydrographer's perspective and introduced me to the Indian Ocean onboard the *Charles Darwin*. Both supervisors are enthusiastic, generous with their time and have contributed greatly to my development as a scientist.

I thank Joël Hirschi and Alberto Naveira-Garabato for taking an active interest in my research and for providing feedback on the chapter drafts. I am very grateful to John Stark for resolving the many technical problems and computer-related issues that arose as part of the model work. I also thank the members of the Ocean Circulation and Climate Dynamics group (Robin Smith, Matthew Brand, Marc Lucas, Clotilde Dubois, Fiona McLay, and Johanna Baehr) for creating a lively forum for scientific discussion.

I would like to thank the following people who I have worked with during my PhD studentship: the crew and scientists of research cruise CD139; Elaine McDonagh, for providing the hydrographic data and estimate of the 2002 flow field; Alex Ganachaud, for providing inverse model data; Bruno Ferron, for providing the Indian Ocean model configuration; Beverly de Cuevas and Andrew Coward, for providing OCCAM data; Detlef Stammer for providing ECCO data; and Paolo Cipollini for advice on spectral analysis.

Thanks to my family and friends – in particular Marc Lucas and Siwan Rees who have shared the experience from start to finish. Finally, thanks to Charlie for her love and support over the last four years.

Chapter 1: Introduction

1.1 The oceans and climate

We live in a world of changing climate. There is little doubt amongst the scientific community that carbon-dioxide levels and global mean temperature have been increasing since the Industrial Revolution and will continue to increase in the near future. Given the potentially disastrous consequences of rising sea level, increased storm activity and a weakening or shutdown of the thermohaline circulation, there has never been a greater need to understand the Earth climate system.

The oceans play a crucial role in the current climate and will have an important influence on future climate change. They cover an enormous area, providing the surface temperature boundary condition for the atmosphere over 70% of the Globe. The oceans are very efficient at absorbing incoming solar radiation and transport huge amounts of heat poleward [*Trenberth and Caron*, 2001]. Atmosphere-Ocean exchange has an important impact on greenhouse gas concentrations and the oceans are a natural source of aerosols, which influence global cloud cover. The oceans have a long memory and respond only slowly to changing atmospheric and radiative conditions [e.g. *Siedler et al.*, 2001].

In order to make predictions about the future climate it is important to understand the current climate. This necessitates an understanding of the present global ocean circulation, of which the Indian Ocean is an integral part (figures 1.1, 1.2).

1.2 Ocean circulation

The ocean circulation determines many of the oceanic properties that are important for climate, such as primary production (and associated uptake of CO_2), local sea level and the transport of heat and freshwater. Here we introduce two aspects of the ocean circulation that are of climatic importance: (i) the ocean gyres (figure 1.1); and (ii) the meridional overturning circulation (figure 1.2).

1.2.1 The ocean gyres

The ocean circulation in the upper 1000m or so is dominated by the influence of the winds. For the mid-latitudes, the result is a series of broad ocean gyres with small equatorward velocities and narrow, intense western boundary currents carrying water poleward (e.g. the Gulf Stream). The rate of subduction (the drawing down of high-latitude surface waters into the ocean interior) in an ocean gyre largely determines dissolved oxygen concentrations, which has important implications for the global carbon budget [*Joos et al.*, 2003]. The gyres and western boundary currents are also important for transporting heat and salt to the high-latitudes, which, it has been suggested, stabilizes the North Atlantic overturning circulation [*Longworth et al., in press*]. Typical mean current speeds in the ocean gyres and equatorial current systems are 10^{-3}–10^{-1} ms^{-1} and the western boundary current speeds are orders of magnitude larger (~1 ms^{-1}). The asymmetry of the gyre circulation arises because of the Earth's rotation and the so-called 'westward intensification' is addressed in a classic paper by Stommel [1948].

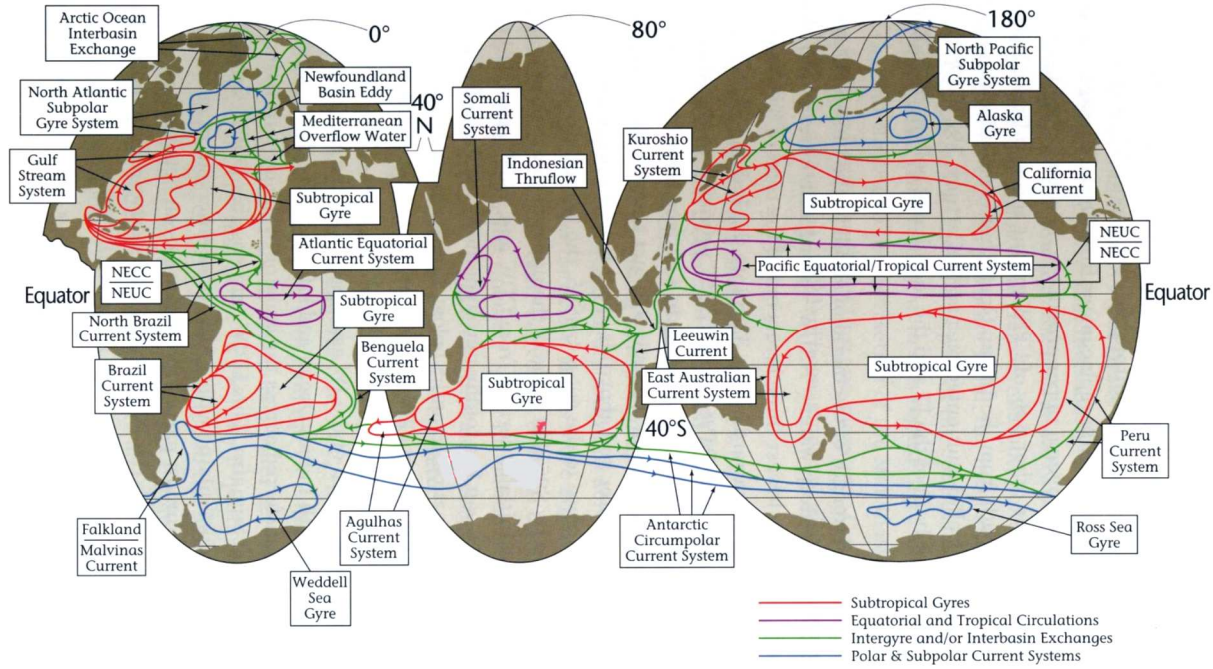

Figure 1.1: A schematic of the surface ocean currents from Schmitz [1996].

1.2.2 The meridional overturning circulation

The meridional overturning circulation (MOC) is the zonally integrated flow within an ocean basin (e.g. figure 1.2). Such a description of the circulation is important as it sets the overall budget of various properties of a given basin, such as the heat and freshwater transport. The MOC of the world ocean is characterised by the formation of North Atlantic Deep Water (NADW) in the Atlantic and the formation of Circumpolar Deep Water (CDW) and Antarctic Bottom Water (AABW) in the Southern Ocean (figure 1.2). These downward branches of the MOC, which occur at a few isolated formation sites, are balanced by upwelling in the ocean interior. Determining and quantifying the return pathways of the deep water masses (particularly NADW) is fundamental to understanding the heat and freshwater transports associated with the deep circulation.

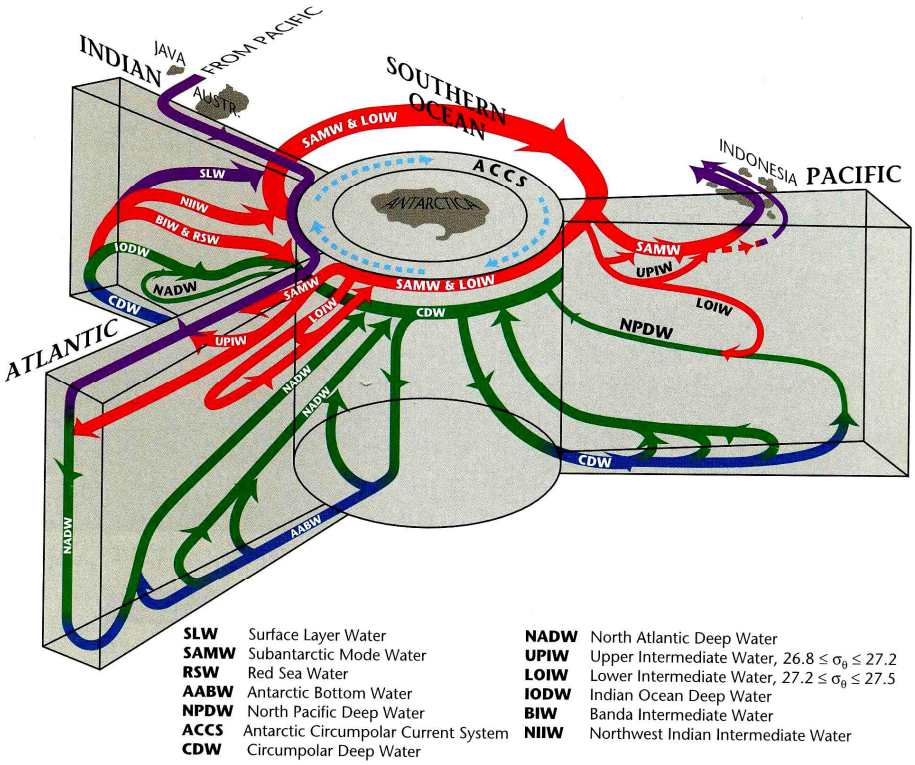

Figure 1.2: A schematic of the World Ocean meridional overturning circulation from Schmitz [1996]. Surface circulations are in purple, intermediate are in red, deep in green and near-bottom in blue.

1.2.3 The 'steady-state' perspective

Measuring the currents in the ocean is a challenging problem because observations are limited and at any given time the velocity field is dominated by the presence of mesoscale eddies (the 'weather systems' of the ocean). This problem is exacerbated in the deep ocean, where observations are few and mean velocities are very small (typically a few mms^{-1}). Traditionally, oceanographers adopted the idea that the ocean circulation is in 'steady-state', in order that observations from different years could be combined to build up a picture of the 'mean' ocean circulation [*Wunsch*, 1996]. There is some justification in this perspective because the interior density structure of the ocean interior adjusts to atmospheric conditions via the translation of baroclinic Rossby waves, which take years or decades to translate across the major ocean basins [e.g. *Gill*, 1982]. It is important to appreciate that many of our conceptual pictures of the ocean circulation have their foundations in steady-state thinking, including those presented in figures 1.1 and 1.2.

Inverse box models [*Wunsch*, 1996] provide a means of estimating the ocean circulation in a way that is consistent with ocean dynamics and some additional constraints, such as simple biology and geochemistry. The steady-state assumption is implicit in this approach, since data from different years are combined to infer the mean

circulation over some time period. Ganachaud [2003a] used hydrographic sections collected as part of the World Ocean Circulation Experiment (WOCE) to estimate the mean global ocean circulation over the period 1985-1996. The model solution is 'optimal' in that it best satisfies a number of constraints, including approximate conservation of mass, heat, salt and silica. Ganachaud's estimate of the flow field near 32°S in the Indian Ocean is used in model experiments presented in chapters 4 and 5.

1.3 The Indian Ocean

The Indian Ocean is the smallest of the world's oceans, accounting for about 14% of the area of the global ocean. It is also perhaps the least well understood in terms of its dynamics, owing to a poor observational database and complex ocean geometry (figure 1.3). The Indian Ocean is unique in exhibiting a seasonally reversing atmospheric and ocean circulation, known as the monsoon system [*Fieux and Reverdin*, 2001] (figures 1.4, 1.5). The ocean has connections to the Pacific via the Indonesian Seas to the east and to the Southern Ocean in the south (figure 1.1). In a global context the Indian Ocean is most notable for providing one of the return pathways for North Atlantic Deep Water [*Gordon*, 1986; *Gordon et al.*, 1992] (figure 1.2). This flux of heat and salt from the Indian Ocean to the South Atlantic around the tip of South Africa has been suggested to have a stabilizing affect on the global MOC [*Weijer et al.*, 2001].

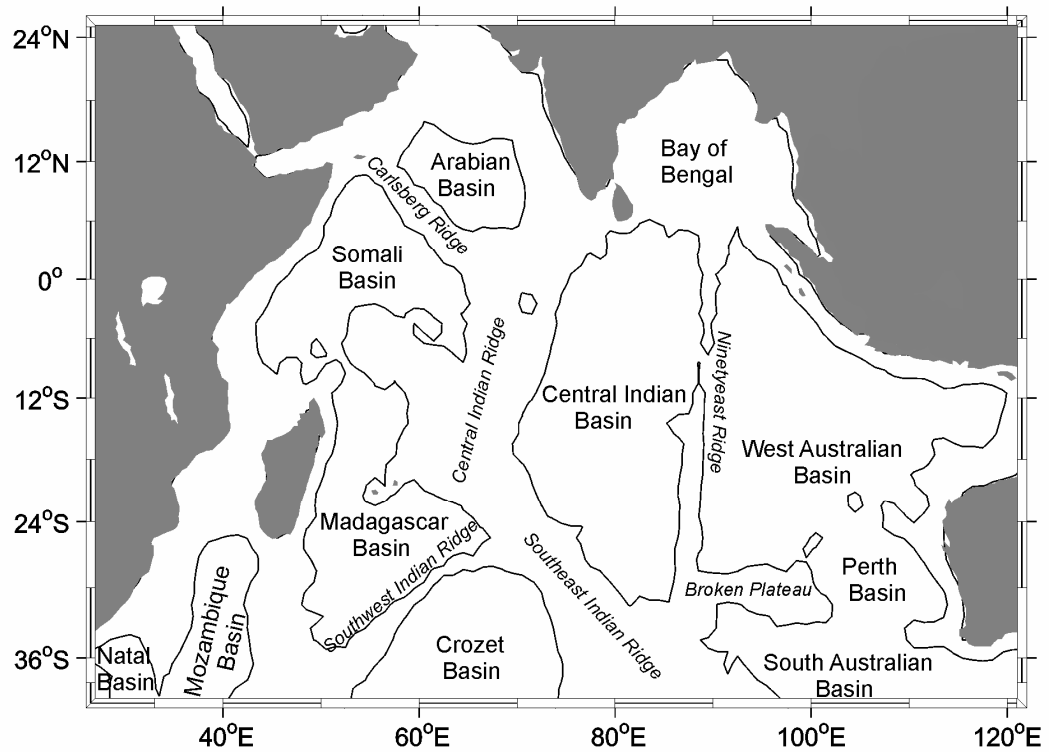

Figure 1.3: Map of the Indian Ocean sub-basins and topographic ridges. The lines are the smoothed 4000m depth contour.

1.3.1 The tropical monsoon circulation

The Indian Ocean is unique among the world's oceans in that it is bounded to the north at mid-latitudes by the Asian continent. The resulting meridional land-sea contrast is responsible for the seasonal reversal of the winds, known as the monsoon (figure 1.4). Associated with the monsoon winds is a dramatic change in the surface ocean currents of the tropical Indian Ocean (figure 1.5). The winter monsoon (Northeast monsoon), which occurs between December and March-April is characterized by north-easterlies north of the equator and the Inter-tropical Convergence Zone (ITCZ) lies zonally at about 10°S (figure 1.4). During the summer monsoon (Southwest monsoon), occurring between June and September-October the winds north of the equator reverse completely. In this phase the monsoon winds are much stronger and the ITCZ meanders over the Asian continent (figure 1.4), bringing the monsoon rains.

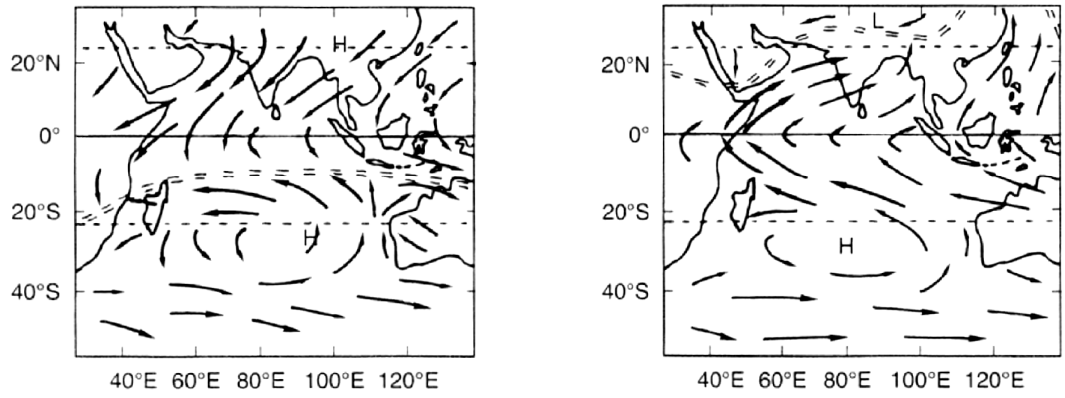

Figure 1.4: Prevailing winds during the Northeast monsoon (left) and Southwest monsoon (right). The location of the ITCZ is indicated by the dashed lines. Figure from Fieux and Reverdin [2001].

The monsoon winds drive some extraordinary changes in the surface currents of the tropical Indian Ocean (figure 1.5). During the Northeast monsoon we observe the formation of the Somlai Current and South Equatorial Countercurrent, which are not present during the Southwest monsoon [*Schott and McCreary*, 2001]. The Southwest monsoon sees a reversal of the flow around the coast of India and Sri Lanka, and the formation of the Southern Gyre and Great Whirl off the African coast.

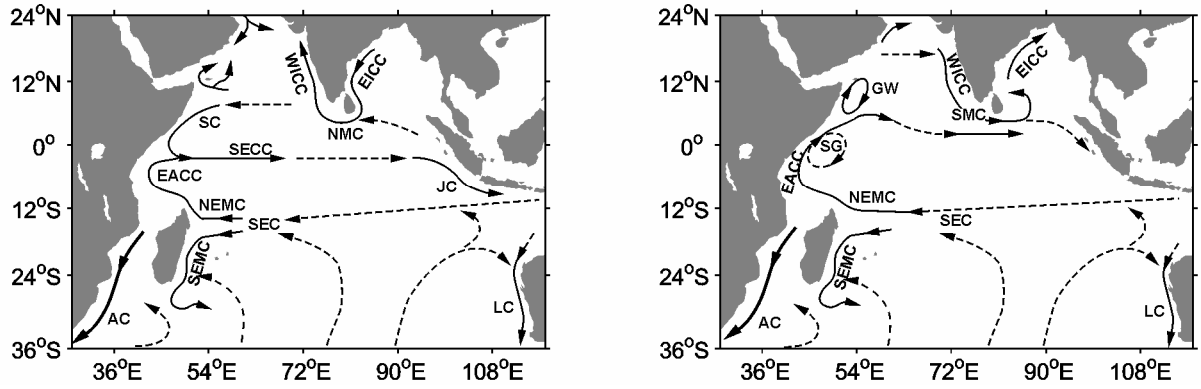

Figure 1.5: The near-surface circulation during the Northeast monsoon (left) and Southwest monsoon (right). Currents indicated are the Agulhas Current (AC), South Equatorial Current (SEC), South Equatorial Countercurrent (SECC), Northeast and Southeast Madagascar Current (NEMC and SEMC), East African Coast Current (EACC), Somali Current (SC), Southern Gyre (SG) and Great Whirl (GW), West Indian Coast Current (WICC), East Indian Coast Current (EICC), Northeast and Southwest Monsoon Current (NMC and SMC), South Java Current (JC) and Leeuwin Current (LC). Figure adapted from Schott and McCreary [2001].

Although the tropical ocean circulation changes radically between seasons, there is little influence of the monsoon south of about 10°S. In a model study, Lee and Marotzke [1998] found that deep circulation of the Indian Ocean showed a monsoonal signal, associated with the changing Ekman transports and a barotropic (depth-mean)

compensation flow. However, the annual mean deep circulation was similar to a previous model solution using annual mean winds [*Lee and Marotzke*, 1997], which suggests that the monsoon has little influence on the deep circulation on long time-scales.

1.3.2 The Agulhas Current and subtropical gyre circulation

South of about 20°S the Indian Ocean has a fairly typical subtropical gyre circulation. There is broad equatorward flow over the ocean interior (figure 1.5) and an intense poleward current at the western boundary – the Agulhas Current. The Agulhas Current is one of the world's most energetic western boundary currents, with velocities reaching 1.8 ms^{-1} [*Beal and Bryden*, 1999] and an estimated mean transport of 70 ± 20 Sv [*Bryden et al.*, submitted manuscript]. The current has a large vertical shear of horizontal velocity and has be observed to exhibit equatorward flow at depth [*Beal and Bryden*, 1997].

Bindoff and McDougal [2000] observed changes in the subantarctic mode water (SAMW) and Antarctic Intermediate Water (AAIW) near 32°S between 1965 and 1987. Both water masses we observed to have freshened and cooled. These water masses are ventilated south of the subtropical gyre, subduct and move northward and become the thermocline waters near 32°S. Using a simple water-mass model [*Bindoff and McDougall*, 1994], the authors showed that the changes could be explained by a surface warming in the SAMW formation region and by increased precipitation formation region of AAIW. Banks and Bindoff [2003] found the same trend in a coupled climate model and classified the cooling and freshening on isopycnals as the fingerprint of anthropogenic climate change.

Bindoff and McDougall also found a decrease in oxygen concentrations between 1965 and 1987, which they explained by slight slowing of the subtropical gyre circulation. McDonagh et al [2005] observed a reversal of the upper thermocline trend in oxygen concentrations and the SAMW properties for data collected in 2002. They suggest that variability in this mode water is due to variations in the air-sea heat flux in the formation region. The implied speed-up of the gyre between 1987 and 2002 opposes the notion of a large-scale reorganization of the ocean circulation in response to anthropogenic forcing.

A high resolution hydrographic section at 32°S in the Indian Ocean has only been occupied twice to date; first in 1987 [*Toole and Warren*, 1993] and then again in 2002 [*Bryden et al.*, 2003b]. The advent of the 2002 repeat section presents an opportunity to investigate changes in the density structure of the upper water column that are associated with a change in the gyre strength. A comparison of the two sections from a dynamic perspective and implications for changes in the gyre circulation are discussed in chapter 4, which is based on the work of Palmer et al [2004].

1.3.3 The Indonesian Throughflow

The Indian Ocean is connected to the Pacific by the Indonesian Seas. The inter-ocean exchange that occurs through the Indonesian Archipelago is known as the Indonesian Throughflow (IT) and has an important influence on the mass, heat and freshwater budgets of the Indian and Pacific Oceans [*Godfrey*, 1996]. The IT brings warm, relatively fresh water into the eastern Indian Ocean with a mean transport of about 10-20 Sv [*Ganachaud*, 2003a; *Godfrey and Masumoto*, 1999; *MacDonald*, 1998]. However, the Throughflow is known to show large variability on time scales from weeks to years and can exhibit westward or eastward transport at any given time [*Sprintall et al.*, 2002]. The effect of the IT on the Indian Ocean circulation includes warming of the Agulhas outflow and a deepening of the ocean-wide thermocline [*Godfrey*, 1996].

1.3.4 The meridional overturning circulation

The MOC of the Indian Ocean is a two cell structure. The first is a shallow, cross-equatorial cell that is a result of subduction in the South Indian Ocean and upwelling north of the equator. The shallow MOC has an estimated size of 6 Sv and is thought to contribute little to the meridional heat transport [*Schott et al.*, 2002]. The second overturning cell is a consequence of deep inflow into the ocean basin from the south and upwelling in the ocean interior. The dense water masses that enter across 32°S are North Atlantic Deep Water (NADW, confined to the west) and Circumpolar Deep Water (CDW) (figure 1.2). The rate at which these water masses flow northward into the Indian Ocean and the route they take before exiting to the south determines the size and structure of the deep MOC. Because the Indian Ocean is closed to the north below 2000m, some authors estimate the MOC simply by calculating the inflow below this depth.

Despite numerous studies using both hydrographic data and numerical models, the size and structure of the deep MOC remains poorly constrained. Toole and Warren [1993]

used a hydrographic section at 32°S and water properties to determine a geostrophic deep inflow of 27 ± 10 Sv. Robbins and Toole [1997] realized that this flow field violated the silica budget and added silica conservation as a constraint. Through an inverse calculation they obtained a weaker deep inflow of 12 ± 3 Sv. Subsequent inverse studies, using the same 1987 section, by Ganachaud et al. [2000] and Sloyan and Rintoul [2001] estimated the MOC as 11 ± 3 and 23 ± 3 Sv, respectively. Bryden and Beal [2001] showed that the size of the MOC was sensitive to the strength of the Agulhas Current. Using acoustic Doppler current profiler measurements in the Agulhas Current to reference a geostrophic flow field they estimated an MOC of 10 Sv.

In contrast to the studies discussed above, most general circulation models (GCMs) have shown a weak deep overturning, typically of a few Sv. These include regional Indian Ocean GCMs [e.g. *Lee and Marotzke*, 1997;1998; *Zhang and Marotzke*, 1999], global ocean GCMs [e.g. *Garternicht and Schott*, 1997; *Stammer et al*., 2002] and coupled ocean-atmosphere GCMs [e.g. *Banks*, 2000]. The exception is the work of Ferron and Marotzke [2003] who invoked an 18 Sv overturning in a regional model of the Indian Ocean. This result was achieved by constraining the model interior to match (within the estimated errors) hydrographic observations made as part of the World Ocean Circulation Experiment (WOCE).

The limitations of Ferron and Marotzke's work are discussed in chapter 5, where we improve upon their model set-up and evaluate the long-term stability of their model solution. We also test the sensitivity of quasi-steady overturning states to the distribution of diapycnal mixing in the model interior – an issue which is not addressed in the previous GCM studies. In chapter 4 we attempt to address the weak overturning that typifies the model studies by using hydrographic sections to force the southern boundary of a regional GCM. This is the first time, to our knowledge that such an approach has been used to investigate the deep MOC of the Indian Ocean.

In our model experiments we do not test the sensitivity of the Indian Ocean deep MOC to the magnitude of the IT. We note that in a coupled ocean-atmosphere model, Banks [2000] finds an increase in the MOC (which is initially small) when the strength of the IT is reduced by restricting the flow with modified bathymetry or by enforcing a zero net IT. However, in a regional Indian Ocean GCM, Ferron and Marotzke [2003] find that their estimate of the MOC is little influenced by the IT strength. We acknowledge the potential of the IT strength to influence the MOC in our model runs but leave such sensitivity studies for future work.

1.4 Research overview

This research presented in the following chapters is concerned with variations in the large-scale circulation of the Indian Ocean on a decadal time scale and on the influence of diapycnal mixing on quasi-steady overturning states. The analysis concentrates on the period from 1987 to 2002, when two complete hydrographic transects across the subtropical Indian Ocean were occupied [*Toole and Warren*, 1993; *Bryden et al.*, 2003b]. The hydrographic observations are used to assess changes in the subtropical gyre circulation and also to infer changes in the basin-integrated meridional overturning, through the use of a general circulation model (GCM). The final piece of research investigates the influence of prescribed diapycnal mixing schemes on the sustainability of overturning regimes in a GCM.

1.5 Summary

- An understanding of the global ocean circulation is essential in order to predict future climatic changes.
- The Indian Ocean is an important component of the global ocean circulation.
- The subtropical gyre and deep overturning circulations are of climatic importance.
- There is controversy about the size and structure of the deep meridional overturning circulation.
- The research in the following chapters investigates:
  (i) decadal changes in the subtropical gyre circulation (chapter 3);
  (ii) influence of conditions near 32°S on the overturning circulation (chapter 4);
  (iii) sensitivity of quasi-steady overturning states to diapycnal mixing (chapter 5).

Chapter 2: Description of the Indian Ocean model

2.1 Introduction

Much of the work presented in this thesis uses the Massachusetts Institute of Technology general circulation model (MITgcm). The model and its capabilities are described in detail by Marshall et al. [1997a; 1997b], some of which is repeated here. MITgcm model documentation and model code is freely available to the research community from http://mitgcm.org. The purpose of this chapter is to review the architecture of MITgcm and describe the Indian Ocean model used in this thesis. Descriptions of the model domain, initial conditions, boundary conditions and model forcings are presented. The model configuration is based on that of Ferron and Marotzke [2003] and we include a summary of their work.

2.2 MITgcm

The MITgcm uses a *z*-coordinate for vertical discretization, where *z* represents the vertical distance from a static ocean surface under hydrostatic balance. These so-called '*z*-coordinate' models are the most widely-used ocean models today. The *z*-coordinate is a good framework for modelling diabatic processes (such as the ocean mixed layer) and the community has many years of experience using this type of coordinate. However, computing advection and diffusion along isopycnal surfaces in z-models requires computationally-costly parameterisations and bathymetry is generally poorly represented [*Griffies et al.*, 2000]. The model domain is separated into many cells, which are cuboids by default, but individual cells can be 'shaved' to improve the representation of ocean bathymetry [*Adcroft et al.*, 1997]. The ocean state variables are staggered in the horizontal plane using an Arakawa C grid [*Mesinger and Arakawa,* 1976], with potential temperature (θ) and salinity (S) averaged over the cell volume and velocity components (u, v, w) located at the centre of the cell faces (figure 2.1).

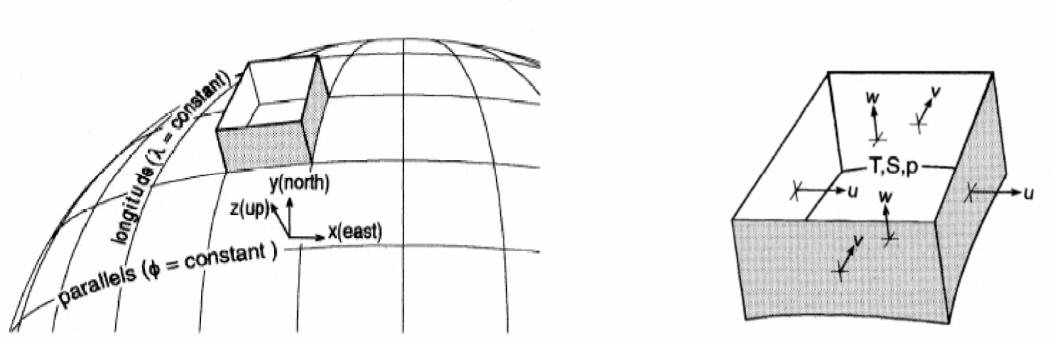

Figure 2.1: (left) A schematic of the model grid with spherical polar coordinates. (right) The relative positions of ocean state variables on the Arakawa 'C' grid. Temperature (T), salinity (S) and pressure are cell mean quantities. Figure adapted from Marshall *et al*. [1997b].

At each model time step, MITgcm solves a simplified form of the incompressible Navier-Stokes equations, under the Boussinesq approximation[*]. The model can be used in hydrostatic and nonhydrostatic modes, making it a very flexible tool for studying oceanographic phenomena over the full range of oceanic length and time scales [*Marshall et al.*, 1997b].

2.3 Model configuration

The basic model configuration used here is derived from the Indian Ocean analysis of Ferron and Martozke [2003] (hereafter referred to as FM), which is discussed in section 2.4. The modifications to the original configuration include modified bathymetry near the southern boundary for some model runs (section 2.3.1) and implementation of an eddy parameterization and an isopycnal mixing scheme (section 2.3.2).

2.3.1 Model domain and resolution

MITgcm is configured for the Indian Ocean over a domain extending from (24ºE, 35ºS) to (123ºE, 26ºN). The limited domain makes best use of available computing resources, but necessitates the use of open boundaries at 122ºE for the Indonesian Throughflow and at 35ºS for the Southern Ocean (figure 2.2). The horizontal resolution is 1º×1° and there are 22 vertical levels with vertical resolution of 10-500m (table 2.1). In keeping with previous modeling work and to minimize computational load, the hydrostatic approximation is made. The complex topography of the Indonesian Throughflow is not

[*] Under the Boussinesq approximation density differences are ignored (ρ is replaced by ρ_o), except where they give rise to buoyancy forces [e.g. *Gill*, 1982].

included in the model. Instead, a single channel representing the Throughflow occurs between the Australian coast and the Indonesian continental shelf (figure 2.2). The Red Sea is also not included in the model.

Model Level	Level Thickness (m)	Level Mid-Point (m)	Level Bottom (m)
1	10	-5	-10
2	10	-15	-20
3	15	-27.5	-35
4	20	-45	-55
5	20	-65	-75
6	25	-87.5	-100
7	35	-117.5	-135
8	50	-160	-185
9	75	-222.5	-260
10	100	-310	-360
11	150	-435	-510
12	200	-610	-710
13	275	-847.5	-985
14	350	-1160	-1335
15	415	-1542.5	-1750
16	450	-1975	-2200
17	500	-2450	-2700
18	500	-2950	-3200
19	500	-3450	-3700
20	500	-3950	-4200
21	500	-4450	-4700
22	500	-4950	-5200

Table 2.1: The vertical levels used in the Indian Ocean model

The default model bathymetry comes from the ETOPO5 (1988) global data set of land and sea floor elevations, which has a $0.08^{o}\times0.08^{o}$ horizontal resolution. The model bathymetry was constructed by applying a simple interpolation routine to the ETOPO5 data and then modifying some of the key regions by hand (for example, near the boundaries and a few deep passages [*Ferron*, pers. comm.]). In some model experiments hydrographic data are used to force the southern boundary, in which case the model bathymetry is modified to reflect bathymetry of the ship track (figure 3.1) or the geostrophic flow field of an inverse box model estimate [e.g. *Sloyan and Rintoul*, 2001; *Ganachaud* 2003a]. The modified bathymetries (figure 2.3) are duplicated over the latitudes 35°S to 32°S in order to allow the relatively noisy high-resolution flow field to adjust to the model dynamics (see chapter 4).

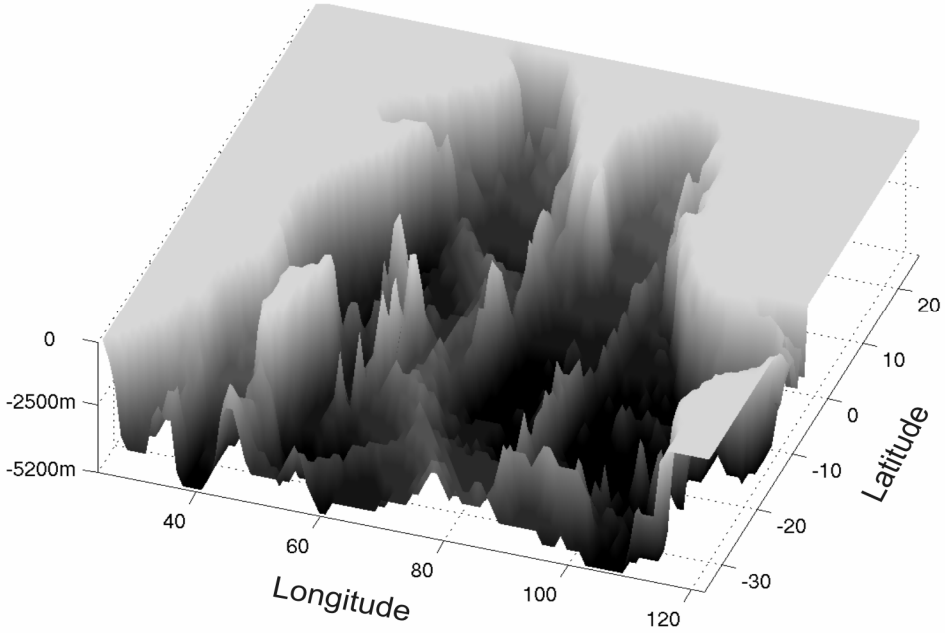

Figure 2.2: A map of the model bathymetry. The data have been smoothed to show the mid-ocean ridges more clearly.

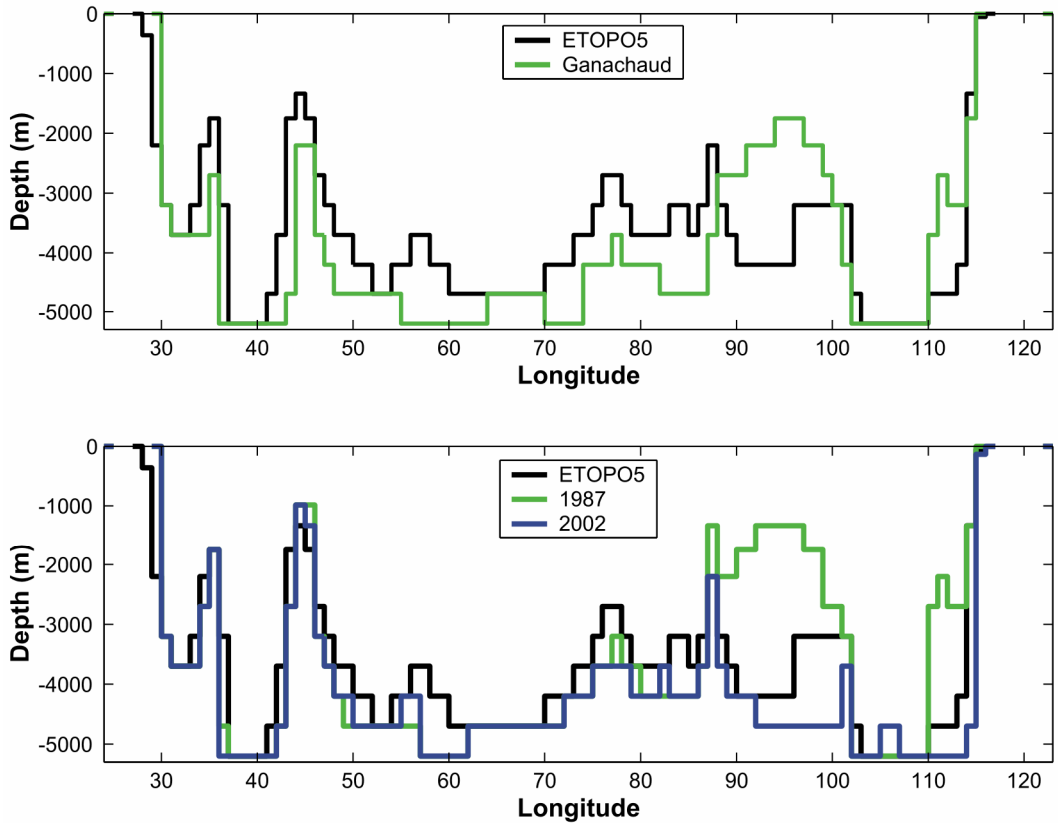

Figure 2.3: The different bathymetries used at the model southern boundary. The ETOPO5 section at 33°S (black); the bathymetry for the Ganachaud [2003a] estimate (upper, green); the McDonagh [in prep.] estimate (upper, blue); the 1987 section bathymetry (lower, green); and the 2002 section bathymetry (lower, blue).

2.3.2 Model parameters

One of the limitations of the FM configuration was the use of horizontal and vertical diffusivities (K_h, K_v) to simulate mixing in the ocean. A more physical representation of mixing is to orient the diffusive flux along isopycnals, using the parameterisation put forward by Redi [1982]. This prevents the spurious diapycnal diffusion caused by sloping isopycnals when using horizontal/vertical mixing, known as the 'Veronis effect' [*Veronis*, 1975]. In MITgcm, isopycnal mixing is combined with the Gent-McWilliams parameterisation to simulate the presence of mesoscale eddies in coarse resolution models [*Gent and McWilliams*, 1990]. The combined GM/Redi parameterisation [*Griffies et al.*, 1998] is used in all model runs presented in the following chapters, though some model runs have been duplicated with the simpler horizontal/vertical mixing scheme to verify the model set-up. The model parameter values appear in table 2.2.

Model Parameter	**Symbol**	**Value**
Domain size (i, j, k)	Nx×Ny×Nz	100×62×22
Vertical eddy viscosity	A_v	2×10^{-3} m^2s^{-1}
Horizontal eddy viscosity	A_h	2×10^{4} m^2s^{-1}
Diapycnal tracer diffusivity (T, S)	K_d	2×10^{-5} m^2s^{-1}
Isopycnal tracer diffusivity	K_ρ	1×10^{3} m^2s^{-1}
Gravitational acceleration	g	9.81 ms^{-2}
Momentum time step	t_m	3600s
Tracer time step	t_T	3600s

Table 2.2: Parameter values used for the Indian Ocean model

2.3.3 Boundary conditions

Where the ocean is bounded by topography, there is a condition of no-flow normal to the solid boundary and a no-slip condition parallel to the boundary. The model has lateral open boundaries (where mass and tracers may leave the model domain) on the southern and eastern edges of the model domain (figure 2.2). At these locations temperature, salinity and velocity normal to the boundary are prescribed at each time step, from a linear interpolation of monthly velocity and tracer fields. At open boundaries the model code requires identical velocity fields (and bathymetry) along j = 1, 2 and i = Nx, Nx-1, where Nx is the number of grid points in the x-direction (figure 2.4). This arises from the need to represent the Coriolis terms in the equations of motion on the 'C' grid

(because the *u* and *v* components are not co-located). A uniform correction velocity is applied to southern boundary to ensure mass/volume conservation in the model interior.

At the surface boundary a 'Rigid Lid' [e.g. *Gill*, 1982] is employed to avoid problems with a free surface and the lateral open boundaries. Surface windstress values are prescribed to simulate the transfer of momentum to the ocean from the atmospheric boundary layer. The surface heat and freshwater forcings are a combination of prescribed fluxes and 30-day restoring to climatological values. During a model run, surface forcings are linearly interpolated from daily surface fluxes and twice-daily wind stress fields. The surface and lateral boundary forcings are described in sections 2.5 and 2.6.

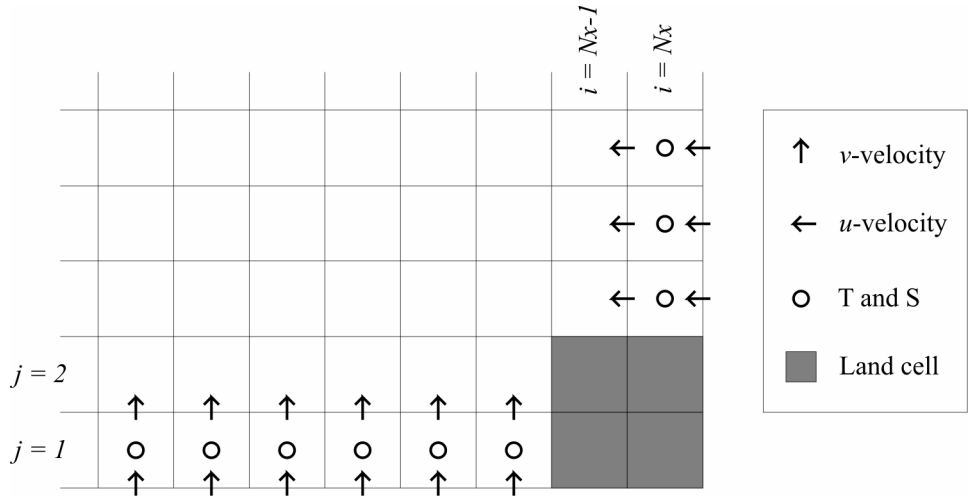

Figure 2.4: A schematic of the open boundary scheme used in the Indian Ocean model. Velocity normal to the boundary is prescribed at each time step over all model levels at j = 1, 2 and i = Nx, Nx-1. Temperature and salinity are prescribed for each time step at j = 1 and i = Nx.

2.3.4 Model initialisation

At the start of a model run initial values for potential temperature (θ), salinity (S) and the *u*- and *v*-components of velocity (*w* is inferred from mass conservation) are required for the ocean part of the model domain. Two different model initialisations are used in the model work (table 2.3). Initializations A and B are used in the modelling work presented in chapters 4 and 5, respectively (table 2.3). The FM surface heat and freshwater fluxes and mean sea-surface θ and S values from the World Ocean Atlas 1994 (hereafter referred to as 'WOA94') [*Levitus and Boyer*, 1994; *Levitus et al.*, 1994] are shown in figures 2.5 and 2.6, respectively. Where hydrography is used to force the open boundary, θ and S between 35°S and 32°S are the observed values.

	Initialisation A	**Initialisation B**
Potential temperature	WOA94 January values [*Levitus and Boyer*, 1994]	10-year model spin-up [*Ferron and Marotzke*, 2003]
Salinity	WOA94 January values [*Levitus et al.*, 1994]	10-year model spin-up [*Ferron and Marotzke*, 2003]
Velocity (*u* and *v*)	$u = v = 0$	10-year model spin-up [*Ferron and Marotzke*, 2003]

Table 2.3: Temperature, salinity and velocity fields for the ocean interior at time = 0.

2.4 The Ferron and Marotzke (FM) Indian Ocean analysis

FM combined an OGCM with World Ocean Circulation Experiment (WOCE) hydrographic observations to analyse the meridional overturning of the Indian Ocean. The basic configuration of their Indian Ocean model is described in the previous sections, using the ETOPO5 bathymetric data throughout the model domain. FM also used a simple horizontal and vertical mixing scheme for θ and S, with values $K_h = 10^3$ and $K_v = 2\times10^{-5}$ m^2s^{-1}. The 4D-variational method (section 2.4.3) used by FM requires 'first-guess' model initial conditions and boundary forcings. These first guess fields are subsequently modified in order that the simulated Indian Ocean circulation fits the observations, within certain error constraints. The modified initialisation and forcings are referred to here as 'optimised' fields because they are associated with an optimal model state. The first-guess data are described in sections 2.4.1-2.4.3 and details of the FM 4D-variational method are reviewed in section 2.4.4. The first-guess and optimised forcings are presented in sections 2.5 and 2.6.

2.4.1 The NCEP/NCAR reanalysis

The FM first-guess surface heat and freshwater fluxes come from the NCEP (Natural Centers for Environmental Prediction)/NCAR (National Center for Atmospheric Research) daily reanalysis values for 1995 [*Kalnay et al.*, 1996] (hereafter referred to as NCEP). The surface wind stress values are twice-daily values from the same year. The NCEP reanalysis combines meteorological observations with a dynamical model of the atmosphere to generate a complete description of past atmospheric states, from 1948 to present. The reanalysis fields (e.g. surface temperature, heat/freshwater flux or surface

wind stress) are a 'best guess' of the spatial distribution of each quantity at a given time. The reanalysis surface data are discretized on a 2.5°×2.5° latitude-longitude grid and linearly interpolated onto the Indian Ocean model 1°×1° grid. The time-mean 1995 surface heat and freshwater fluxes are presented in figure 2.5 and the monthly mean wind stress for January and July 1995 in figure 2.7.

2.4.2 The World Ocean Atlas 1994

The FM first guess model initial conditions and lateral boundary forcings for θ and S come from the WOA94. The data consist of quality controlled hydrographic cast (reversing thermometers and water samples), CTD (Conductivity/Temperature/Depth probe), STD (Salinity/Temperture/Depth probe) and bathythermograph observations between 1900 and 1994 [*Boyer and Levitus*, 1994]. The data have been combined and interpolated onto a 1º×1º horizontal resolution grid with depth as the vertical coordinate. The vertical resolution is 10m near the surface and 500m for the deepest 8 levels, with a maximum depth of 5500m. FM used the WOA94 climatological January θ and S values for the first-guess initial conditions and the monthly-mean values to force the southern and eastern boundaries. The annual mean θ and S for the ocean surface and southern and eastern boundaries are presented in figures 2.6, 2.8 and 2.9, respectively.

2.4.3 The ECCO global ocean model

The FM first-guess open boundary velocities are monthly mean values from a preliminary run of the ECCO (Estimating the Circulation and Climate of the Ocean) global ocean estimation [*Stammer et al.*, 1997]. In this preliminary run the ECCO model was constrained by TOPEX/POSEIDON sea-surface height data [*Fu et al.*, 1994] using the 4D-variational method described in the following section. Since the work of FM, the ECCO model has been improved to include more observational constraints and the resolution has been increased from 2°×2° with 20 vertical levels to 1°×1° with 22 vertical levels [*Stammer et al.*, 2002] (this latter data set is used in modelling presented in Chapter 4). The time-mean velocity fields for the first-guess at the southern and eastern boundaries are presented in figures 2.8 and 2.9.

2.4.4 The 4D-variational method

FM analysed the meridional overturning of the Indian Ocean using a 4D-variational method [e.g. *Le Dimet and Talagrand*, 1986; *Thacker and Long*, 1988] and WOCE hydrographic data. The 4D-variational approach is an iterative process that uses a forward model and the adjoint of its tangent-linear model. During the time integration of the forward model, the cumulated misfits between model and target values (observations) are computed using a pre-determined cost function. The model-data misfits are weighted by error covariances chosen by the analyst. Following the forward model run, the adjoint model is integrated backward in time to calculate the gradient of the cost function to some independent variables of the model (the control variables). A descent algorithm is then used to calculate the amplitude of the control variables so that, at the next iteration, the model trajectory is closer to the observations. Iterations of the forward model run with updated control variables, followed by the adjoint model run are continued until the model trajectory is consistent with the observations.

FM used the model forcings and initial conditions as control variables and 1995 WOCE data throughout the Indian Ocean as the target observations. The forward model was the MITgcm configured for the Indian Ocean – identical to that described here. The adjoint model of the GCM [*Marotzke et al.*, 1999] was generated using the tangent-linear and adjoint model compiler [*Giering and Kaminski*, 1998]. The forward model was integrated for one year and the authors completed 20 iterations to arrive at an 'optimal' model trajectory. Error covariances were based on depth-dependent errors in CTD (Conductivity-Temperature-Depth) salinity and temperature.

The 4D variational method requires initial model conditions and model boundary forcings, the so-called 'first-guess'. The FM first-guess surface forcings came from the 1995 NCEP surface fluxes of freshwater, heat and momentum (Kalnay et al). Open boundary forcings were a combination of monthly-mean WOA94 values for θ and S, and velocities from the 2°×2° ECCO global ocean model [*Stammer et al.*, 1997]. The first-guess initial conditions came from year 10 of a model spin-up using the forcings described above. During the spin-up T and S were relaxed to WOA94 monthly mean values over the top 12 model levels to limit model drift (with restoring coefficient of 10 days for level 1 and 30 days for levels 2-12).

2.5 Model surface forcings

In this section we present the surface forcings used in the modelling work. The surface T and S forcings are a combination of daily prescribed heat and freshwater fluxes (figure 2.5) and a restoring to monthly-mean WOA94 surface values with a 30-day time scale (figure 2.6). The atmosphere-ocean momentum transfer is simulated using 12-hrly surface wind stress values (figure 2.7).

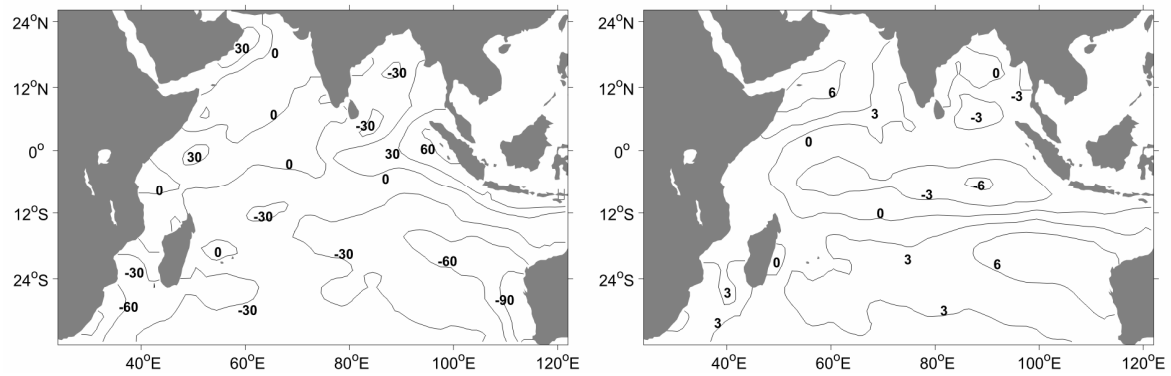

Figure 2.5a: The annual mean heat flux (left) and freshwater flux (right) for the FM first-guess (NCEP 1995 values [*Kalnay et al.*, 1996]). The units of heat flux are Wm^{-2} and positive values indicate heat input into the ocean. The units of freshwater flux are $Kgm^{-2}s^{-1}\times10^{-8}$ and positive values indicate net evaporation.

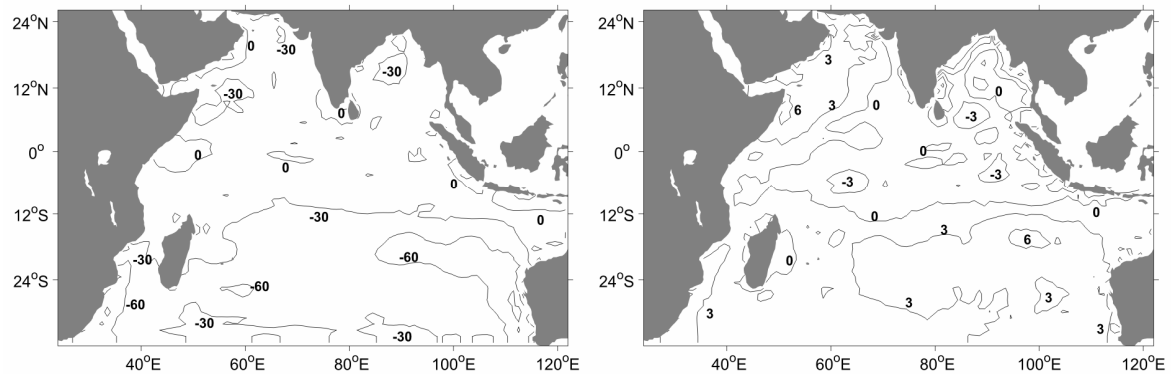

Figure 2.5b: The optimized annual mean heat flux (left) and freshwater flux (right) fields from the FM solution. The units of heat flux are Wm^{-2} and positive values indicate heat input into the ocean. The units of freshwater flux are $Kgm^{-2}s^{-1}\times10^{-8}$ and positive values indicate net evaporation.

The FM first-guess (NCEP) heat flux (figure 2.5a) shows the Indian Ocean to be a region of oceanic heat loss in 1995, with a mean value of -14.2 Wm^{-2} north of 32°S. Most of the oceanic heat loss occurs south of the Equator. Areas of greatest heat loss include the Agulhas current region (east coast of southern Africa); the Leeuwin current region (west coast of Australia) and the eastern part of the subtropical gyre; and a tongue between 12°S and 24°S that is probably associated with Indonesian Throughflow (IT) waters. The areas

of greatest heat gain occur near the Equator off the coast of Somalia and Indonesia; and in the north-west Arabian Sea, off the coast of Oman.

The first-guess freshwater flux (figure 2.5a) shows the Indian Ocean to be an area of net evaporation, with a freshwater loss of 1.4×10^{-8} Kgm^2s^{-1} north of 32°S. South of about 10°S the areas of net heat loss and net evaporation appear to be well-correlated. The Arabian Sea shows strong evaporation, particularly in the north-west. The largest area of freshwater input just south of the Equator, associated with the Inter-Tropical Convergence Zone. There is also a small area of freshwater convergence off the coast of Burma, which is probably associated with river run-off.

The optimized heat flux (figure 2.5b) shows substantial changes to the first-guess field (figure 2.5a) with maximum changes exceeding ± 80 Wm^{-2} and a mean value of -27 Wm^{-2}. The area of heat loss south of 10°S has spread over most of the ocean, but the peak values adjacent to the African and Australian coasts are reduced. The equatorial area of oceanic heat input near Indonesia has vanished, as have heat convergence areas off the north-east African coast and in the north-west Arabian Sea.

There are also substantial differences between the first-guess (figure 2.5a) and optimized (figure 2.5b) freshwater fluxes, but the two fields are qualitatively more similar than their heat flux counterparts. The main change effected by the optimization seems to be a reduction in peak values of freshwater flux. Again, the optimized field is noisier than the first-guess field. After the optimization net evaporation north of 32°S is reduced from 1.4×10^{-8} to 1.2×10^{-8} $Kgm^{-2}s^{-1}$.

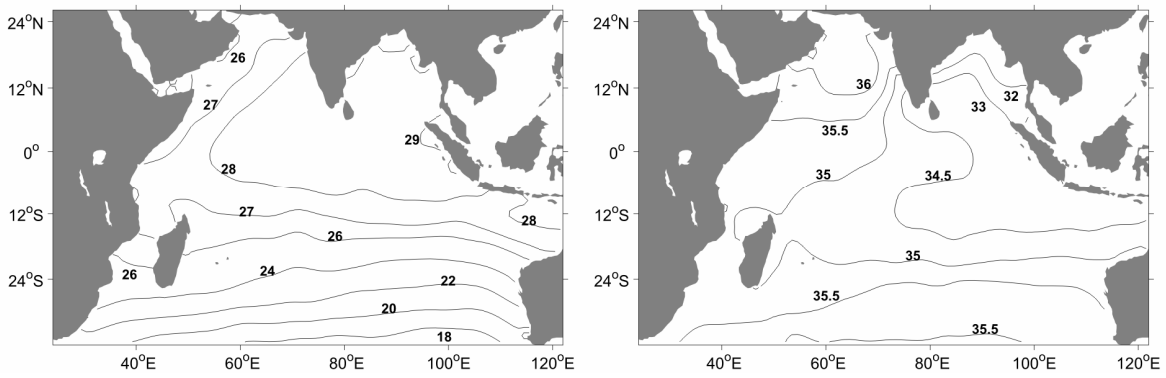

Figure 2.6: The annual mean sea surface temperature in °C (left) and sea surface salinity (right) from WOA94.

The WOA94 sea surface temperature shows a predominantly zonal distribution over the southern mid-latitudes (figure 2.6). The heat-advection influence of the southward flowing Agulhas and Leeuwin currents is apparent in the 'dipping' isotherms near the African and Australian coasts. North of the equator surface isotherms run in a north-east to south-west direction in the western Arabian Sea. The warmest waters occur near the equator, adjacent to Indonesia and in the central north Indian Ocean.

WOA94 sea surface salinity shows a similar zonal pattern to temperature in the southern mid-latitudes (figure 2.6). North of the equator, values either side of the Indian peninsular are split between freshwater inputs in the east and freshwater loss in the west. The freshwater input in the east is most likely river run-off from the Asian continent. The high salinity in the west arises from evaporation over the Arabian Sea and saltwater input from the Red Sea and Persian Gulf.

The first-guess (NCEP) January winds (figure 2.7a) show strong north-easterlies in the north, which are typical of the winter monsoon (see chapter 1). Strong south-easterly winds are adjacent to the Australian coast and extend over the ocean interior. There is also a low-pressure synoptic weather system off the coast of Madagascar. The July winds (figure 2.7c) show weaker and less coherent winds in the north, though there is some evidence of the south-westerlies associated with the summer monsoon. Further south, the low-pressure system seen in the January data has moved eastward over the ocean. The southern mid-latitudes show a wind-direction distribution for July that is similar to January.

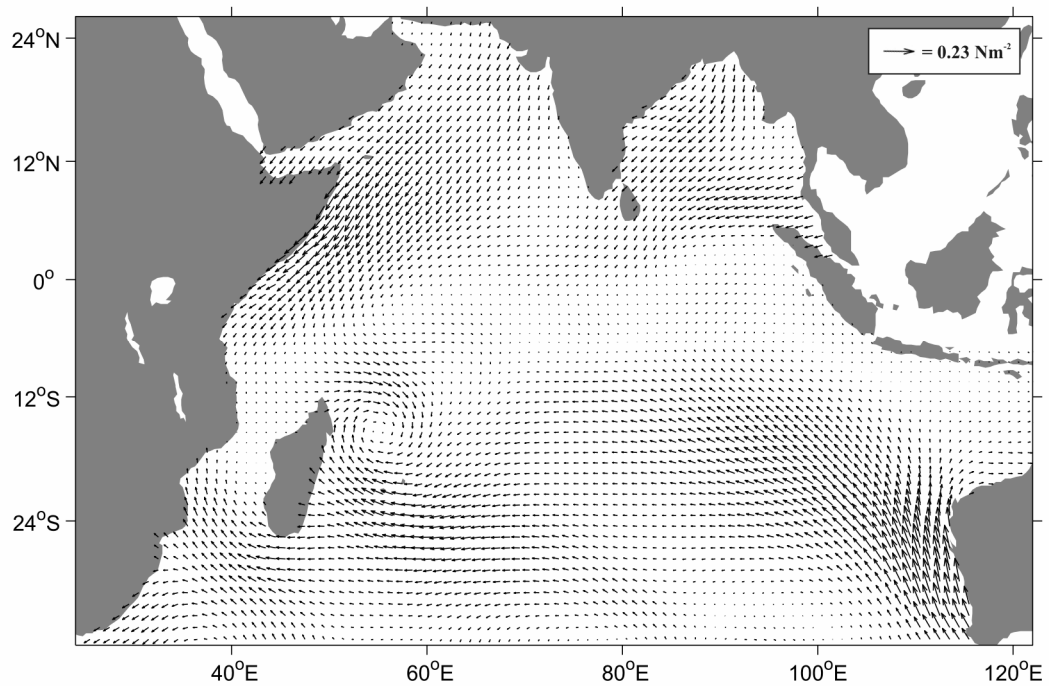

Figure 2.7a: The mean surface wind stress for January of the FM first-guess (NCEP 1995 values [*Kalnay et al.*, 1996]).

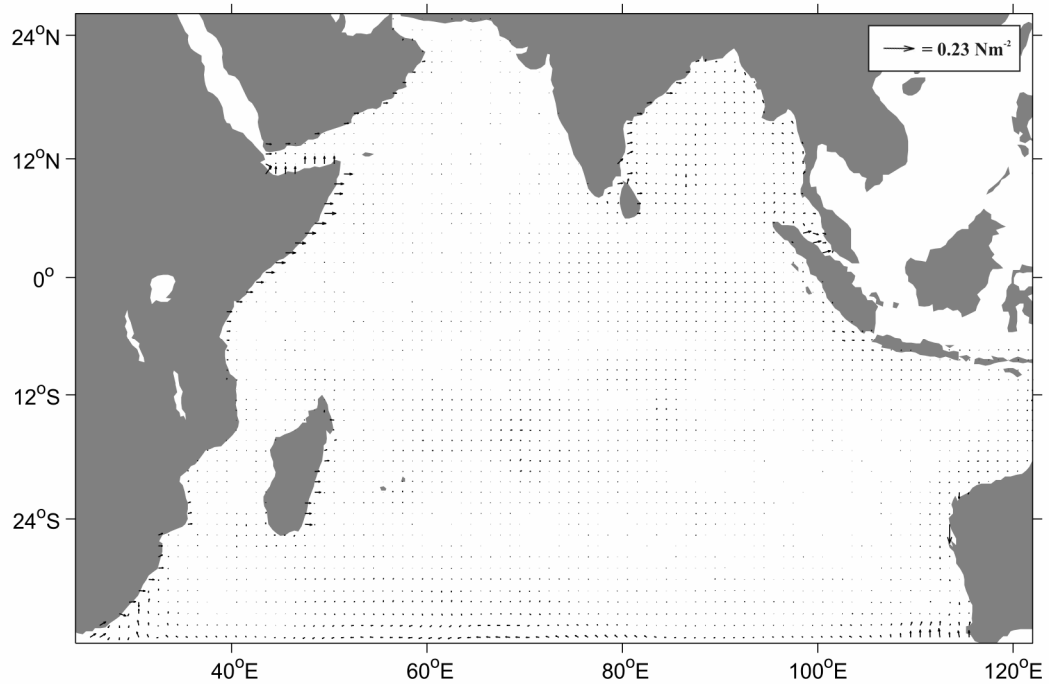

Figure 2.7b: FM optimized wind stress minus the first-guess for January.

There are no substantial large-scale differences between the FM first-guess and optimized surface wind stress fields over the ocean interior. The changes that occur are limited to a few coastal regions and are unlikely to alter the wind-driven overturning cell substantially. For January, many coastal regions develop an extra offshore component after the optimization. This implies that there may be more alongshore transport and perhaps

increased upwelling in these coastal regions. The optimized winds for July also show some changes in coastal regions, but to a lesser extent than those in January.

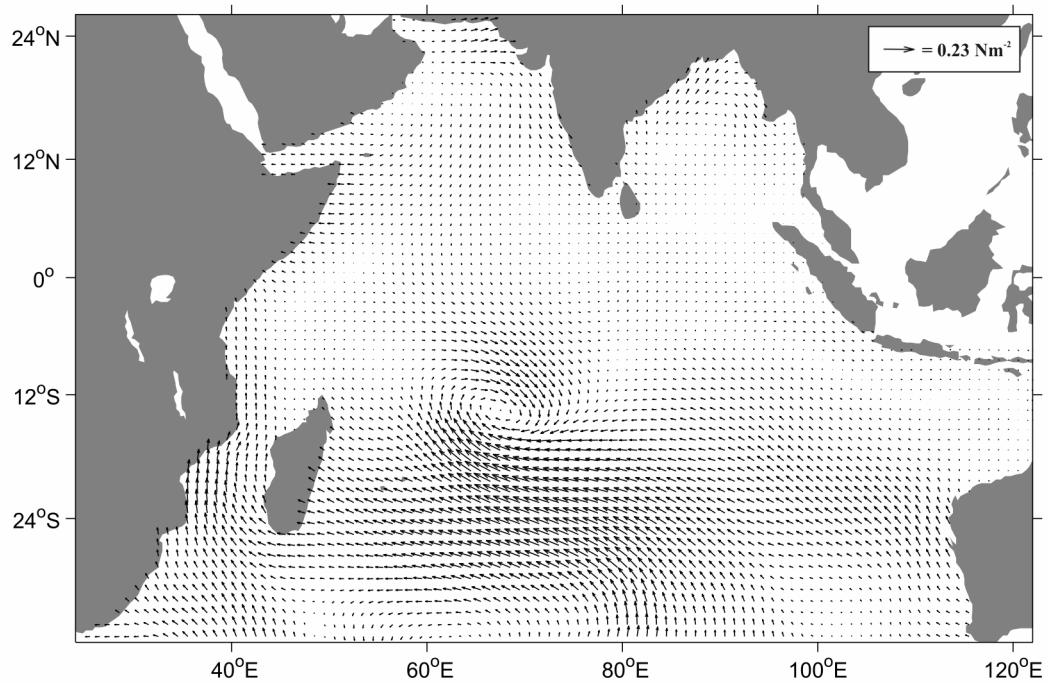

Figure 2.7c: The mean surface wind stress for July of the FM first-guess (NCEP 1995 values [*Kalnay et al.*, 1996]).

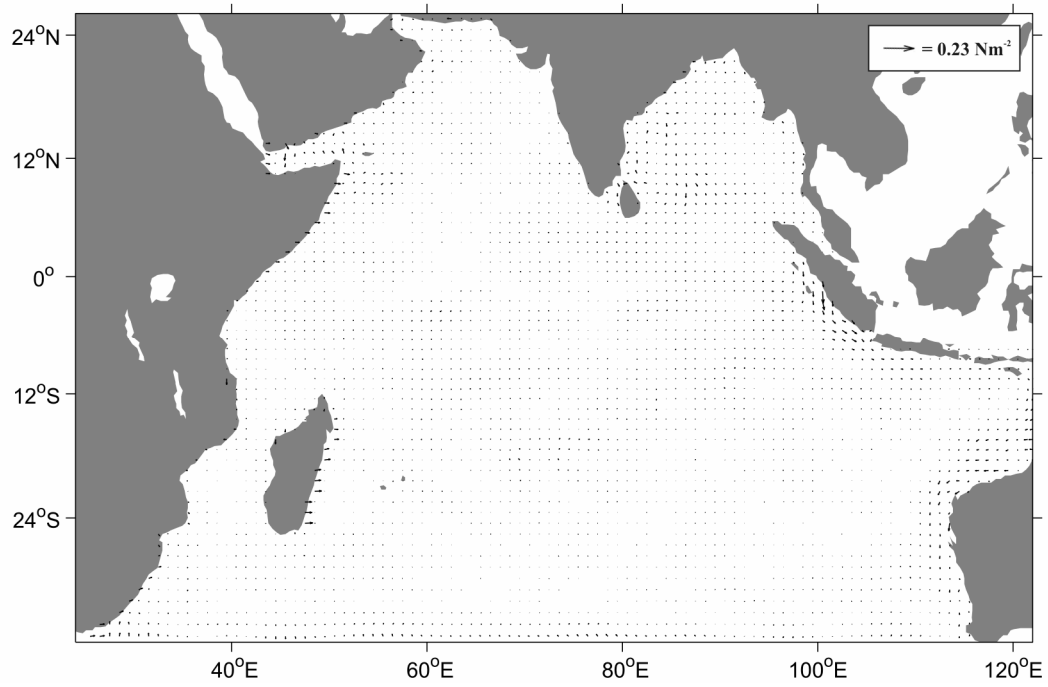

Figure 2.7d: FM optimized wind stress minus the first-guess for July.

2.6 Model open boundary forcings

Potential temperature, salinity and velocity normal to the boundary are prescribed at the southern and eastern open boundaries at each time step. Here we present the FM first-guess (WOA94/ECCO) and optimized open boundary forcings (see section 2.4.1). The eastern boundary conditions presented here are adopted throughout the work with MITgcm. Those southern boundary conditions that incorporate hydrography are presented in chapter 5.

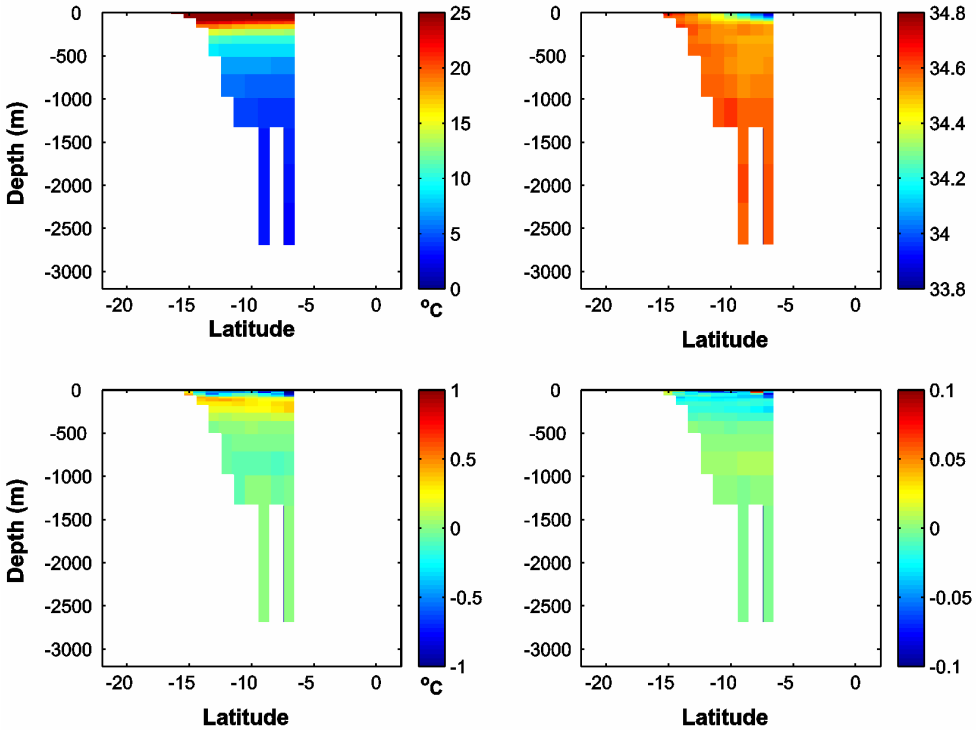

Figure 2.8a: First guess (WOA94) time-mean temperature (upper left) and salinity (upper right) fields for the eastern boundary. Optimized temperature minus first guess (lower left) and optimized salinity minus first guess (lower right).

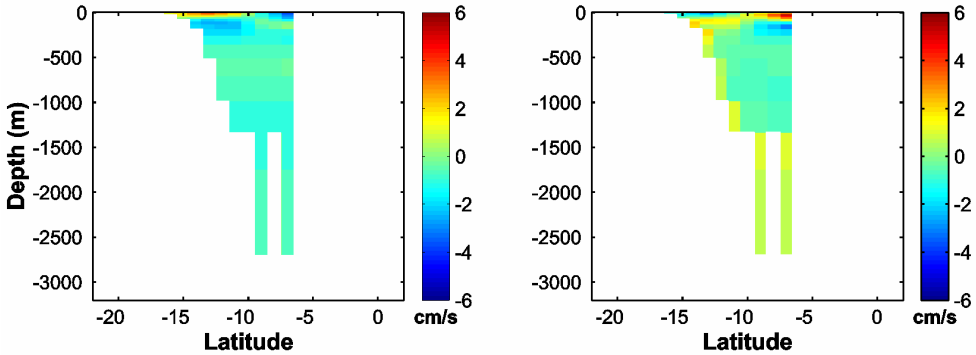

Figure 2.8b: First guess (ECCO) time-mean *u*-velocity for the eastern boundary (left) and optimized velocity minus the first guess (right). Positive (negative) values indicate eastward (westward) flow.

The first-guess (WOA94) eastern boundary temperatures are approximately constant with latitude and show a typical strong depth-dependence. The surface temperature values exceed 25°C and this influence of the IT is felt by the Indian Ocean interior (figure 2.6). In contrast the first-guess salinities are approximately depth-independent, except for some low values in the north in the upper 100m. The changes to T and S caused by the FM optimization are mainly in the upper 200-300m. For temperature we observe a cooling of the surface layers and a warming below about 50m after the optimization. For salinity there is a general freshening above 200m, with an isolated surface grid-cell of increased salinity.

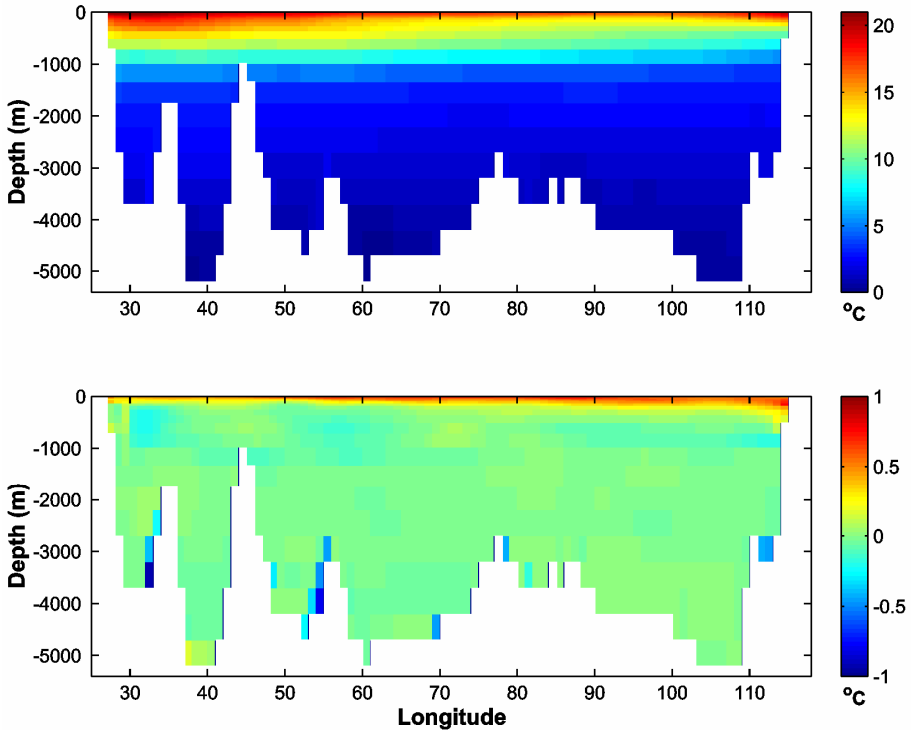

Figure 2.9a: First guess (WOA94) time-mean potential temperature for the southern boundary (upper panel) and FM optimized temperature minus the first guess (lower panel).

The first-guess (ECCO) zonal velocities show predominantly westward flow, with an eastward surface flow south of 10°S. The largest velocities occur in the upper 300m. The change effected by the FM optimization seems to remove the meridional asymmetry of the flow above 300m and reduces the westward flow in the two deep channels. There is also a reduction in westward flow along the southern flank of the main channel (these changes may be related to changes in the topography as one enters the model domain). These changes must lead to an increase in mean temperature of the IT waters entering the Indian Ocean.

The first-guess (WOA94) southern boundary temperature field (figure 2.9a) shows the rapid drop in temperature with depth that is common to all ocean basins. The isotherms gently slope downwards in the east-west direction, which is a by-product of the subtropical gyre circulation. The temperature distribution is much smoother than one would expect from a single hydrographic section (see chapter 3). The optimized field of potential temperature at the southern boundary (figure 2.9a) shows a surface warming in excess of 1°C. This warming penetrates to greater depth as one moves eastward, eventually reaching a depth of about 500m adjacent to the Australian Coast. There are a few areas of slight warming and cooling at mid-depths (20 to 1200m) and some strong cooling features at the sea floor, though not at the deepest levels.

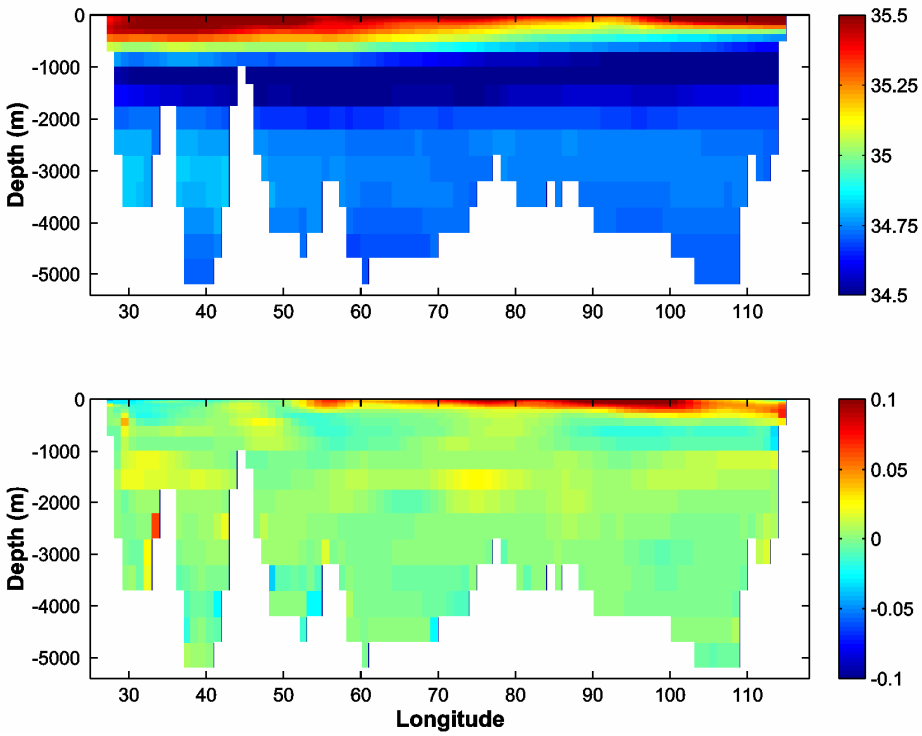

Figure 2.9b: First guess (WOA94) time-mean salinity at the southern boundary (upper panel) and optimized salinity minus the first guess (lower panel).

The first-guess (WOA94) southern boundary salinities (figure 2.9b) highlight the sub-surface salinity minimum indicative of Antarctic Intermediate Water (AAIW). This water mass is transported northwards with the subtropical Indian Ocean gyre. One can also make out the salinity maximum in the western basin at about 3000m depth, associated with North Atlantic Deep Water (NADW). The optimization process led to an increase in salinity in the surface layers, east of about 50°E and a slight freshening in the west (figure 2.9b). There are relatively small changes in salinity throughout the mid-depth ocean and some isolated larger changes adjacent to topography at depth.

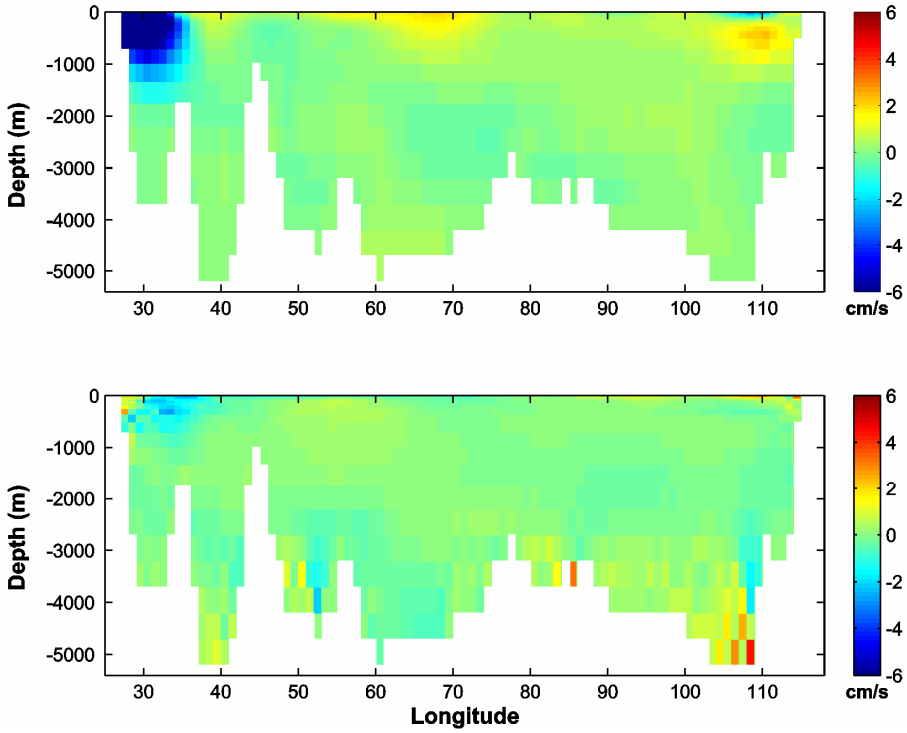

Figure 2.9c: First guess (ECCO) time-mean *v*-velocity for the southern boundary (upper panel) and optimized velocity minus first guess (lower panel).

The first-guess (ECCO) meridional velocities show a much broader Agulhas current than is observed in the real Indian Ocean (figure 2.9c). The Agulhas undercurrent [*Beal and Bryden*, 1997] is not present in the ECCO 2°×2° model. The most conspicuous differences in the optimized field are at the western boundary in the surface layers and in the deepest model layers (figure 2.9c). In particular, we see large increases in northward velocity in the deep Perth Basin (100°E to 110°E). The coarse depth resolution at these levels means that these velocities must be associated with a large increase in northward transport.

2.7 Summary

- The Indian Ocean model has a domain extending from (24°E, 35°S) to (123°E, 26°N), with realistic bathymetry.
- Open boundaries are prescribed at 35°S and 123°E to simulate the influence of the Southern Ocean and Indonesian Throughflow, respectively.
- The Ferron and Marotzke optimization modified the surface fluxes substantially, but had little effect on the wind stress.
- The Ferron and Marotzke optimized fields for θ, S and v show substantial modification at the open boundaries. These changes are concentrated near the surface and at a few isolated places at depth.

Chapter 3: The gyre circulation of the subtropical Indian Ocean[†]

[†] Part of this chapter has been published in: Palmer, M. D., H. L. Bryden, J. Hirschi, and J. Marotzke, Observed changes in the South Indian Ocean gyre circulation, 1987-2002, *Geophysical Research Letters*, *31*(15), art. no.-L15303, 2004.

3.1 Introduction

At mid-latitudes the large-scale circulation in the upper 2000m of the ocean is characterised by the ocean gyres: a western boundary current and a slower return flow over the ocean interior that are in approximate mass balance (in the absence of a meridional overturning circulation). The gyre transport can be estimated by measuring the density structure of the water column and integrating the geostrophic shear from thermal wind balance. This can be done with a full hydrographic section [*Hall and Bryden*, 1982] or using measurements near the basin edges and confining the calculation above any intersecting topography [e.g. *Marotzke et al.*, 1999]. In both cases one must determine reference level velocities or, equivalently, the barotropic velocity field to obtain absolute transports.

Lavín et al. [1998] estimated the circulation in the subtropical North Atlantic by requiring that the ocean interior transport balance the Gulf Stream transport through the Straits of Florida and the Ekman transport over the Atlantic. Such an approach was largely made possible by cable measurements that measured the total Gulf Stream transport. A similar method has been applied to the Indian Ocean by Bryden and Beal [2001]. Their study used current meter data from 1995 to constrain the mean Agulhas current transport and Lowered Acoustic Doppler Current Profiler (LADCP) data to find the zero-velocity surface across the current.

For the Indian Ocean the temporal variability in the Agulhas Current remains a source of doubt for such transport estimates [*Bryden et al.*, submitted manuscript] as does lack of knowledge about the barotropic flow across any hydrographic section. An additional complication is the Indonesian Throughflow (IT), the size of which is poorly constrained by observations [*Godfrey*, 1996; *Sprintall et al.*, 2002]. It remains unclear how the IT transport is compensated in the southern Indian Ocean. Therefore the analysis presented here concentrates on relative changes in the density structure of the water column over the ocean interior and the associated transports relative to a uniform zero-velocity surface (ZVS).

A method for estimating the relative gyre transports over the ocean interior is presented using hydrographic data from 1987, 1995 and 2002 using a uniform ZVS at 2200m. While the analyses focus on the comparison of the two complete hydrographic sections taken in 1987 and 2002 it is useful to include data from the partial occupation of the 32^{o}S section in 1995.

3.2 Data

3.2.1 Hydrographic data

Salinity, temperature, and pressure data are used from 2 CTD (Conductivity-Temperature-Depth) sections at nominal latitude of 32°S taken in November-December 1987 [*Toole and Warren*, 1993] and March-April 2002 [*Bryden et al.*, 2003b]. A supplementary data set comes from two partial occupations in June-July and March-April of 1995: WOCE sections I5W ([*Donohue and Toole*, 2003] stations 611-677) and I5E ([*Talley and Baringer*, 1997], stations 394-442). These three sections generally overlie each other in the west, but deviate east of 80°E (figure 2.1), following or avoiding a zonal ridge-crest (Broken Plateau).

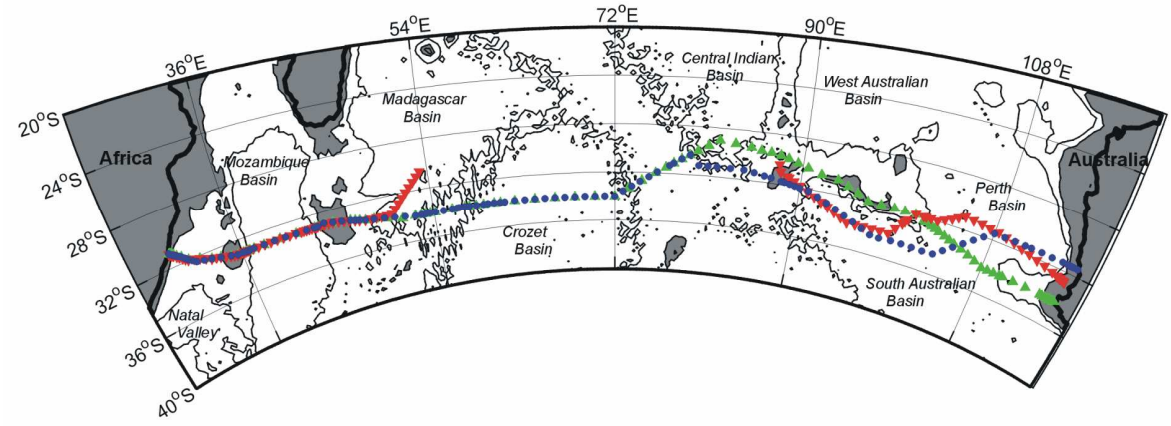

Figure 3.1: South Indian Ocean bathymetry (0, 2000, and 4000m isobaths, depths shallower than 2000m shaded gray) with hydrographic station locations (1987 ▲, 1995 ▼, 2002 ●).

The raw CTD data are continuous profiles of salinity (from conductivity) and temperature as a function of pressure. The salinity and temperature data are calibrated using water samples collected during the CTD cast at each station, to correct for any drift or bias in the sensors. The raw profiles have a lot of short length-scale noise, which is associated with sensor response (figure 3.2). The hydrographic data were box-averaged into 20 dbar bins to remove high-wavenumber noise and create a regular depth grid. The vertical coordinate of pressure was converted to depth using the UNESCO International Equation of State (IES 80), as described in Fofonoff [1985].

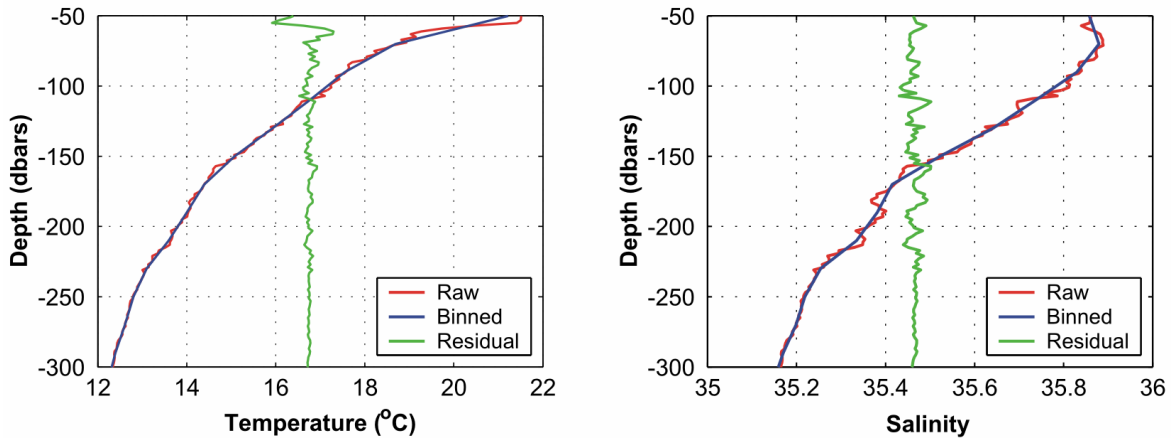

Figure 3.2: CTD profiles of potential temperature (left) and salinity (right) for 50-300 dbar at 31.2°S and 83.2°E from 2002.

Before making any geostrophic transport calculations the density structures of the 1987 and 2002 sections are examined, using sigma-theta (σ_θ) as the density coordinate [*Pond and Pickard*, 1983]. There are three places where the isopycnals diverge substantially between the two sections (figure 3.3): the σ_θ = 26.5 kg m^{-3} between 50ºE and 70ºE; between 600-2200m depth, near Madagascar Ridge (45ºE to 55ºE); and at 800-2200m depth, near Broken Plateau (85ºE to 110ºE). There is a particularly striking feature in the 2002 section at about 104ºE, where the station tracks are re-converging at the end of Broken Plateau. These differences suggest that the geostrophic flow field has changed between 1987 and 2002. Bryden *et al*. [2003a] and McDonagh *et al.* [2005] discuss the changes in water mass properties that occurred between 1987 and 2002 at 32ºS. They report an increase in salinity on potential temperature surfaces for the upper thermocline waters, reversing a trend noted by Bindoff and McDougall [2000] prior to 1987. The observed water mass changes are zonally coherent and do not seem to offer any explanation for the changes in the density field presented here.

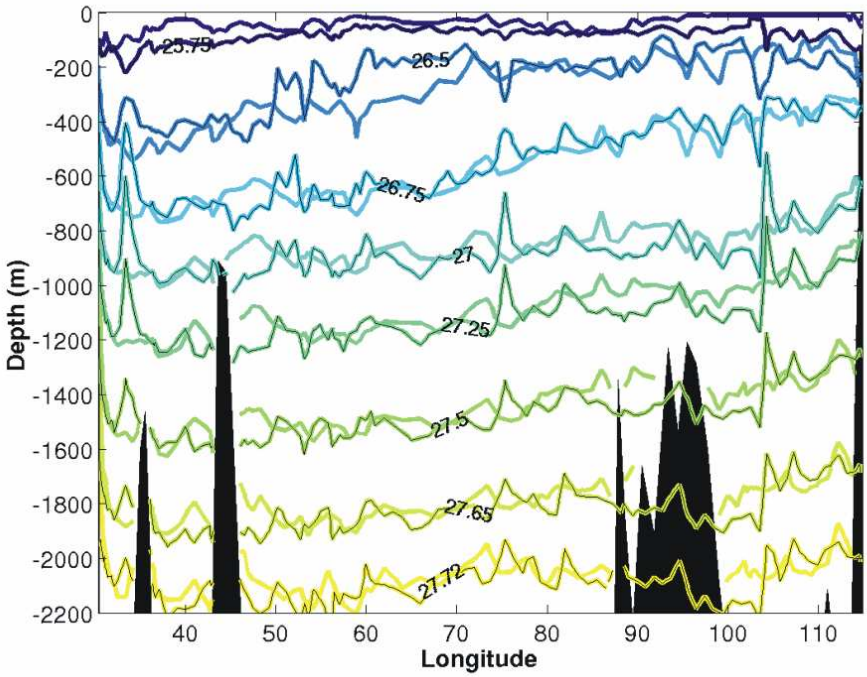

Figure 2.3: Contours of density (σ_θ) for 1987 and 2002 (reinforced with black lines). The bathymetry (from left to right) is Mozambique Plateau, Madagascar Ridge and Broken Plateau.

3.2.2 Model data

Data from the Ocean Circulation and Climate Advanced Modelling Project ocean model (OCCAM [*Webb et al.*, 1998]) are used to estimate the uncertainty in measuring the gyre transport when using a single hydrographic section. OCCAM is a z-coordinate model based on the primitive equations under the hydrostatic and Boussinesq approximations [*Gill*, 1982]. The model equations are discretized using finite-difference schemes on an Arakawa B grid [*Mesinger and Arakawa*, 1976]. Data from two different model configurations were used in the error analysis (table 3.1).

Model configuration OCCAM.25 (table 3.1) is used to investigate the influence of sub-annual variations in the density field at 32ºS on the estimated transports over the ocean interior. For this error estimate, it was imperative to have a long time series with a non-climatological windstress field. OCCAM.125 data (table 3.1) is used to assess the spatial uncertainty associated with the sampling of the hydrographic data at 32ºS because it has better representation of mesoscale eddies than the OCCAM.25 data. Both model configurations were initialized from year 8 of the 0.25º×0.25º model spin-up [*Webb et al.*, 1998]. OCCAM has a very large number of grid cells and manipulating the global data or even that of the Indian Ocean was impractical for this analysis. Therefore, data from only a few lines of latitude near 32ºS in the Indian Ocean were extracted from the global data set.

	OCCAM.25	**OCCAM.125**
Horizontal Resolution	0.25º×0.25º	0.125º×0.125º
Vertical Resolution	36 levels @ 20-250m	36 levels @ 20-250m
Surface Temperature	Restoring to Levitus and Boyer [1994]	Restoring to Levitus and Boyer [1994]
Surface Salinity	Restoring to Levitus *et al*. [1994]	Restoring to Levitus *et al*. [1994]
Windstress Forcing	6-hourly ECMWF (1993-1999)	Monthly ECMWF (1986-1988), Climatology
Integration Time	6 years	2 years
Data Type	5-day time averages (years 1-6)	15-day snapshots (year 2)

Table 3.1: The configurations of the OCCAM model used in the error analysis of gyre transports at 32ºS.

It is helpful to include some details about the representation of the Indian Ocean in OCCAM. As the OCCAM.25 is the longer run, the analysis is based on this data set. The Agulhas Current has a mean barotropic transport of 54.6 ± 8.4 Sv and the Indonesian Throughflow strength is 12.7 ± 4.6 Sv, based on the 5-day average velocity fields. The Agulhas transport is significantly lower than recent observations [*Bryden et al.*, submitted manuscript] and the IT is within the range of current estimates [*Godfrey*, 1996; *Sprintall et al.*, 2002]. The deep overturning cell at 32°S has an average magnitude of 4.5 Sv with the northward deep inflow occurring below 3700m and mass balance achieved at a depth of approximately 1400m.

The magnitude of the time-mean velocity field at 32ºS shows where the largest persistent currents occur (figure 3.4, upper panel); near the surface, western and eastern boundaries and adjacent to mid-ocean topography. The areas of greatest variability were determined by computing the standard deviation of the time series. In the following analyses the data used were restricted to between 40ºE and 105ºE, in order to avoid the large coherent variability associated with the Agulhas Current at the western boundary and the Leeuwin Current at the eastern boundary (figure 3.4, lower panel). The zonally averaged model velocity field over these longitudes exhibited a zero crossing at 1770m, using linear interpolation, which was chosen for the ZVS in model-based geostrophic reconstructions. Note that the areas of largest meridional velocities do not always coincide with the areas of largest variability, for example, the strong velocities on the eastern flanks of the ridges in the ocean interior.

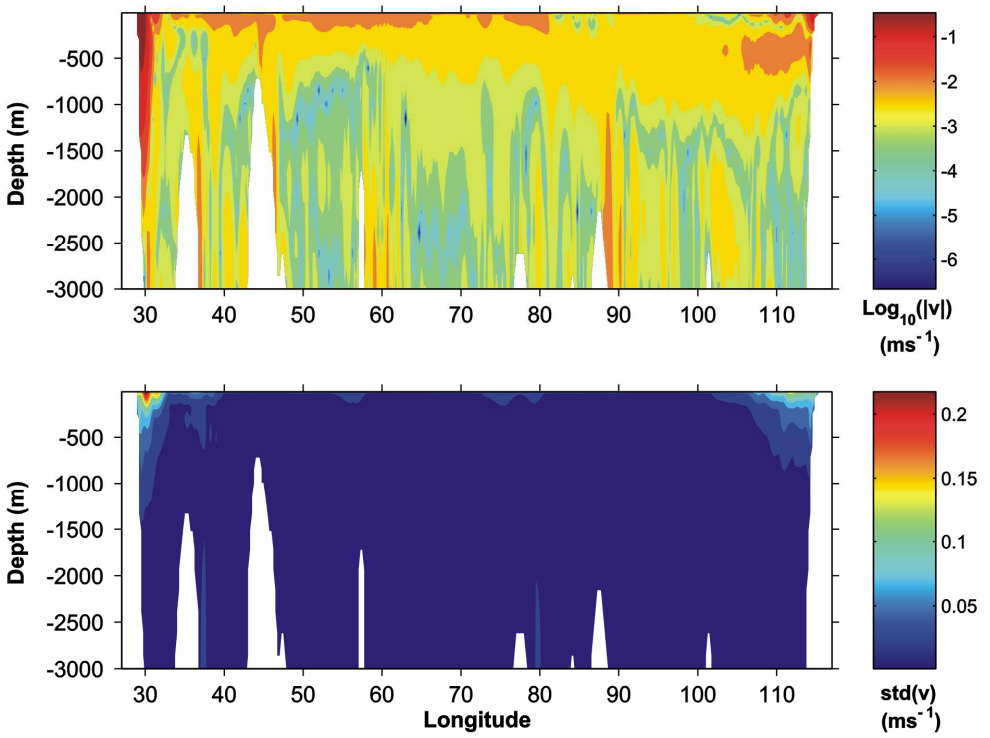

Figure 3.4: Velocity data at 32ºS from the OCCAM.25 configuration: (upper panel) $\log_{10}$ ($|v|$) and (lower panel) standard deviation of (v) for the top 3000m. The model bathymetry is shown in white.

3.3 Methods

The geostrophic transport between each station pair is computed by calculating geopotential anomaly and integrating upward from a ZVS at 2200m [*Pond and Pickard*, 1983]. The ZVS is chosen at a depth of minimum velocity shear in the ocean interior for the 3 sections. Changing the ZVS by as much as 800m affects the transport estimates by less than 3% (figure 3.5). Where there is topography above 2200m, the ZVS is set to the deepest common level of the station pair. This only occurs at the Madagascar Ridge and across Broken Plateau for the 1987 section (figure 3.3).

The profile of geostrophic meridional-velocity shear between each station pair is calculated by applying thermal wind balance to the geopotential anomaly fields. The thermal wind equation [e.g. *Gill*, 1982] provides a relationship between zonal density differences ($\partial\rho/\partial x$) and vertical meridional-velocity shear ($\partial v/\partial z$):

$$-f\frac{\partial v}{\partial z}=\frac{g}{\rho_0}\frac{\partial \rho}{\partial x}, \qquad \text{(Eq. 3.1)}$$

where f is the planetary vorticity, g is the gravitational acceleration and ρ_0 is the reference density. For each station pair equation 3.1 is integrated in the vertical with v = 0 at 2200m, or v = 0 at the bottom (if there is topography above 2200m). Where topography is encountered it is treated as horizontal between adjacent hydrographic stations at the deeper of the two levels. Transports are calculated for the upper 2200m from the velocities for 1987, 1995 and 2002.

The primary interest is the large-scale flow field, so the data are filtered with a Gaussian of 8º-longitude length-scale to remove the high wavenumbers. The filtering process also provides a means of assessing the transport uncertainty associated with the mesoscale eddy and internal wave fields (section 3.4). The estimates of the gyre transport across 32ºS and changes in the geostrophic flow field among the three sections are discussed in section 3.5.

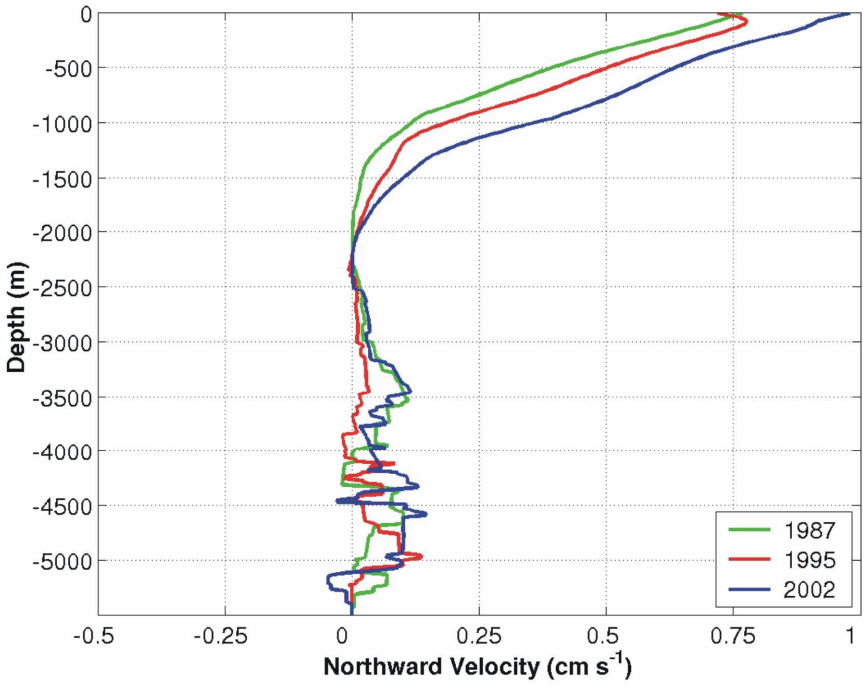

Figure 3.5: The mean velocity profiles between 40ºE and 110ºE referenced to 2200m. The velocities have been interpolated onto a regular 0.5º grid.

3.4 Error analysis

Three potential sources of transport error are addressed in this section:

i. *The uncertainty in transport estimates caused by hydrographic sampling strategy.*
ii. *The uncertainty in geostrophic transport associated with sub-annual variations in the density field.*
iii. *The uncertainty in transports associated with mesoscale eddies and the internal wave field.*

The first two error sources are estimated using data from the OCCAM global ocean model. The final source of error is estimated using hydrographic data. We note here again that the estimated gyre strengths are not sensitive to the choice of ZVS. Increasing the depth of the ZVS by 800m changes the transport estimates by less than 3%.

3.4.1 Hydrographic sampling

Uncertainties in the transport estimates associated with hydrographic sampling (figure 3.1) are estimated using data from the OCCAM.125 configuration (table 3.1) at 32ºS. The model is sampled at every second grid point near the Agulhas Current and at every sixth grid point over the ocean interior. This provides a sampling distribution similar to that of the observations, with the simplification of sampling at constant latitude. A comparison of the mean hydrographic station separations and the separation of the OCCAM sampling are shown in table 3.2.

Mean station separation:	**Hydrography**		**OCCAM.125 (sub-sampled)**
	1987 section	**2002 section**	
Agulhas Region	0.35º	0.22º	0.25º
Mid-Ocean	0.86º	0.73º	0.75º

Table 3.2: The mean distance between hydrographic stations for 1987, 2002 and the sub-sampled OCCAM data.

A total of 38 snapshots at 15-day intervals were used from year 2 of the OCCAM.125 run. For each model snapshot the geostrophic transport at 32ºS is computed in the upper 1770m for the ocean interior (40ºE to 105ºE), first using every model grid point and then the sub-sampled model data. These longitudes correspond approximately to the area over which the hydrographic transports are computed. The calculations were

performed using a ZVS of 1770m, which was determined by analysis of the model meridional velocities. In each case the same end stations are used in the calculation, which means that any differences in total transport must be associated with hydrographic sampling around topography (where there is a change in the ZVS). The standard deviation between the complete and sub-sampled OCCAM transports was 1.9 Sv, with the mean of the sub-sampled transports 0.5 Sv larger than the mean of the complete transports. The same calculation was repeated with a ZVS near 2200m, similar to that used in the analysis of hydrographic data. In this case the standard deviation was 1.0 Sv with the sub-sampled transports underestimated by 0.5 Sv on average.

3.4.2 Sub-annual variability of geostrophic transports

The estimate of transport uncertainty due to sub-annual variations in the density field at 32ºS was assessed using the OCCAM.25 data. Although these data are at coarser resolution than that used for the previous error analysis, they are from a longer model run and use non-climatological winds; both attributes are crucial for a meaningful analysis of the sub-annual variability. The data are 5-day time averages, which are necessary to prevent aliasing of oceanic signals by the high-frequency wind forcing [*Jayne and Tokmakian*, 1997]. A time series of geostrophic transport for the upper 1770m is calculated using a ZVS at 1770m and a second time series is generated on absolute model velocities (figure 3.6, upper panel). As one would expect, the geostrophic time series lacks the high-frequency variability of the absolute transports. The standard deviation of the residual of the two time series is 5.3 Sv, with the mean absolute transport 2.2 Sv larger than its geostrophic counterpart. The bias in transports may result from the northward transport contribution from the surface wind-driven Ekman flow, which is not included in geostrophic transport calculations. Despite this bias, the geostrophic flow field seems to provide a good indication of the absolute transports over the ocean interior.

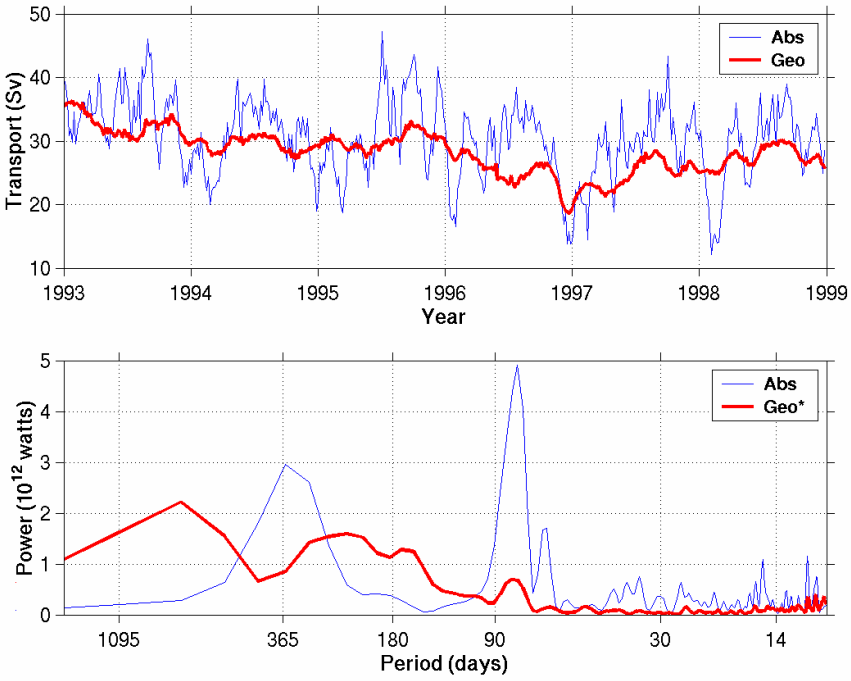

Figure 3.6: Transport time series (upper panel) for the upper 1770m based on OCCAM absolute velocities are geostrophic flow referenced to 1770m for 40°E to 105°E. The corresponding power spectrum (lower panel) using a 3-year Hanning window with a 2/3 overlap. *The geostrophic power spectrum has been multiplied by a factor of 10.

The power spectrum of the absolute transports (figure 3.6, lower panel) reveals a peak at the annual period and at about 60-70 days. Presumably some of this variability is related to the monsoon winds. The geostrophic time series exhibits a small peak at the 60-70 day period, but most of the variability is at periods longer than 6 months. The largest peak for the geostrophic transports is beyond the annual period and is likely to be related to translation time of baroclinic Rossby Waves.

The geostrophic transports do not appear to exhibit a seasonal cycle, so uncertainty associated with sub-annual changes in the density field is treated as random. For each year of the time series the mean geostrophic transport and the standard deviation about the mean was calculated. The mean of the six standard deviations was found to be 1.7 Sv and is taken as the transport uncertainty associated with sub-annual variability.

3.4.3 Mesoscale eddies and internal waves

As discussed earlier, the geostrophic velocities computed from hydrography are filtered with an 8º Gaussian in order to extract the large-scale flow field from the data. The 8º length-scale filter is used because it offers substantial smoothing without much loss of edge data. The error associated with mesoscale eddies and internal waves is estimated by

subtracting the filtered transport curve from the unsmoothed curve (figure 3.7) and computing the standard deviation of the residuals between 35ºE and 110ºE. This procedure yields an uncertainty of ± 4.2 Sv for the 1987 data and ± 6.4 Sv for the 2002 data. Due to the lack of observations over the ocean interior for 1995 (figure 3.1) there were not sufficient data to form a reliable the estimate, so the 2002 value is used.

The three sources of uncertainty were combined by computing the square root of the sum of the variances, thereby making the assumption that they are independent of each other. The final error estimates for the three hydrographic sections are: ± 4.9 Sv for 1987, ± 6.9 Sv for 1995, and ± 6.9 Sv for 2002[‡]. For comparison, Ganachaud [2003b] estimates a geostrophic transport error of ± 3.8 Sv for the upper 2000m at 36ºN in the Atlantic. The contribution of mesoscale variability (± 2 Sv) was lower than that reported here, probably because Ganachaud used a 1/4º ocean model for the analysis, rather than hydrography.

3.5 Gyre transports

The filtered transports above the 2200m ZVS accumulated from west to east (figure 3.7) show significant differences among the three sections. The most obvious difference among the three transport curves is the weaker Agulhas transport in 2002 than in 1987 and 1995, which offsets the transport profiles in the vertical. However, the main concern is the northward gyre transport, east of about 40ºE as the Agulhas is known for its large amplitude high frequency variability [*Bryden et al.*, submitted manuscript], and may not be representative of the ocean state at the time of the section. From 1987 to 2002 the point of maximum southward transport consistently moves westward. The estimate of the gyre strength is defined as the maximum transport that can be attributed to each filtered curve over the ocean interior, between 35ºE to 110ºE. Therefore the transport calculation is made between 55ºE and 110ºE for 1987; 47ºE and 110ºE for 1995; and 40ºE and 110ºE for 2002. The gyre transport estimates are presented below (table 3.3). Although there are no hydrographic data for 1995 between 52ºE and 90ºE the transport estimate is unaffected, because there is no intersecting topography above the ZVS between these longitudes [*Marotzke et al.*, 1999].

[‡] These are revised values and are slightly lower than the ± 5.1 and ± 7.0 reported in Palmer et al. [2004]. The differences arise from a small error in processing some of the OCCAM data in the original analyses.

The 1987 and 1995 sections show large residual transports that, if taken at face value, require a large ITF or deep inflow (or combination of both) to achieve mass balance. However, the use of a uniform ZVS means that the focus is on changes in the *relative* transports (since the true ZVS is very unlikely to be uniform), so we do not make inferences about changes in the ITF strength or deep inflow.

Year	Transport	Uncertainty
1987	41 Sv	± 4.9
1995	42 Sv	± 6.9
2002	58 Sv	± 6.9

Table 3.3: Gyre strength estimates based on hydrography for 1987, 1995 and 2002. 1 Sv = 10^6 m^3s^{-1}.

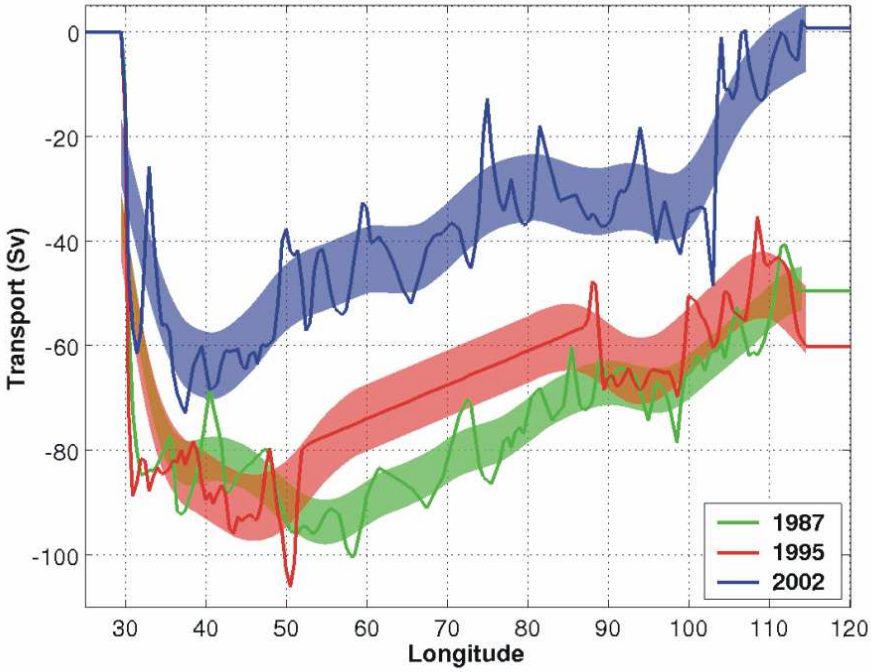

Figure 3.7: Cumulative transports for 1987, 1995 and 2002 calculated on the station grids (lines) with the corresponding filtered transports at one standard deviation (shaded areas). Transports are computed for the upper 2200m.

The 2002 data show a large northward transport at about 105ºE (figure 3.7), coincident with a step-like change in the isopycnal depths (figure 3.3) over a deep trench in the section bathymetry. It remains unclear what causes this sharp discontinuity in ocean water properties. It has been hypothesized that this could be due to a boundary current flowing along Broken Plateau and then northward, through Perth Basin. What causes this extraordinary feature is the subject of ongoing research. For the 1995 curve, there is an

area of southward transport at about 112ºE (figure 3.7), near the Australian coast. This is probably due to the Leeuwin Current, which has its maximum southward velocities in April-May, near the time this part of the section was taken [*Feng et al.*, 2003].

Perhaps the most striking feature of the changes in geostrophic velocity (figure 3.8) is the apparent westward migration of the area of southward flow, centred at about 50ºE in 1987. The greatest difference between the 1987 and 2002 sections occurs at about 50ºE, where southward flow in 1987 is replaced by northward flow in 2002. This change is consistent with a change from downward sloping isopycnals in the west-east direction in 1987 to upward sloping isopycnals in 2002 in this area (figure 3.3). Just west of Broken Plateau (80ºE to 88ºE) there is a change from predominantly northward flow in 1987 to southward flow in 2002, which can also be inferred from the differences in slope of the isopycnals in this area (figure 3.3). Associated with this change is the intensified northward flow east of Broken Plateau in 2002, centred on the 'step' in the isopycnals discussed earlier.

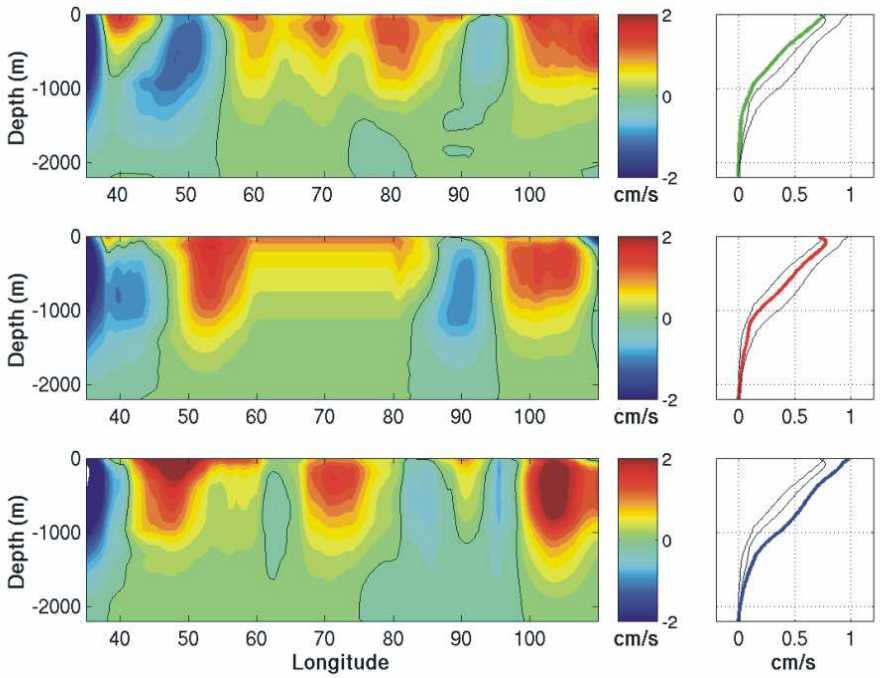

Figure 3.8: Contours of geostrophic velocity for 1987 (upper panel), 1995 (middle panel) and 2002 (lower panel) after applying an 8º-longitude Gaussian filter (positive values represent northward velocities and zero contours are drawn in black). The panels on the right show the zonally averaged velocity profiles (from 40ºE to 110ºE) for 1987 (green), 1995 (red), and 2002 (blue).

The 1995 data give the impression that there has been a persistent change between the flow structure of the 1987 and 2002 sections. The transition can be seen in the zonally averaged velocity profiles (figure 3.8), which suggest that as well as differences in the

zonal structure of the transports, the gyre has strengthened over the period 1987 to 2002. The northward velocities penetrate to greater depth in 2002 than 1987.

In the comparison of the 1987 and 2002 data, one is most confident of the results where the station locations overlie, i.e. west of 80ºE. In this region there are clear differences in the geostrophic flow field, mainly in terms of the zonal structure. It is recognised that the different station tracks east of 80ºE and the strong feature in the isopycnals at 104ºE in 2002 means that the estimates of the relative gyre strengths should be taken with caution.

3.6 Discussion

The size of the gyre transport is estimated using hydrographic data and a zero-velocity surface at 2200m for 1987 (41± 4.9 Sv), 1995 (42 ± 6.9 Sv) and 2002 (58 ± 6.9 Sv). The estimates for 1987 and 1995 are consistent within one standard deviation and the 2002 estimate shows a 40% increase. The largest uncertainty in these estimates comes from eddy and internal wave noise on the sections. There is a change in the zonal structure of the gyre transports between 1987 and 2002. The principal areas of change are east of Madagascar Ridge and either side of Broken Plateau. The 1995 data suggest that there has been a persistent change in the flow structure over the period 1987 to 2002.

Bindoff and McDougall [2000] noted a 20% slowdown of the Indian Ocean gyre circulation between 1962 and 1987 based on transport calculations and changes in dissolved oxygen concentrations. The authors also reported a freshening of the upper thermocline waters. In 2002 the upper thermocline waters were found to be saltier on isotherms [*Bryden et al.*, 2003a] and dissolved oxygen measurements imply a 20% speed-up in the gyre since 1987 [*McDonagh et al.*, 2005]. These findings suggest that there is a link between the water mass changes and gyre strength. The increased gyre strength suggested by McDonagh *et al.* [2005] is qualitatively consistent with results presented here, but they observe zonally coherent changes in water mass properties between 1987 and 2002. In contrast, the differences in isopycnal depth happen in specific areas: just east of Madagascar Ridge and around Broken Plateau in the deep isopycnals at between 50ºE and 70ºE in the upper thermocline. The differences in the zonally integrated velocity profiles below 1000m (figures 3.5, 3.8) suggest that some of the transport changes between 1987 and 2002 are not related to the shallow water mass changes reported earlier.

The possibility of changes in the wind forcing being responsible for the observed changes has been ruled out for two reasons. Firstly, the hydrographic measurements show the largest changes at depth – away from the influence of the wind stress. Even if, somehow, the changes in wind stress were manifested at depth, the values of Sverdrup Transport across 32ºS cannot account for the large gyre transport for 2002. The most likely explanation for the increased apparent gyre strength is a change in the deeper circulation. The meridional overturning cell could have changed magnitude, changed its vertical position, or the locations of the return southward flow may have changed horizontal position.

3.7 Conclusions

- The Indian Ocean subtropical gyre strength at 32ºS is estimated as 41± 4.9 Sv for 1987, 42 ± 6.9 Sv for 1995 and 58 ± 6.9 Sv for 2002. This represents a 40% increase from 1995 to 2002.
- The changes in hydrography responsible for the large 2002 estimate occur at depth and adjacent to topography.
- Analysis of the wind-driven Sverdrup Transport at 32ºS shows consistency with the 1987 and 1995 values, but cannot account for the large increase for 2002.
- The evidence points to a change in the deeper circulation, which can influence the apparent gyre strength based on hydrography.

Chapter 4: Decadal variability in the deep circulation?

4.1 Introduction

The poor agreement between hydrography-based and model studies represents a source of controversy in estimating the size of the meridional overturning circulation (MOC) of the Indian Ocean. Estimates based on one or more hydrographic sections suggest a 10-27 Sv (1 Sv = 10^6 m^3s^{-1}) deep MOC [e.g. *Toole and Warren*, 1993; *Bryden and Beal*, 2001; *Talley et al.*, 2003; *Ganachaud*, 2003a], whereas most general circulation models show a weak overturning (typically < 5 Sv [e.g. *Garternicht and Schott*, 1997; *Lee and Marotzke*, 1997; *Zhang and Marotzke*, 1999]). In this chapter we combine hydrographic observations with a regional model of the Indian Ocean to investigate decadal variability in the deep MOC, in an attempt to address the disparity between hydrography-based and model-based studies. This is the first time, to our knowledge, that hydrographic data have been used directly to force a regional model of the Indian Ocean.

Recent work by Palmer et al [2004] on changes in the subtropical gyre circulation suggests that there has been a change in the deep baroclinic structure over the Indian Ocean interior at 32°S. The authors report a greater geostrophic velocity shear at 1000-2000m depth in 2002 than in 1987, with changes occurring near topography. A natural extension to the work of Palmer et al. is to consider how the changes in the hydrography may affect the Indian Ocean MOC. Therefore, the aim of the work presented in this chapter is twofold: (i) to investigate the sensitivity of the Indian Ocean circulation to water properties near 32°S; and (ii) to force the Indian Ocean model with our current best estimate of a 1987 and 2002 flow field and compare the resulting circulations. By doing this, we hope to establish the plausibility of a change in the deep overturning between 1987 and 2002 and identify ways in which the circulation may have changed.

In section 4.2 we describe our regional model of the Indian Ocean. The hydrographic data and its transformation onto the model grid are discussed in sections 4.3 and 4.4. In section 4.5 we present a method for re-constructing the Indian Ocean meridional velocity field at 32°S and discuss two estimates of the flow field at 32°S in 1987 and 2002. Section 4.6 deals with the adjustment time scale of the Indian Ocean model to the prescribed boundary conditions. In section 4.7 we consider the sensitivity of the MOC to changes in potential temperature, salinity and meridional velocity at the southern boundary. Finally, in section 4.8, we compare a plausible Indian Ocean circulation for 1987 and 2002.

4.2 The Indian Ocean model

We use the MIT ocean general circulation model [*Marshall et al.*, 1997a; 1997b] configured for the Indian Ocean. The model domain extends from (24ºE, 35ºS) to (122ºE, 26ºN) with open boundaries at 122ºE for the Indonesian Throughflow (IT) and at 35ºS for the Southern Ocean. The horizontal resolution is 1º×1° and there are 22 vertical levels (10m resolution near the surface and 500m for the deepest six levels). Bathymetry is interpolated from the ETOPO5 [1998] data set. The model uses a combination of the Gent and McWilliams [1990] mesoscale eddy parameterization and mixing along isopycnals [*Redi*, 1982], known as a GM/Redi scheme. This mixing scheme avoids the spurious diapycnal mixing due to tilting isopycnals under the more traditional vertical/horizontal-mixing scheme, known as the 'Veronis effect' [*Veronis*, 1975]. Diapycnal transfers in the model are parameterized by prescribed vertical diffusivity coefficients and a convection algorithm.

The initial conditions for temperature and salinity are the mean January values from the World Ocean Atlas 1994 [*Levitus and Boyer*, 1994; *Levitus et al.*, 1994]. Model runs are started with the ocean at rest ($u = v = w = 0$). Surface heat and freshwater forcings are a combination of daily 1995 NCEP fluxes [*Kalnay et al.*, 1996] and a 30-day restoring to monthly mean sea surface temperature (SST) and salinity (SSS) from the World Ocean Atlas 1994 (hereafter WOA94). The atmosphere-ocean momentum transfer is simulated by prescribed 12-hourly wind stress fields, using the 1995 NCEP values. At open boundaries potential temperature (θ), salinity (S) and velocity normal to the boundary are prescribed at each time step, interpolated from monthly values. The eastern boundary forcings for θ and S are the monthly mean values from the WOA94 (figure 2.8a). Velocities at the eastern boundary are monthly mean fields from the ECCO 2°×2° global ocean model [*Stammer et al.*, 1997] (figure 2.8b). For all experiments the time-mean IT transport is -10 Sv (into the model domain) except where noted. Near the southern boundary the model bathymetry is modified between 35°S and 32°S according to the prescribed southern boundary conditions (section 4.4.1).

4.3 Hydrographic data

Salinity, temperature and pressure data from two CTD (Conductivity-Temperature-Depth) sections at nominal latitude of 32°S are used in this analysis. The sections were occupied in November-December 1987 [*Toole and Warren*, 1993] and March-April 2002 [*Bryden et al.*, 2003b] (figure 3.1). The raw CTD data have been sorted into 20 dbar bins to remove high-wavenumber noise and create a regular depth grid. The vertical coordinate of pressure is converted to depth in metres using the UNESCO International Equation of State (IES 80), as described in Fofonoff [1985]. The in-situ temperatures are converted to potential temperature for use at the model southern boundary. The fundamental difference in sampling of the 1987 and 2002 sections is the ship track (figure 3.1). The 1987 section crossed Broken Plateau (92°E to100°E) and sampled over more of the Australian continental shelf. The 2002 ship track deviates from the 1987 section east of 80°E to avoid these regions of shallow bathymetry.

For the 2002 section only, direct velocity measurements were made at each hydrographic station. The data are from three Acoustic Doppler Current Profilers (ADCPs [e.g. *King et al.*, 2001]), which provide full-depth profiles of velocity. An additional data set comes from the shipboard ADCP, which estimated absolute velocities for the upper few hundred metres. These data were used by E. McDonagh to provide reference-level velocities for an estimate of the geostrophic flow field during the 2002 Indian Ocean crossing [*McDonagh et al.*, in prep.].

4.4 Transformation of hydrographic data onto the model grid

In this section we describe how θ, S and *v* are transformed onto the model grid. First we describe the transformation process for *v*, as this determines the model bathymetry used later for θ and S on the model grid.

4.4.1 Transformation of v onto the model grid

There are four estimates of the transport across 32°S that require transformation onto the model grid: the first two are the baroclinic transport fields for 1987 and 2002, calculated on a regular 20 dbar grid (section 4.5.1); the second two are estimates of the absolute transport fields for 1987 and 2002 (supplied by A. Ganachaud and E. McDonagh) based on isopycnal layers (section 4.5.2). All data are derived from the 1987 and 2002 hydrographic sections and have relatively high horizontal resolution (~ 0.5°), but irregular station separation.

The data on the 20 dbar grid are interpolated onto the model vertical grid in the following way. For the upper 7 model levels (135m) a linear interpolation scheme is used, because the model vertical resolution is similar to that of the hydrographic grid. For the deeper model levels, a 'box average' procedure is used, which exactly conserves the section-integrated transports (see section 4.4.3). The absolute transport fields in isopycnal layers are transformed onto the model vertical grid using exclusively box-averaging.

In all cases the bathymetry at the southern boundary is determined by the estimated transport field: wherever any transport occurs in the location of a model grid cell, that grid cell is set to an ocean cell. Any grid cells with no transport attributed to them at the end of the transformation are set as land cells. In this way the model bathymetry is determined by the estimated flow field and we are best able to preserve the integrated transports of the hydrographic grid. Any transport that occurs below the model sea floor (5200m) is added to the deepest model grid cell (4700-5200m).

At this stage all transport estimates are on the model vertical grid and the hydrographic horizontal grid. The transformation onto the model horizontal grid is achieved through the same box-averaging approach used for the vertical grid. After this final step, the transports are converted to velocities by dividing the total transport attributed to each grid cell by the area of that cell. The re-constructed and absolute estimates of the southern boundary velocity fields are shown in figures 4.5 and 4.9, respectively.

4.4.2 Transformation of θ and S onto the model grid

The first step in the transformation of θ and S onto the model grid is to remove the land-points in the hydrographic data. This is achieved by linearly interpolating across topographic features, such as ocean ridges, and extrapolating the deepest values downwards (figure 4.1). This process prevents contamination of the data with missing values in the later stages of the transformation. The next step is to transform the data onto the model vertical grid. For the upper seven model vertical levels, the vertical resolution of the model grid is similar to the observations. For these vertical levels a simple linear interpolation scheme is used to determine the values on the model grid. For the deeper model levels a more sophisticated 'box averaging' algorithm is used, which is designed to preserve the section-integrated properties (see section 4.4.3). Once the hydrographic data have been transformed onto the model vertical grid they are transformed onto the model horizontal grid, again using the box-averaging method. The exceptions are the grid cells adjacent to the eastern and western boundaries. At these locations, water properties are determined by 'hand picked' hydrographic stations of sufficient depth to reach the model sea floor. This avoids contamination of the data near the boundaries (one can think of the boundaries as topography that cannot be interpolated across). In the final step the tracer field is masked with the appropriate model bathymetry. The transformation process is shown pictorially in figure 4.1.

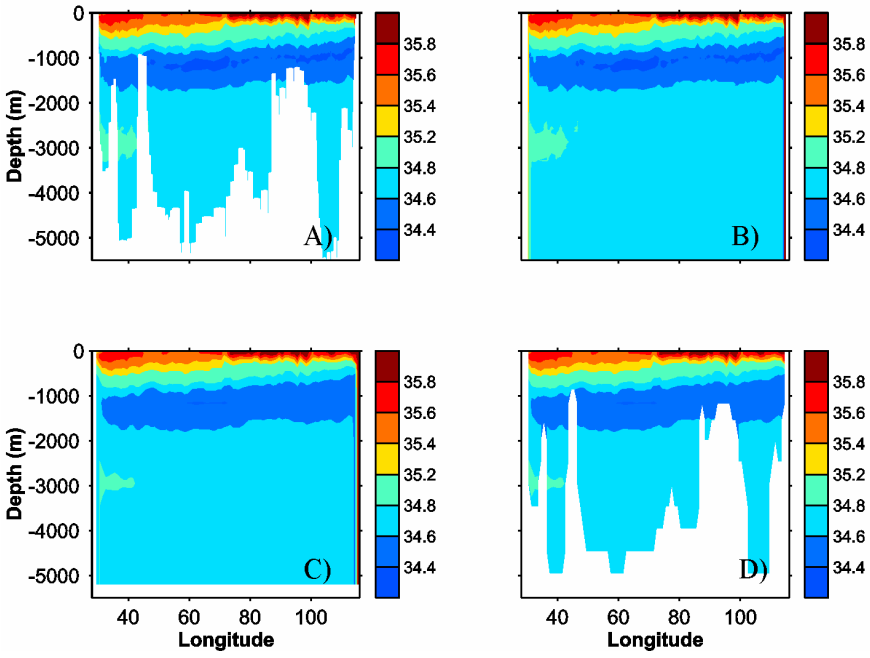

Figure 4.1: Contour plots of S for the 1987 section to illustrate the transformation of hydrographic θ and S onto the model grid. A) the original hydrographic section [106×303 matrix]; B) interpolated across bathymetry and filled downwards [106×303 matrix]; C) area-mean transformed data on model grid [100×22 matrix]; D) Masked data on model grid [100×22 matrix].

4.4.3 Box averages

Here we describe the 'box average' method that is used in the transformation of data from the hydrographic grids to the model grid.

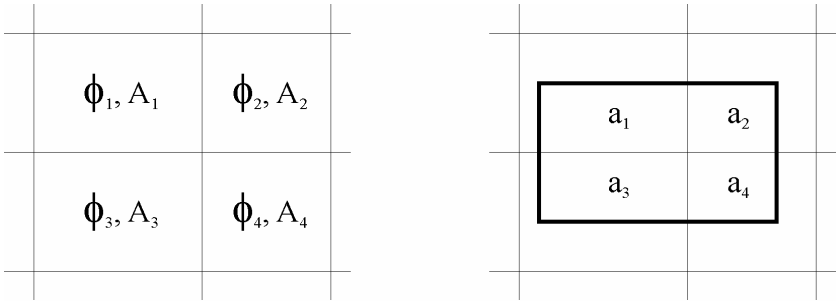

Figure 4.2: A schematic of the hydrographic grid (left) and again with a single model grid cell overlaid on top (right). ϕ_1-ϕ_4 represent water mass properties, A_1-A_4 are areas of the hydrographic grid cells and a_1-a_4 represent sub-areas within the model grid cell.

Referring to the schematic (fig. 4.2), ϕ is the water mass property we want to transform onto the model grid (θ or S) and A is the area on the hydrographic grid associated by each value of ϕ. When we overlay the model grid, a number hydrographic grid cells either completely or partly contained within the borders of each model grid cell. If a_n is the area of each of the sub-box contained within each model cell, the value of ϕ attributed to the model grid box is calculated as:

$$\phi_{\text{model}} = \frac{\sum_{n=1}^{4} \phi_n a_n}{\sum_{n=1}^{4} a_n} \qquad \text{(Eq. 4.1)}$$

The calculation is performed in a two-stage process, making first a 1-D 'line average' in the vertical, followed by the same routine oriented in the horizontal. The net effect is exactly that described in figure 4.2. The advantage with the box-average approach over less-sophisticated interpolation routines is that it conserves the section integrated quantities.

4.5 Velocities at the southern boundary

In this section we describe two ways in which we obtain a complete meridional velocity field for the model southern boundary. In the first instance, we carry out a dynamical reconstruction of the flow using a combination of hydrographic, global GCM and surface re-analysis data (4.4.1). The resulting southern boundary forcings are later compared with control experiments to test the sensitivity of the MOC to the southern boundary conditions (section 4.7). In the second instance, we take two existing estimates of the flow field near 32°S, one for 1987 and one for 2002, and transform them onto the model grid (section 4.4.2). We then use these flow fields to force the southern boundary and compare the resulting circulations (section 4.8). The results give an indication of how the Indian Ocean circulation may have changed between 1987 and 2002.

4.5.1 Re-construction of velocities at 32°S

Following Lee and Marotzke [1998], the local meridional velocity field *v*(x, y, z) is re-constructed using three dynamical components:

$$v(x,y,z) = \frac{1}{H}\int_{-H}^{0} v(x,y,z)dz + \left[v_e(x,y,z) - \frac{1}{H}\int_{-H}^{0} v_e(x,y,z)dz \right] + v_{sh}(x,y,z)\,, \qquad \text{(Eq. 4.1)}$$

where the total depth, *H*, is a function of x and y. The first term on the right-hand-side of equation 4.1 is the depth-averaged or *barotropic* meridional flow. The second term is the Ekman flow (v_e) minus its vertical average. This term represents the surface Ekman flow and the barotropic compensation beneath the surface. The final term represents the vertical shear in the meridional velocity field, or *baroclinic* flow. In our case, this shear comes entirely from the geostrophic thermal wind shear balanced by zonal density gradients (Eq. 3.1). The prescribed Ekman flow and barotropic flow prescribed at the southern boundary depend on the method of velocity reconstruction.

Using the hydrography, the thermal wind equation is integrated from the seafloor to determine the mean geostrophic flow between each station pair (section 3.3). The calculation is made such that the depth-integrated velocity equals zero. This baroclinic velocity field is converted to a transport field and then transformed onto the model grid using box-averaging (section 4.4.1). Any transport that occurs below the model sea floor

(5200m) is included in the deepest model level. The transports are then converted back to velocities by dividing the geostrophic transport attributed to each grid cell by the grid cell area. The barotropic flow field comes from monthly mean values of the ECCO (Estimating the Circulation and Climate of the Ocean) 1°×1° global ocean model [*Stammer et al.*, 2003]. The model was run with realistic forcings over the period 1993-2000. The ECCO barotropic velocity field is adjusted to take into account the different model bathymetry for 1987 and 2002, so that volume transport is conserved. The Ekman term (v_e, eq. 4.1) is computed under the assumption that the Ekman transport = $\tau^x/(f\rho)$ [*Gill*, 1982] (τ^x is the zonal wind stress, f the Coriolis parameter and ρ is water density) and that this transport occurs entirely in the uppermost model level. The zonal wind stress values (τ^x), are monthly means of the NCEP reanalysis data for 1995 [*Kalnay et al.*, 1996]. Therefore, in the velocity reconstruction the barotropic and Ekman flow have a seasonal cycle, but the baroclinic flow is time-constant.

4.5.2 Velocities from observation-based studies

Our current best estimates of the absolute oceanic flow field come from inverse box models [*Wunsch*, 1978]. The technique makes the assumption that the hydrostatic and geostrophic approximations hold and that the basin-integrated oceanic fluxes are in steady state. The models consist of one or more boxes bounded horizontally by hydrographic sections or land and separated into discrete vertical layers (usually according to potential density). It is expected that integrated water properties should be conserved over each layer. The 'inverse' part of the box model refers to the adjustment of the geostrophic flow field by the model machinery to satisfy basic requirements, such as mass, heat and salt conservation. This is achieved by changing the reference levels used to calculate the geostrophic flow field across each hydrographic section, from an original 'first guess' circulation, to arrive at a model state that best fits the constraints.

We use the Ganachaud [2003a] global inverse box model estimate of the flow across 32°S as our southern boundary condition for 1987 and a first-guess velocity field for 2002 supplied by E. McDonagh [*McDonagh et al.*, in prep.]. Each data set provides a time-mean estimate for all terms in eq. 4.1. The data made available were net transport for each model layer between each station pair and the depths of the layer interfaces for each station pair. The process of transforming the transports onto the model grid is described above (section 4.4). The Ganachaud and McDonagh estimates of the flow field on the model grid are show in figure 4.9. The transformation of the flow field from isopycnal coordinates to

vertical coordinates reduces the deep overturning in both cases. The 11 ± 3 Sv deep inflow reported in Ganachaud [2003a] is reduced to 9 Sv. The McDonagh deep inflow is reduced from 17 Sv to 16 Sv. At the time of this investigation no error estimate is available for the McDonagh flow field.

4.6 Adjustment timescale of the overturning circulation

When a model initially at rest is integrated forward in time, the model state evolves as it adjusts to the imposed boundary conditions. In this chapter we are interested in circulation changes on the order of decades, since our goal is to compare a plausible 1987 and 2002 circulation. We would like to find an optimal integration time for the model runs – optimal in the sense that enough time has passed for the initial model adjustment, but not long enough so that the distribution of diapycnal diffusivity dominates the solution (this is dealt with in chapter 5).

In order to study the adjustment time of the basin we set up model runs with time-constant boundary forcings. The time-constant forcings are necessary to resolve the model adjustment that occurs in the first year. Since we don't know what the appropriate distribution of K_d should be, we test the sensitivity of the model evolution to different K_d fields. Three plausible mixing regimes are used: (A) uniform K_d of 2×10^{-5} m^2s^{-1}; (B) uniform K_d of 1.2×10^{-4} m^2s^{-1}; (C) a 2-D observation-based estimate of K_d, which is a function of depth and latitude[*]. In all cases we use the same time-mean forcings and model set-up (experiment 87D, section 4.7.1).

Experiment	Diapycnal Mixing Regime
A	Uniform $K_d = 2\times10^{-5}$ m^2s^{-1}
B	Uniform $K_d = 1.2\times10^{-4}$ m^2s^{-1}
C	2-D estimate of K_d(lat,depth)

Table 4.1: The mixing regimes used in the model experiments

The uniform K_d field used in experiment A is from Ferron and Marotzke [2003] and approximately the value that is suggested by direct measurements of the upper water column [e.g. *Ledwell et al.*, 2000]. The uniform K_d field used in experiment B is the basin-

[*] The observational estimates of K_d are courtesy of A. Naveira-Garabato. See chapter 5 for details.

mean value estimated from recent observations in the Indian Ocean and is close the canonical value put forward by Munk [1966] and Munk and Wunsch [1998]. The distribution of K_d used in experiment C comes from two zonal hydrographic sections occupied in 1995: I01 at 10ºN (I01W stations 901-933, 935, 939-956 and I01E stations 971-1004, 1008-1013 [*Shi et al.*, 2002]); I02 at 10ºS (stations 1077-1105, 113-114, 1127-1156, 1167-1227 [*Johnson et al.*, 1998; *Warren and Johnson*, 2002]); and a crossing of the Indian Ocean at 32ºS in 2002 [*Bryden*, 2003b], CD139 (figure 5.1). We construct depth-profiles of K_d using the zonal mean value for each section and then linearly interpolate between latitudes to produce a K_d field that is a function of model level and latitude (figure 5.3).

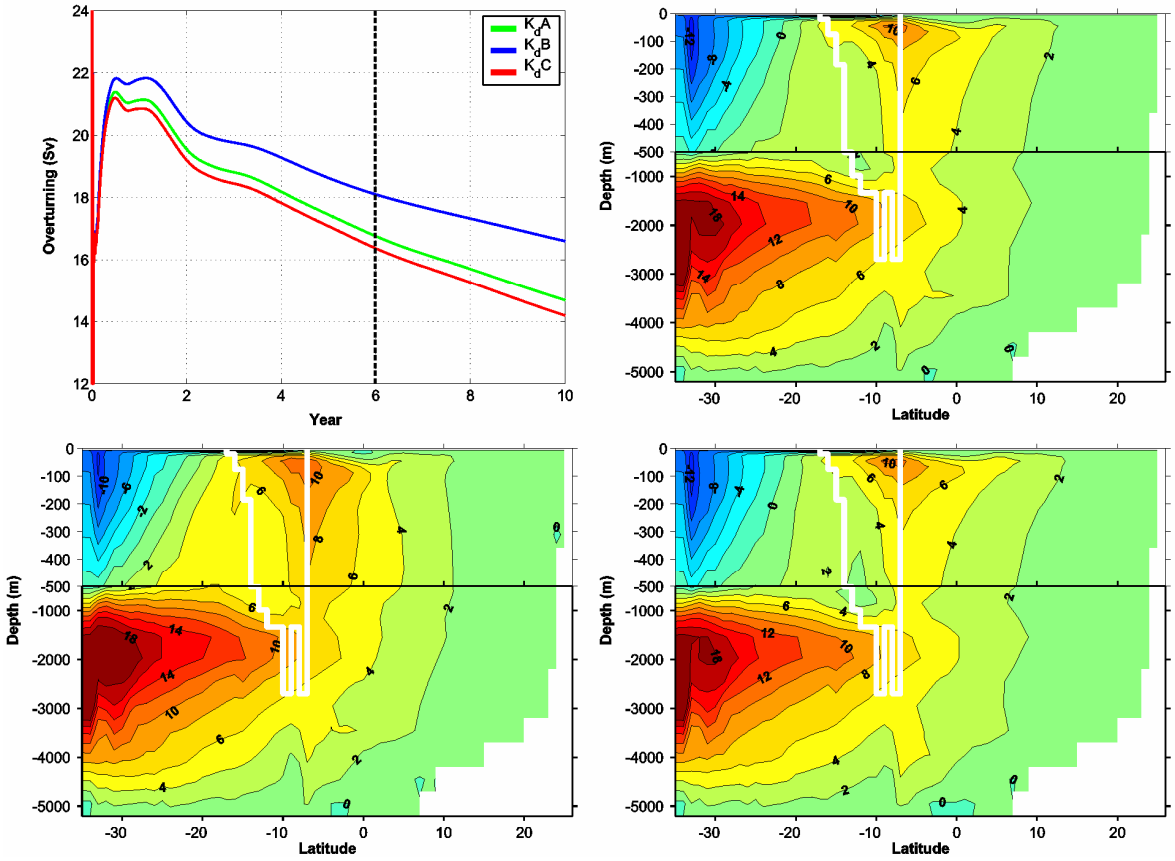

Figure 4.3: The upper left panel shows the evolution of the overturning streamfunction† at 28°S for 3 different mixing regimes. The streamfunctions shown are for year 6 of experiment A (upper right), experiment B (lower left) and experiment C (lower right). Flow is anticlockwise (clockwise) around positive (negative) features. Units are Sv (1 Sv = 10^6 m^3s^{-1}). The white line shows the location of the Indonesian Throughflow.

† We adopt the convention of Ferron and Marotzke [2003] and compute the streamfunction in the region of the Indonesian Throughflow as if the model were a closed basin. Thus the depth-integrated value south of the Throughflow is equal to the Throughflow strength.

A time series of the deep overturning at 28°S (figure 4.3) shows three characteristic periods of adjustment. Over the first few days of model integration we observe large oscillations in the overturning streamfunction. These oscillations must be related to the barotropic adjustment in the model and response in the sea surface height because of the short timescale associated with these changes. Next we see some longer period oscillations with an associated time scale of a few months. The oscillations do not appear to persist beyond about year 4 of the model integration and are associated with the baroclinic adjustment to the boundary forcings. Using observations, Chelton and Schlax [1996] found that the basin-crossing time for a first baroclinic Rossby Wave in the subtropical Indian Ocean is a few years. The final adjustment time scale is shown by the divergence of the model solutions and must be associated with the distribution of K_d. This divergence is apparent after a few months of model integration and increases as each model run proceeds toward an equilibrium state (see chapter 5).

The evolution of the streamfunction under our chosen K_d regimes is qualitatively similar and differences do not exceed 2 Sv over the first 6 years. Examination of the streamfunction for year 6 reveals that the zonally integrated circulation is similar in all 3 cases (figure 4.3). In this part of our investigation we do not want consider the longer evolution of the model solutions, since we don't know what the appropriate mixing should be. Therefore we will use the model circulation from year 6 as our reference state. This is long enough for the initial model adjustment to take place, but not long enough for diapycnal mixing to dominate the solution. The evolution of the model to quasi-equilibrium states will be addressed in chapter 5.

4.7 Sensitivity of the MOC to southern boundary conditions

In this section we investigate the sensitivity of the model overturning circulation to the southern boundary conditions. There are two model configurations on account of the different bathymetry of the 1987 and 2002 hydrographic sections. For each model configuration we carry out four experiments (table 4.2). Each experiment has a different combination of prescribed velocity (v) and density field (θ and S) at the southern boundary.

4.7.1 Experimental configurations

Experiment A, is the control run. Velocities at the southern boundary are from the ECCO 1°×1° global ocean model and θ and S are prescribed the WOA94 monthly climatological values. These model forcings are similar to those used in the control run of Ferron and Marotzke [2003]. In experiment B, the values for θ and S are replaced by the hydrographic data (fig. 4.4). For experiment C, we retain the climatological values for θ and S, but replace the ECCO *v*-field with a reconstruction that incorporates geostrophy applied to the hydrographic section (figure 4.5). Finally in experiment D, we use the hydrography for θ and S and the velocity reconstruction for *v*. In all cases a uniform offset velocity is applied at the southern boundary to ensure an annual mean Indonesian Throughflow of 10 Sv into the model domain.

The major qualitative difference between the θ and S fields derived from the 1987 and 2002 hydrographic sections and the WOA94 is the smoothing applied to the latter data set (figure 4.4). One of the criticisms of the WOA94 is that the objective interpolation used to create the data base removes much of the fine-scale structure. It has been suggested that the smoothing of gradients associated with deep western boundary currents could explain why some of the previous modelling efforts have been unsuccessful in producing a substantial deep overturning in the Indian Ocean [*Lee and Marotzke*, 1997]

Experiment	**Southern boundary condition**	
	Temperature and salinity	**Meridional velocity**
87A	World Ocean Atlas 1994	ECCO global GCM
87B	1987 Hydrography	ECCO global GCM
87C	World Ocean Atlas 1994	Reconstruction
87D	1987 Hydrography	Reconstruction
02A	World Ocean Atlas 1994	ECCO global GCM
02B	2002 Hydrography	ECCO global GCM
02C	World Ocean Atlas	Reconstruction
02D	2002 Hydrography	Reconstruction

Table 4.2: The southern boundary configurations used to investigate the model sensitivity to conditions at the southern boundary. Details of the velocity reconstructions are given in section 4.5.1.

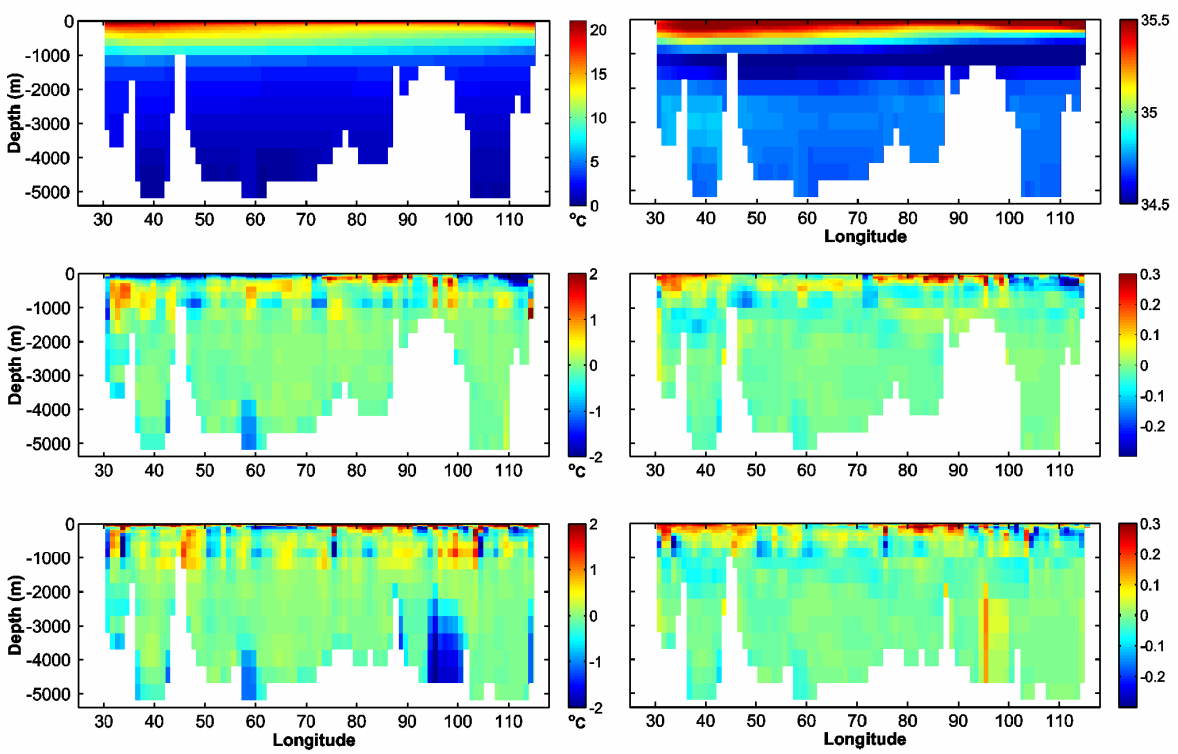

Figure 4.4: The mean θ (upper left) and S (upper right) fields at 32°S from the World Ocean Atlas 1994 (WOA); 1987 section minus WOA (middle panels); and 2002 section minus WOA (lower panels). All data have been transformed onto the model grid.

The anomaly fields of the 1987 and 2002 sections from WOA94 reveal the mesoscale signal inherent in the hydrographic data (figure 4.4). As one would expect, the greatest differences occur in the near surface, where there are strong vertical gradients of θ and S. There are also some substantial differences at depth, mostly occurring near topographic features. These differences are largely due to short-comings of the process used to combine the WOA94 data with the modified bathymetry at the southern boundary. For example, the removal of Broken Plateau in the 2002 hydrographic section leads to an apparent cooling and loss of freshwater relative to WOA94. As our principal aim is to test the model sensitivity to changes in θ and S at the southern boundary, such differences in deep water properties are not considered problematic.

What is not obvious from the θ and S anomaly fields is the different character of the mesoscale noise of the 1987 and 2002 sections. The reconstructed velocity fields show that the most intense noise in the 1987 flow field appears to be limited to the upper 1500m (figure 4.5). In 2002 the amplitude of the noise is greater and also seems to penetrate much deeper in the water column. In particular, there are a few areas of deep intense southward flow for the 2002 section (33°E, 50°E, 75°E, 81°E and 103°E). West of Broken Plateau (88°E) the bathymetry is similar for the hydrographic sections (and therefore, so is the

depth-mean flow), so the difference between the flow fields must be primarily due to differences in their vertical structure. The reconstructed velocity fields are strikingly different from the ECCO velocity, which shows broad, relatively weak velocities rather than the intense 'stripy' flow fields of the observations.

The cumulative transports of the reconstructed flow fields (figure 4.6), show a weaker Agulhas Current transport in 2002 than 1987. This is due to the weaker horizontal gradients in θ and S in 2002, which lead to a less intense southward flow under a similar barotropic flow regime. The 1987 reconstruction is in qualitative agreement with the accepted view of the Indian Ocean MOC: there is a net northward transport below 2200m and southward transport in the upper 1335m. The deep inflow is 16 Sv, which is consistent with the estimate of MacDonald [1998] and within 1 Sv of the range estimated by Robbins and Toole [1997] and Ganachaud [2003a]. The 2002 section however, shows a net southward flow below 2200m and net northward flow above this depth. This is a complete reversal of the accepted picture of the Indian Ocean MOC. This net flow regime arises because of the combination of the smoothly varying barotropic flow field from the ECCO model and some exceptionally strong horizontal gradients observed near 105°E in the 2002 hydrographic section.

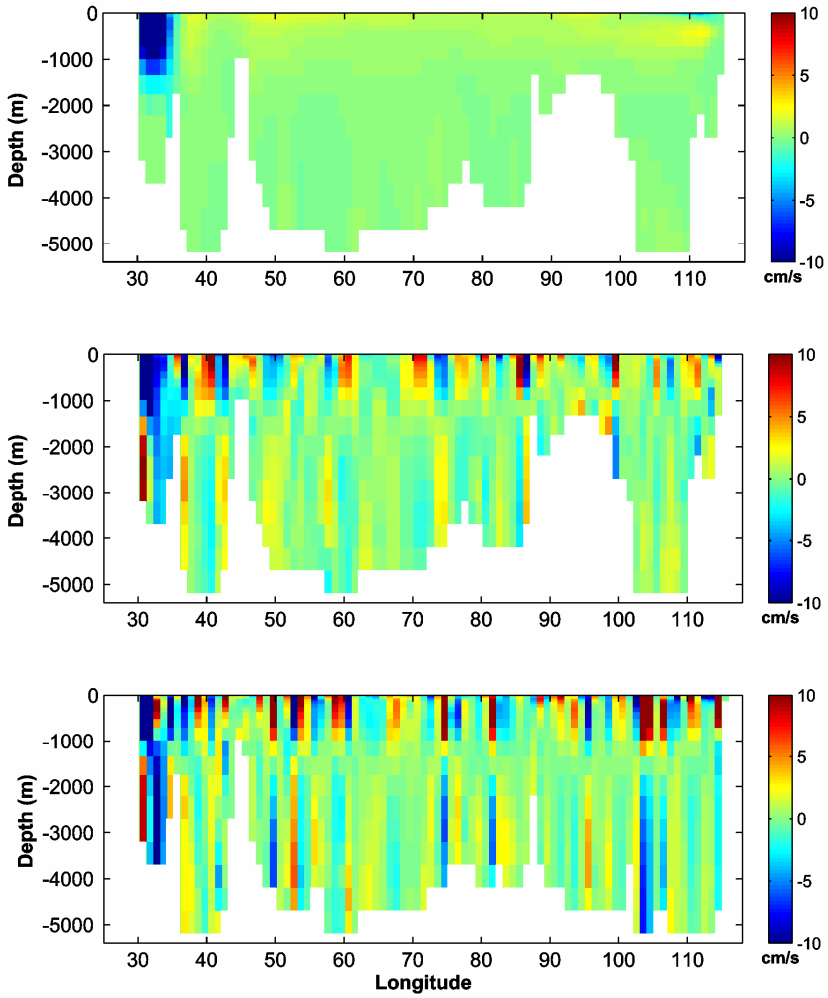

Figure 4.5: The time-mean velocity field at the southern boundary from the ECCO model (upper panel); reconstructed velocity field using the 1987 hydrography (middle panel); and reconstructed velocity field using the 2002 hydrography (lower panel). Positive values indicate northward flow.

Palmer et al. [2004] note a remarkable 'step-like' feature in the isopycnals of the 2002 hydrography at about 105°E. Under the approximation of geostrophy, the large zonal density gradient requires a large vertical shear of meridional velocity (Eq. 3.1). The mean meridional velocity profile computed from the thermal wind equation is such that the flow becomes increasingly southward at depth. In order to maintain a northward deep transport (or even a zero net deep inflow) requires a large northward barotropic flow. The barotropic flow from the ECCO model is only ever weakly northward or southward away from the boundaries, so the result in the velocity reconstruction has to be southward transport at depth (see figures 4.5 and 4.6, 2002 reconstruction near 105°E). This unrealistic flow regime highlights the difficultly in combining model data with hydrographic observations.

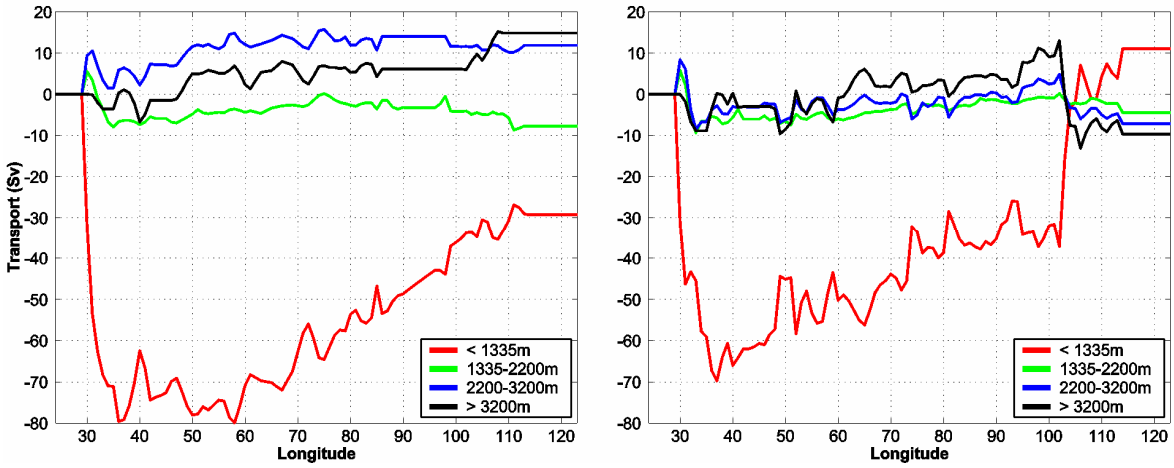

Figure 4.6: The cumulative transports for the reconstructed velocity fields for 1987 (left) and 2002 (right).

4.7.2 1987 configuration results

The influence of θ and S on the MOC is established by comparing experiment 87A with 87B and 87C with 87D. Experiments 87A and 87B show very similar overturning streamfunctions (figure 4.7), with a weak deep overturning that is consistent with many previous GCM results [e.g. *Garternicht and Schott*, 1997; *Lee and Marotzke* 1997;1998; *Zhang and Marotzke*, 1998]. The similarity demonstrates that the inclusion of θ and S from the 1987 hydrography has little influence on the overturning circulation. This result is supported by the similarity between the overturning streamfunctions for experiment 87C and 87D, which use the reconstructed *v*-field at the southern boundary and use θ and S from WOA94 and the 1987 hydrography, respectively.

The impact of the reconstructed *v*-field on the circulation is seen in the comparison of experiments 87A with 87C and 87B with 87D. Regardless of the θ and S fields used the different *v*-fields have a dramatic effect on the overturning circulation. The very weak deep overturning of 87A and 87B is replaced with a vigorous cell, which exceeds 16 Sv and penetrates the basin to the equator for both 87C and 87D. The overturning cell depth is about 2000m and most of the southward flow occurs below 500m depth. This overturning circulation regime is consistent with the estimate of MacDonald [1998] and within ± 2 Sv of the estimates of Robbins and Toole [1997], Ganachaud [2003a] and Talley [2003].

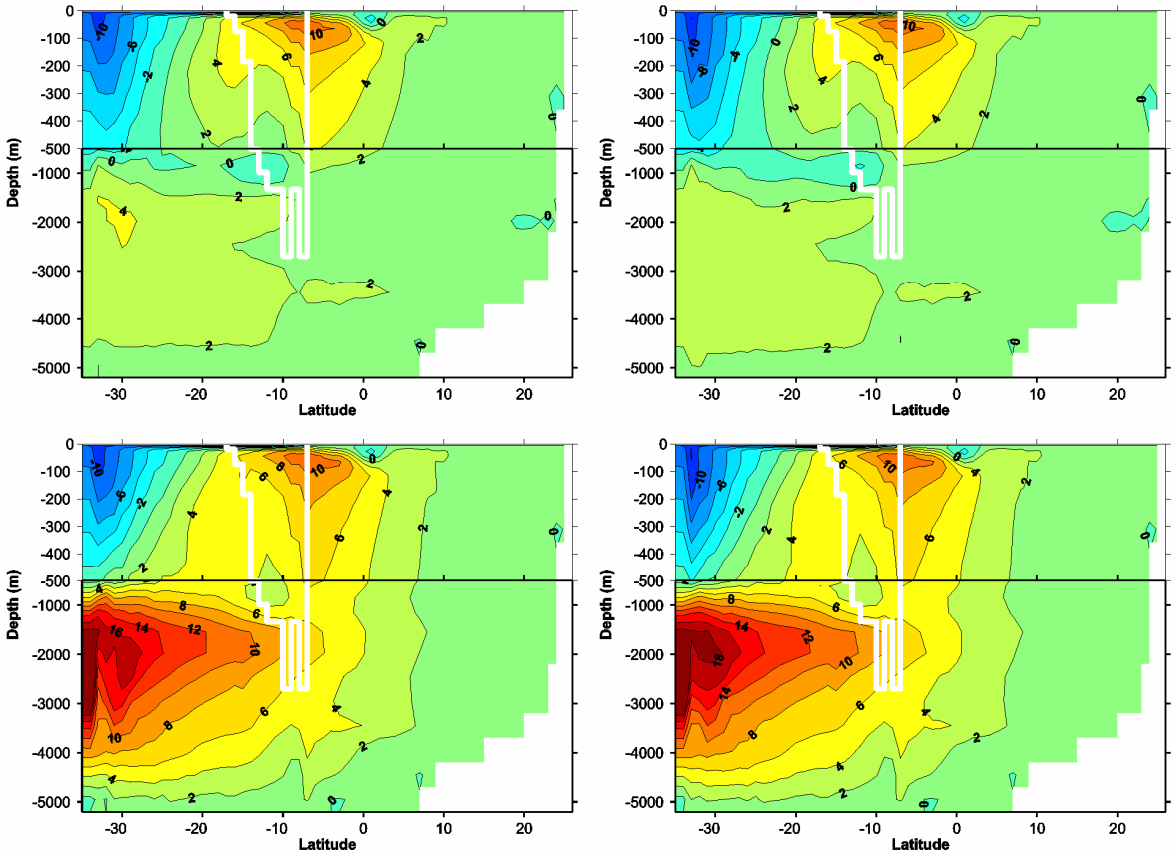

Figure 4.7: The mean meridional overturning streamfunction for year 6 of experiments 87A (upper left); 87B (upper right); 87C (lower left); and 87D (lower right). Units of transport are 10^6 m^2s^{-1}. Transport is anticlockwise (clockwise) around positive (negative) features. The location of the Indonesian Throughflow is shown by the white line.

4.7.3 2002 configuration results

To investigate the influence of θ and S on the 2002 configuration we compare experiment 02A with 02B, and 02C with 02D. The results are similar to the 1987 configuration – the model deep MOC shows little sensitivity to the imposed changes θ and S. The only difference between experiment 87A and 02A is the bathymetry at 35°S to 32°S. The main change in bathymetry is the removal of Broken Plateau and some of the Australian continental shelf, which produces an ocean about 2000m deeper between 88-100°E and 110-115°E for the 2002 configuration. The effect is to slightly weaken the deep overturning throughout the basin and to give rise to a weak three-cell structure near the southern boundary (figures 4.7 and 4.8). It is unclear whether it is the bathymetric changes or changes in the θ and S fields which are primarily responsible for the different overturning, but the anomalously high θ and low S found at the locations of the removed bathymetry in the '02 configuration are likely to play a role (figure 4.4). This hypothesis is supported by the results of experiment 02B (figure 4.8). In this case there much less

interpolation of θ and S is required and the resulting MOC looks very similar to experiment 87B.

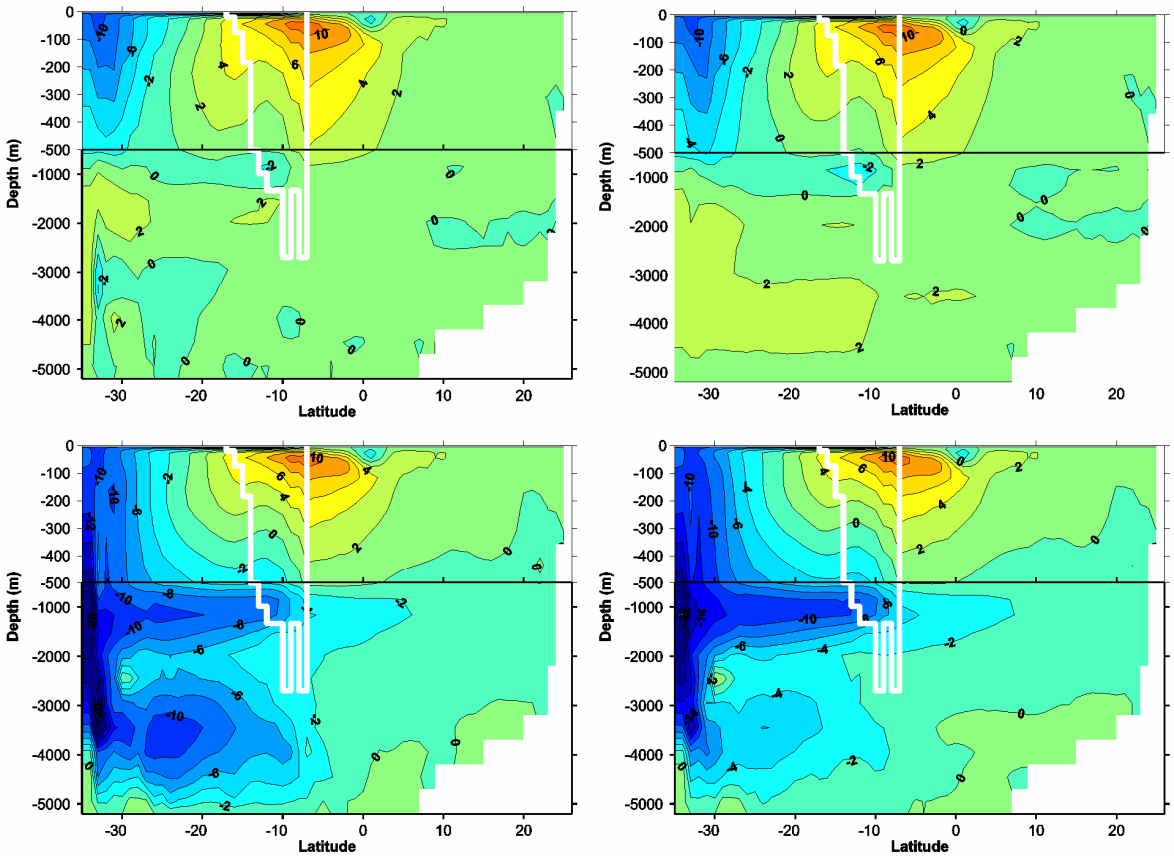

Figure 4.8: The mean meridional overturning streamfunction for year 6 of experiments 02A (upper left); 02B (upper right); 02C (lower left); and 02D (lower right). Units of transport are 10^6 m^2s^{-1}. Transport is anticlockwise (clockwise) around positive (negative) features. The location of the Indonesian Throughflow is shown by the white line

Experiments 02C and 02D demonstrate a dramatic change in the circulation when one implements the reconstructed *v*-field. The main difference between the MOC of 02C and 02D is a stronger negative deep overturning cell centred at 3500m and 24°S in the former experiment (figure 4.8). Experiments 02C and 02D show surface waters between 20°S and 30°S being drawn down into the deep circulation and exiting the Indian Ocean at the southern boundary at depth. This circulation regime is strikingly different to the accepted picture of deep and bottom inflow across 32°S upwelling and returning south higher up the water column. As discussed in section 4.7.1, net outflow at depth is the result of an ill-suited combination of hydrographic and model data. The circulations of 02C and 02D are not consistent with any of the previous work on the Indian Ocean MOC.

The work presented in the previous section has highlighted the model sensitivity to the *v*-field prescribed at the southern boundary and the short adjustment time of the model. These results imply that the model is capable of detecting decadal changes in the deep circulation using velocity information near 32°S. In the following section we use two current 'best' estimates of the flow field for 1987 and 2002 to force the model southern boundary. This is done in an attempt to detect decadal changes in the deep circulation.

4.8 Comparison of a '1987' and '2002' circulation

In this section we use current 'best' estimates of the 1987 and 2002 flow field near 32°S to force southern boundary. The simulated '1987' and '2002' circulations are compared, with emphasis on changes in the deep currents.

4.8.1 Experiment configuration

In each case the model θ and S fields come from the 1987 [*Toole and Warren*, 1993] and 2002 [*Bryden et al.* 2003b] hydrography. The flow field for the 1987 configuration comes from the global inverse box model of Ganachaud [2003a]. The 2002 flow field is a combination of thermal wind applied to the hydrography and the barotropic flow estimated from ADCP data, provided by McDonagh et al. [in prep.]. The transformation of the two flow fields onto the model grid is described in section 4.4.1.

Besides the different hydrography used (and corresponding model bathymetry) the two model configurations also have different IT strengths: 16 Sv for the 1987 estimate and 22 Sv for the 2002 estimate. Both values are toward the upper end of estimates for the size of the IT [*Godfrey*, 1996; *Sprintall et al.*, 2002]. The model initial conditions are the same as used in the previous model work, with some small differences owing to the modified bathymetry between 35°S and 32°S. The model surface and eastern boundary θ and S forcings are identical to the previous experiments in this chapter. The *u*-velocity field at the eastern boundary is modified from previous experiments to ensure an IT strength of -16Sv and -22 Sv for the '1987' and '2002' configurations, respectively. This is achieved by applying an additional time-constant and uniform westward velocity at the boundary.

Experiment	Southern boundary conditions:		Indonesian Throughflow
	θ and S	*v*-velocity	
'1987'	1987 hydrography	Ganachaud [2003a]	-16 Sv
'2002'	2002 hydrography	McDonagh [in prep.]	-22 Sv

Table 4.3: The southern boundary configurations for the Ganachaud ('1987') and McDonagh ('2002') model simulations. The negative values for the Indonesian Throughflow indicate westward transport.

The 1987 and 2002 estimated flow fields show very different characters (figure 4.9). For 1987, the largest variations in velocity appear to be confined to the upper 1500m, whereas large velocities can be found throughout the water column in the 2002 flow field. The fact that large velocities are present throughout the water column for 2002 indicates a stronger barotropic component to the transports. This is confirmed by the cumulative transports of the southern boundary velocity fields (figure 4.10).

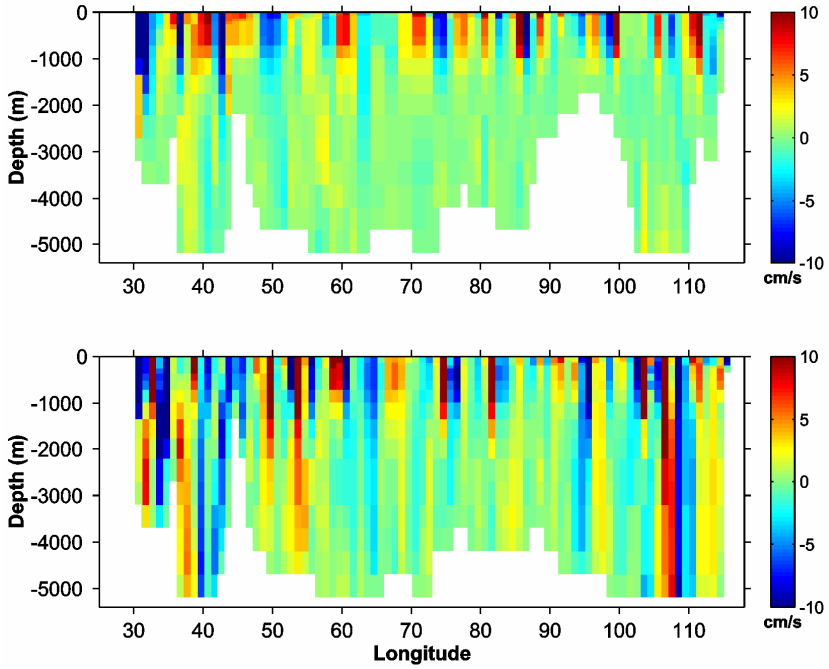

Figure 4.9: The southern boundary meridional velocity field for the '1987' (upper panel) and '2002' model configuration (lower panel). Positive values indicate northward velocity.

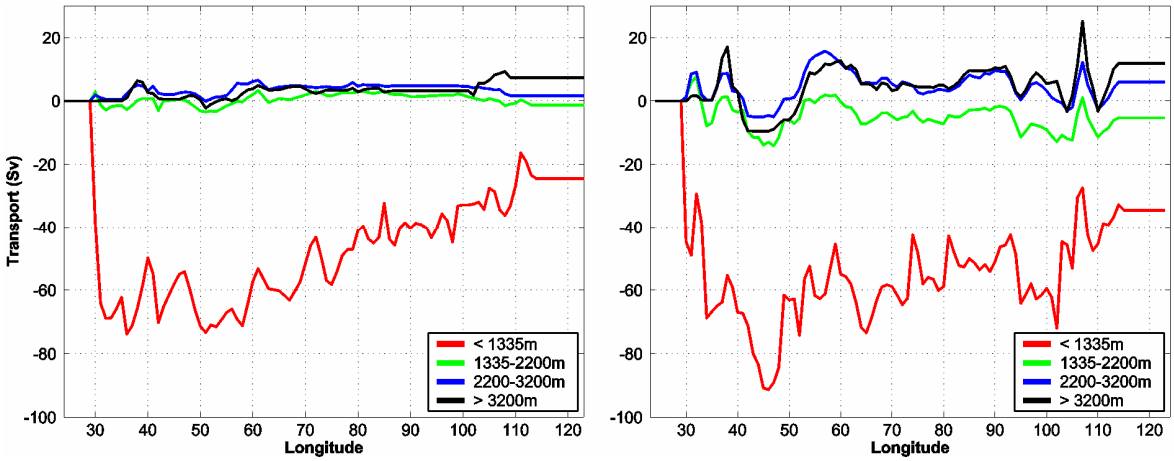

Figure 4.10: The cumulative transports for the '1987' (left) and '2002' (right) boundary conditions.

The 1987 cumulative transports show fairly uniform and weak barotropic transport (figure 4.10). These transports are qualitatively similar to previous estimates of the flow field of the 1987 section [e.g. *Toole and Warren*, 1993; *Robbins and Toole*, 1997; *Bryden and Beal*, 2001]. In contrast, the 2002 cumulative transports show excursions of transport of >10 Sv, which appear to be largely barotropic. The areas of net deep northward flow for the 1987 *v*-field occur between 50°E to 70°E (Madagascar Basin) and 100°E to 110°E (Perth Basin). The 2002 flow field shows a net northward deep inflow east of about 40°E. The locations of greatest net northward flow are 45° to 60°E (Madagascar Basin) and 110°E to 115°E (Perth Basin). The 1987 and 2002 section-integrated transports are qualitatively similar, even if their zonal structure is not. Both estimates of the flow field near 32°S fit our basic expectation of the time-mean circulation, i.e. net northward flow below 2000m and southward flow above.

The dramatic differences in the character of the two estimates of flow field can be rationalised when one thinks about their origins. The 1987 estimate [*Ganachaud*, 2003a] uses a 'first-guess' velocity field, which is based on the traditional approach of using a barotropic flow informed from water mass properties. It is unlikely that hydrographers would favour large barotropic velocities away from the boundary currents, because that is not what is traditionally expected of a 'steady-state' ocean. The choice of barotropic flow is subsequently modified in order that isopycnal layers maintain approximate mass, heat and salt balance (among other things). This is very much a 'steady-state' approach. The 2002 estimate [*McDonagh et al.*, in prep.] is informed using a 'snapshot' of the barotropic flow field from ADCP data. No constraints, such as mass balance have been applied to this 'first guess' velocity field. Putting aside the difficulties in ADCP estimates themselves, one may have concerns about the aliasing of the data due to changes in the barotropic flow that

might have occurred during the 6 weeks it took to complete the hydrographic section. One might also question how representative such an estimate of the flow field is – was the Indian Ocean sampled in a transient state? Some comfort is afforded in the face of such questions by the values of the section-integrated transports, which are qualitatively consistent with the 1987 estimates. In any case, it is remarkable that we see such the large barotropic wave-like signals in the 2002 data. It is natural to speculate whether we would observe a similar picture were there ADCP measurements available for the 1987 section.

4.8.2 '1987' and '2002' overturning circulations

The '1987' solution invokes only a weak circulation in the ocean interior, despite the 9 Sv deep northward flow prescribed at the southern boundary. The overturning cell penetrates the model interior to about 10°S has a 4 Sv magnitude at 2000m depth and a very narrow vertical extent. The maximum overturning away from the southern boundary is 6 Sv, but this only reaches as far north as 30°S. Below 2500m depth, there is only a very small MOC. It is not clear why the interior model dynamics are only weakly consistent with the southern boundary flow field. The complex Indian Ocean bathymetry may be a factor as there is potential for topographic blocking of the prescribed flow just a few grid cells into the model domain.

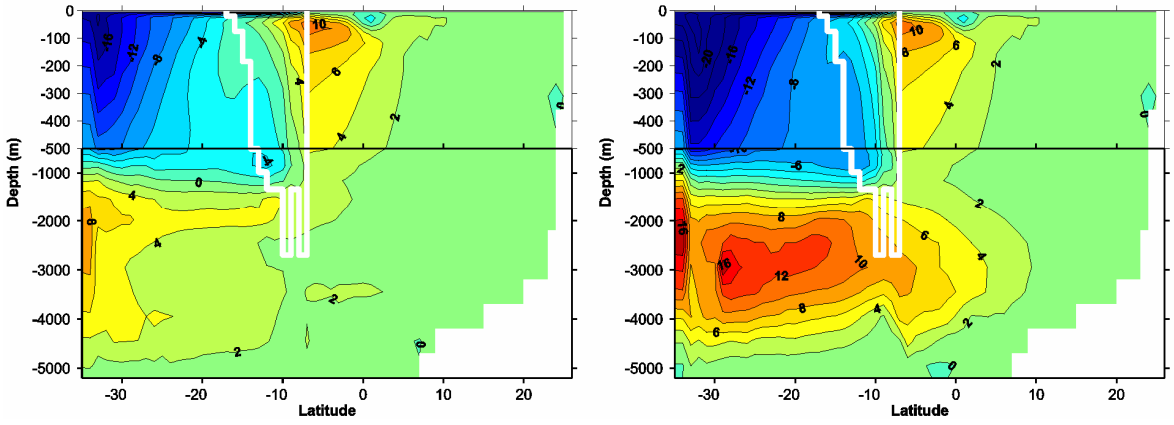

Figure 4.11: The annual mean overturning streamfunction for year 6 of the '1987' (left) and '2002' (right) model configuration. Flow is anticlockwise (clockwise) around positive (negative) features. Units are Sv (1 Sv = 10^6 m^3s^{-1}). The white line shows the location of the Indonesian Throughflow.

The '2002' MOC exhibits a vigorous and far-reaching cell, with a peak value of 16 Sv. The 4 Sv streamline shows that the vertical extent of the MOC spans 4500-1500m and penetrates the basin beyond the equator. The closed streamlines adjacent to the southern boundary show some inconsistency between the model interior dynamics and prescribed

velocities. Despite this apparent inconsistency, the resulting MOC is of the same magnitude as that prescribed at the southern boundary.

Given the large differences in the simulated 1987 and 2002 deep MOC, we now look more closely at the deep circulation in each of the model runs to determine their zonal structure.

4.8.3 Changes in the deep circulation

To investigate how the deep circulation in the 1987 and 2002 model circulation has changed we compute the mean velocity in the deepest 3 model levels (i.e. deeper than 3700m). The most interesting aspect of the deep circulation maps (figures 4.12 and 4.13) is the completely different flow regime we see below 3700m [*Ganachaud*, 2003a] invoked by the 1987 and 2002 boundary conditions. For the 1987 configuration the deep northward flow occurs primarily through the Perth Basin and on into the West Australian Basin. There is also a smaller northward flow which occurs in the Madagascar basin. A small southward flow adjacent to the western wall of the Central Indian Basin acts to reduce the deep overturning. There appears to be a weak boundary current in the southwest Somali Basin and relatively large northward velocities in the south Arabian Basin.

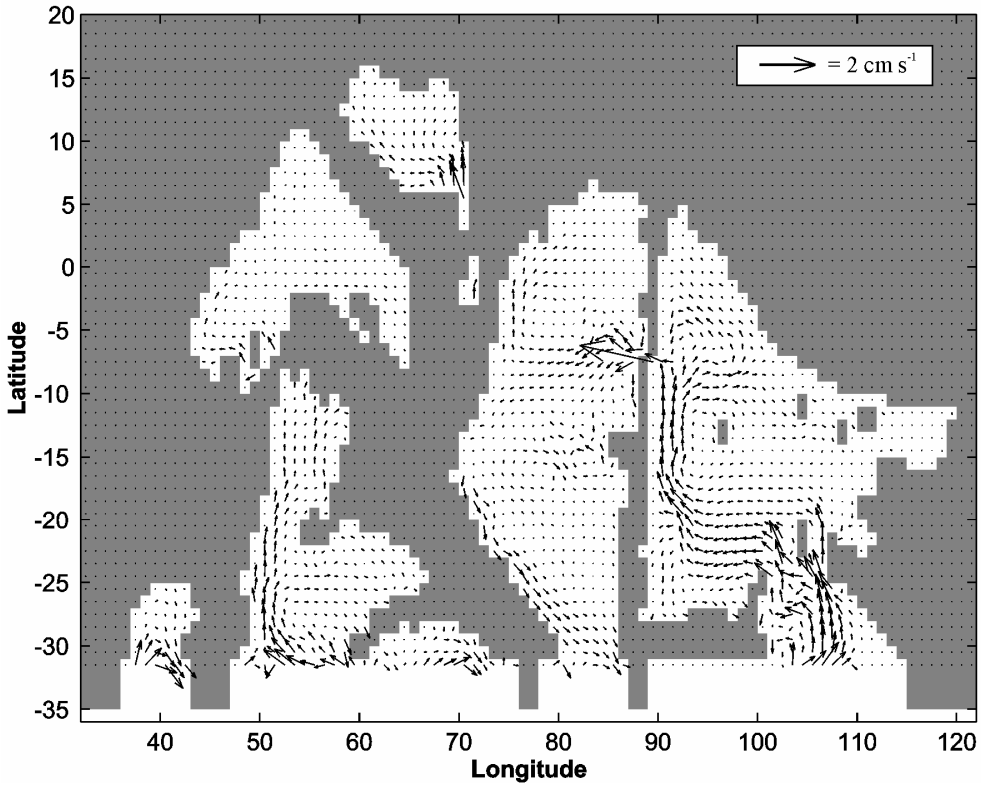

Figure 4.12: The mean circulation north of 32°S below 3700m for the '1987' southern boundary conditions. Velocities are computed as the mean of the deepest 3 model levels.

The distribution of deep northward flow for the 2002 configuration has the dominant contribution in the Madagascar Basin. The next largest deep inflow occurs in the Central Indian Basin, showing a complete reversal of the flow direction from the 1987 circulation. There is also a contribution to the northward flow in the Perth and West Australian Basins, but it is weaker than the 1987 experiment. The Somali Basin exhibits some very large velocities in the south-west and the Arabian Basin shows a circulation similar to the 1987 configuration. Both the 1987 and 2002 experiments show substantial westward flow across at gap in the Ninetyeast Ridge, which is documented in the observations [*Warren and Johnson*, 2002].

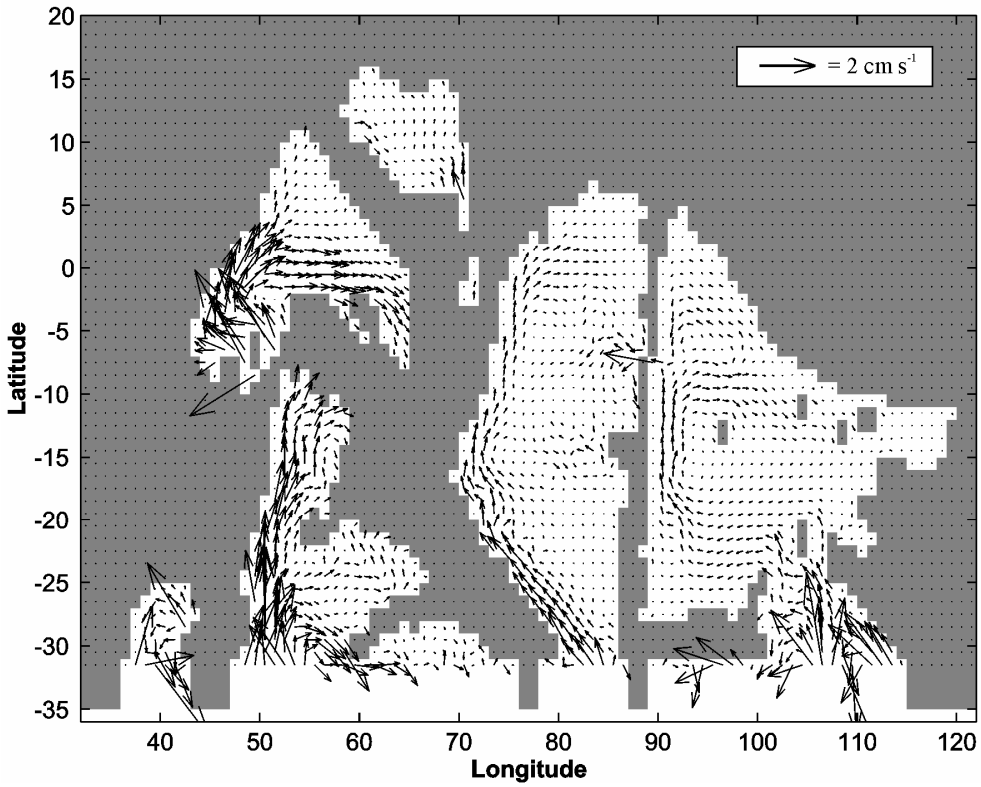

Figure 4.13: The mean circulation north of 32°S below 3700m for the '2000' southern boundary conditions. Velocities are computed as the mean of the deepest 3 model levels.

4.9 Discussion

The initial adjustment of the Indian Ocean occurs in the first 5-6 years of model integration. This is roughly consistent with what one would expect based on the translation speed of a first-baroclinic Rossby Wave in the mid-latitude Indian Ocean [*Chelton and Schlax,* 1996]. Over this time scale we do observe the MOC to be greatly influenced by prescribed diapycnal diffusivities. If the short model adjustment time is applicable to the real ocean there is the potential for substantial differences in the deep circulation on decadal time scales.

We have described a new method for estimating the absolute velocity field across 32°S by combining hydrographic data with the barotropic flow from a global ocean model. For the 1987 section the estimate provides a flow field that is consistent with the estimate of MacDonald [1998] and much closer to hydrography-based estimates than many previous model-based studies. However, there are problems when the same technique is applied using the 2002 section. A 'step-like' feature in the isopycnals near 105°E creates a large vertical shear of meridional velocity and leads to net southward transport of the deep waters. This estimate is not considered realistic, but can be supported by the model dynamics, at least on decadal time scales. The peculiar flow field highlights the difficulty in trying to combine high-resolution hydrographic data with data from a 1°×1° global ocean model. As models increase in resolution and sophistication, the method outlined here may prove useful.

We have tested the sensitivity of the model deep MOC to the meridional velocity field (v) and density field (θ and S) applied at the southern boundary. We find that v has a greater impact on the model solution than the prescribed values of θ and S. This result is in contrast to previous work of Ferron and Marotzke [2003]. However, the changes imposed in θ and S mainly introduce noise, rather than changing their fundamental distribution. The changes to v also introduce noise, but the net flow is drastically modified from the original boundary conditions.

The estimates used for the simulation of the 1987 and 2002 Indian Ocean circulation come from Ganachaud [2003a] and McDonagh et al. [in prep.], respectively. These two estimates of the flow across 32°S have very different characters. For the 1987 estimate, the largest transport variability is confined to the upper 1500m and there is generally a weak barotropic signal away from the boundaries. The 2002 estimate shows a

large barotropic signal, with wave-like structures that persist over 100s of km. Despite this difference, the zonally integrated transports for 1987 and 2002 are qualitatively consistent.

When applied as the southern boundary condition the 2002 estimate produces a much larger overturning in the model ocean interior than the 1987 estimate. The overturning estimate is 6 Sv for 1987 and 16 Sv for 2002. The 1987 overturning is largest near the southern boundary and confined above 2500m north of about 28°S. The 2002 overturning shows the peak value at about 30°S and occupies a large depth range for the entire region south of the equator. As well as these changes in the zonally-integrated circulation, we also observe changes in the zonal structure of the deep circulation. The main area of deep northward flow for 1987 is in the Perth and West Australian Basins, with additional northward flow in the Madagascar Basin and southward flow in the Central Indian Basin. For 2002 the main area of deep northward flow has switched to the Madagascar Basin, with a relatively weak northward flow in the Perth Basin. For 2002, northward flow in the Central Indian Basin also contributes to the larger overturning circulation.

One is naturally cautious about extrapolating the model results here to the real world, particularly in light of the much greater barotropic signal in the 2002 estimate of the flow field near 32°S. From equation 4.1 we know that interaction between the barotropic flow and topography can contribute to an overturning circulation. However, it should be remembered that the southern boundary flow field is ‘dynamically smoothed’ over the first 3 model grid cells, over which the topography is held constant. We therefore conclude that the Indian Ocean may be capable of supporting different deep flow regimes on decadal time scales. This model work suggests that the deep MOC of the Indian Ocean may have changed between 1987 and 2002.

4.10 Conclusions

- The initial adjustment of the Indian Ocean model to the imposed southern boundary conditions occurs in the first 5-6 years of model integration. This implies that substantial changes in the deep circulation could occur on decadal timescales.
- The prescribed velocity at the southern boundary is more important than the prescribed density in determining the interior circulation, at least on the sub-decadal time scales investigated here.
- The estimated flow fields at 32°S for 1987 and 2002 from Ganachaud [2003a] and McDonagh [in prep.] produce very different deep MOC regimes. The peak value is 6 Sv for 1987 and 16 Sv for 2002. We observe a change in the zonal structure of the deep circulation, with the main deep inflow for 1987 occurring in the Perth Basin and in the Madagascar Basin for 2002.
- The Indian Ocean model is capable of supporting different deep flow regimes on decadal time scales and our model suggests that the deep MOC changed between 1987 and 2002.

Chapter 5: Diapycnal mixing and the meridional overturning circulation*

* The diagnosed and observation-based diapycnal estimates presented in this chapter are the work of A. Naveira-Garabato.

5.1 Introduction

In this chapter we re-visit the work of Ferron and Marotzke [2003] (hereinafter referred to as FM) on the meridional overturning circulation (MOC) of the Indian Ocean. FM used hydrographic sections and a sea surface climatology combined with a general circulation model (GCM) through a 4D-variational method to diagnose the Indian Ocean MOC (see chapter 2 for details). Their study was the first using a regional GCM to exhibit a strong deep overturning in the Indian Ocean overturning, which was more consistent with the observation-based estimates than previous GCM studies (table 5.1).

Although FM were successful in showing the presence of a strong deep overturning in a regional model of the Indian Ocean there are limitations to their work. Firstly, the forward part of the run under the optimized forcings was only integrated for 1 year, so nothing is known about the long-term stability of the solution. Secondly, FM used horizontal and vertical mixing rather than the preferred isopycnal mixing and eddy parameterization of a GM/Redi scheme [see *Gent and McWilliams*, 1990; *Griffies et al.*, 1998 for a review; *Redi*, 1982], which detracts somewhat from their findings. To address these problems we extend the forward run of the FM solution to 200 years using a GM/Redi scheme and investigate the evolution of the overturning streamfunction. In subsequent model experiments, we use an observation-based estimate of diapycnal mixing and also diagnose the mixing required to sustain the FM solution indefinitely, using the approximation of a 1D advective-diffusive balance. In a final model experiment we apply diagnosed mixing to a model forced with the Ganachaud [2003a] (hereafter referred to as G03) estimate of the flow field across 32°S. The primary aim of this work is to establish whether a large MOC can be supported in a regional GCM of the Indian Ocean in a quasi-steady-state.

Observation-based estimates		**GCM-based estimates**	
Toole and Warren [1993]	27 Sv	Garternicht and Schott [1997]	3 Sv
Robbins and Toole [1997]	12 ± 3 Sv	Lee and Marotzke [1997; 1998]	2 Sv
MacDonald [1998]	17 ± 5 Sv	Zhang and Marotzke [1999]	2 Sv
Bryden and Beal [2001]	10 Sv	Banks [2000]	3 Sv
Sloyan and Rintoul [2001]	23 ± 3 Sv	Stammer et al. [2002]	4 Sv
Ganachaud [2003a]	11 ± 4 Sv	Ferron and Marotzke [2003]	18 Sv
Talley et al. [2003]	18 Sv		

Table 5.1: Estimates of the deep meridional overturning in the Indian Ocean. 1 Sv = 10^6 m^3s^{-1}.

5.2 Observational estimates of diapycnal mixing

Recent observational estimates of diapycnal mixing in the ocean [e.g. *Naveira-Garabato et al.*, 2004] have shown locally enhanced mixing values far exceeding the canonical value of 10^{-4} m^2 s^{-1} [*Munk*, 1966; *Munk and Wunsch*, 1998], which has traditionally been adopted in GCMs. Enhanced diapycnal mixing is often associated often associated with the breaking of internal waves generated as flows (e.g. tidal flows) interact with rough topography [e.g. *Ledwell et al.*, 2000]. Owing to the rough topography of the Indian Ocean one might anticipate large mixing rates in the Indian Ocean and a correspondingly large MOC [e.g. *Toole and Warren*, 1993]. Hasumi and Suginohara [1999] have investigated the effects of enhanced vertical mixing over rough topography in a global GCM. They found the 3-D circulation to be sensitive to the distribution of vertical mixing.

We use estimates of diapycnal diffusivity (K_d), obtained by applying an internal wave dynamical model to observations of density (from Conductivity-Temperature-Depth data) and velocity fine structure (from acoustic Doppler current profilers) following Naveira-Garabato [2004][†]. The data come from World Ocean Circulation Experiment (WOCE) hydrographic sections occupied in 1995: I01 at 10ºN (I01W stations 901-933, 935, 939-956 and I01E stations 971-1004, 1008-1013 [*Shi et al.*, 2002]); I02 at 10ºS (stations 1077-1105, 113-114, 1127-1156, 1167-1227 [*Johnson et al.*, 1998; *Warren and Johnson*, 2002]); and a crossing of the Indian Ocean at 32ºS in 2002 [*Bryden et al.*, 2003b], CD139 (figure 5.1). We take the zonal mean of each of the 3 sections and then interpolate the data onto the model levels using an area-weighted mean to conserve the depth-integrated value for K_d. We then apply a simple 2-D linear interpolation between the 3 depth profiles to arrive at a mixing field that is a function of depth and latitude (figure 5.3).

[†] the results of these calculations will be presented in: Naveira-Garabato, Bryden and McDonagh, manuscript in preparation

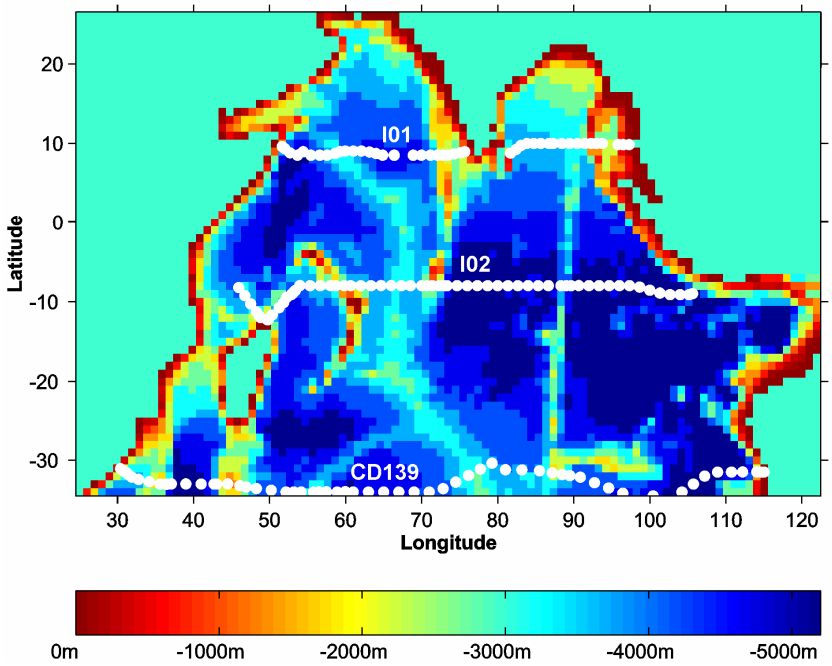

Figure 5.1: The station locations of hydrographic data used to construct the observational estimate of turbulent diapycnal mixing. The bathymetry shown is that of the GCM used in this investigation.

5.3 Diagnosed diapycnal mixing estimates

In this section we consider an alternative method for selecting a diapycnal mixing distribution in the Indian Ocean model. We employ an adaptation of the method used by Naveria-Garabato [*pers. comm.*] to estimate the Indian Ocean MOC from estimates of diapycnal diffusivity. Under the approximation of steady state and a 1-D advective-diffusive balance, any combined density and velocity field has an implied diapycnal mixing distribution. In our case the velocity field is that applied to the model southern boundary and the density field is that over the whole Indian Ocean.

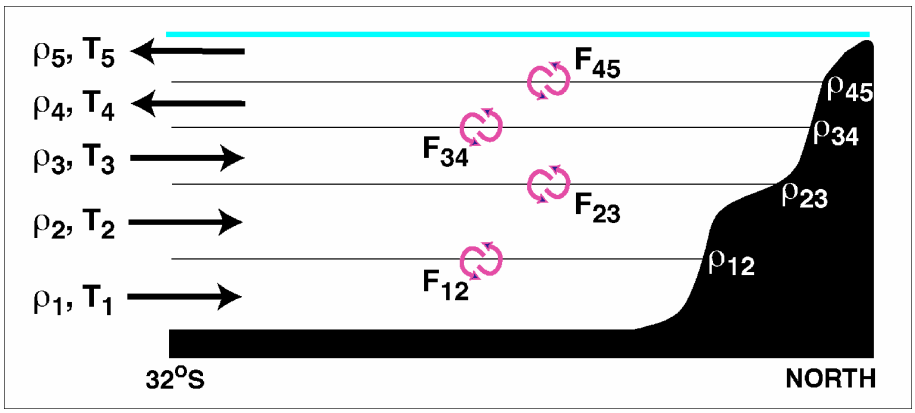

Figure 5.2: A schematic example of the zonally integrated flow field in the Indian Ocean using five isopycnal layers. Figure courtesy of A. Naveira-Garabato.

Referring to the schematic of the zonal mean flow field and isopycnals in the Indian Ocean (figure 5.2):

ρ_n = mean potential density of layer *n*;

$\rho_{n(n+1)}$ = potential density of interface between layers *n* and *n*+1;

T_n = advective volume transport into layer *n*.

The turbulent mass transport across the interface between layers *n* and *n*+1 is given by:

$$F_{n(n+1)} = -K_d \partial\rho/\partial z A_{n(n+1)}, \qquad \text{(Eq. 5.1)}$$

where K_d is the local diapycnal diffusivity, $\partial\rho/\partial z$ is the density gradient across the interface and $A_{n(n+1)}$ is the area of the interface.

For layer *n*, conservation of mass in a steady state dictates that the net advection of mass into each layer must equal the net turbulent diffusion out of each layer:

$$(\rho_n - \rho_{n(n+1)})\, T_n + (\rho_{(n-1)n} - \rho_{n(n+1)}) \sum_{i=1:(n-1)} T_i = F_{n(n+1)} - F_{(n-1)n} \qquad \text{(Eq. 5.2)}$$

The density field and velocity field (and therefore T_n and $\partial\rho/\partial z$) are prescribed at the model southern boundary, so these fields are steady-state by definition. We obtain the area of each density interface ($A_{n(n+1)}$) using WOCE data [*Gouretski and Koltermann*, 2004] and arrive at a 1-D profile for K_d (figure 5.3) at the southern boundary, which is a function of density interface. This 1-D profile is converted to a depth profile, using mean layer depths and applied to the entire model interior.

5.4 Model configuration

We use the MIT ocean general circulation model [*Marshall et al.*, 1997a; 1997b] configured for the Indian Ocean. Our model domain extends from (24ºE, 35ºS) to (122ºE, 26ºN) with open boundaries at 122ºE for the Indonesian Throughflow and at 35ºS for the Southern Ocean (figure 5.1). The horizontal resolution is 1º×1° and there are 22 vertical levels (10m resolution near the surface down to 500m for the deepest six levels). The model bathymetry is interpolated from the ETOPO5 [1998] data. Isopycnal and diapycnal mixing processes in the model are parameterized using a GM/Redi scheme and a convection algorithm, respectively. At the open boundaries temperature (T), salinity (S) and velocity (v) normal to the boundary are prescribed at each time step.

The model set-up is exactly the same as that described in FM (see chapter 2), but with the addition of a 30-day restoring to sea surface T and S from the World Ocean Atlas 1994 [*Levitus and Boyer*, 1994; *Levitus et al.*, 1994]. All experiments are conducted with identical surface forcings and the same eastern boundary conditions for θ and S. Experiments that used the FM southern boundary conditions have a mean Indonesian Throughflow of -10 Sv (into the model domain). For the final model experiment, the FM southern boundary conditions are replaced by the hydrographic section of Toole and Warren [1993] and the flow field across 32°S from G03 (section 5.3.2 for details). In this case a uniform offset is applied to the eastern boundary to ensure a mean IT strength of -16 Sv to preserve the G03 flow field at the southern boundary. Four different diapycnal mixing fields are used (table 5.2) and in each case the model is integrated for 200 years. Experiment A uses the same spatially uniform K_d of 2×10^{-5} m^2s^{-1} implemented in the work of FM; experiment B uses a uniform K_d that is the basin-integrated average of the observational estimate; experiment C has an observationally-estimated K_d field, which is a function of depth and latitude (figure 5.3); experiment D has diagnosed values for K_d that are only a function of depth (figure 5.3). Note that the basin-average K_d of experiment B is very close to the Munk value of 1×10^{-4} m^2s^{-1} [*Munk*, 1966; *Munk and Wunsch*, 1998].

Experiment	Southern Boundary	Diapycnal Mixing	Run Time
A	Ferron and Marotzke	Uniform 2×10^{-5} m^2s^{-1}	200 years
B	Ferron and Marotzke	Uniform 1.2×10^{-4} m^2s^{-1}	200 years
C	Ferron and Marotzke	2D observational estimate, $K_d(y,z)$ (figure 5.3)	200 years
D	Ferron and Marotzke	Diagnosed, $K_d(z)$ (figure 5.3)	200 years
E	Ganachaud	Diagnosed, $K_d(z)$ (figure 5.3)	200 years

Table 5.2: Diapycnal mixing configurations used in the model experiments.

5.4.1 Diapycnal mixing fields

The zonal mean of the observationally-estimated K_d show large values at depth (as high as $10^{-2.5}m^2s^{-1}$) and generally much smaller values above 3000m. There is progressively stronger mixing over most of the water column as one moves south of section I01 (figure 5.3). The FM diagnosed mixing profile shows K_d values that increase with depth and that are much larger than the observations, except at the deepest model level. The K_d values diagnosed from the G03 flow field are smaller than for FM, but still substantially larger than the observations for the upper 3000m. The diapycnal mixing values here are based on the flow field after transformation onto the model grid and therefore differ from the values reported in Ganachaud [2003a].

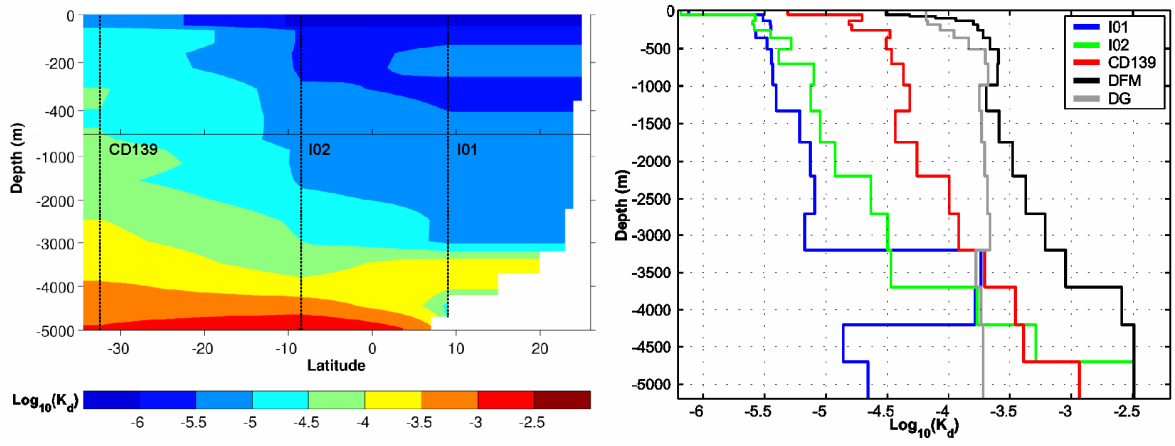

Figure 5.3: The left panel shows the 2-Dimensional mixing field based on the observations with hydrographic section locations indicated in black. The right panel shows the K_d-profiles for each hydrographic section and the K_d-profiles diagnosed from the Ferron and Marotzke [2003] and Ganachaud [2003a] solutions (DFM and DG).

5.4.2 Southern boundary conditions

The origins of the FM southern boundary conditions are the World Ocean Atlas 1994 [*Levitus and Boyer*, 1994; *Levitus et al.*, 1994] and a 2°×2° global ocean model [*Stammer et al.*, 1997]. The resulting optimised T, S and *v* fields vary smoothly in space and are time-dependent. The size of the Agulhas Current (AC) is 65 Sv (1 Sv = 10^6 m^3s^{-1}) and the IT strength is 10 Sv. The deep inflow at the southern boundary is confined to below 3200m and occurs mainly in the Perth Basin (100-110°E, figure 5.4). These southern boundary conditions are applied in experiments A-D.

Experiment E uses T and S from the Toole and Warren [1993] hydrographic section and *v* from the flow field at 32°S estimated by G03 (chapter 4 for details). The T, S and *v* fields contain a lot of mesoscale signal and are much spikier than the FM boundary conditions (figure 5.9). Under these conditions the model bathymetry is modified to fit the hydrographic data and held constant over the latitudes 35-32°S[‡]. The size of the Agulhas Current and Indonesian Throughflow is 70 Sv and 16 Sv, respectively. In this case some of the deep inflow occurs above 3200m and at three zonal locations (approx. 35-40°E, 55-65°E, 100-110°E, figure 5.9).

5.5 'Ferron and Marotzke' configuration results

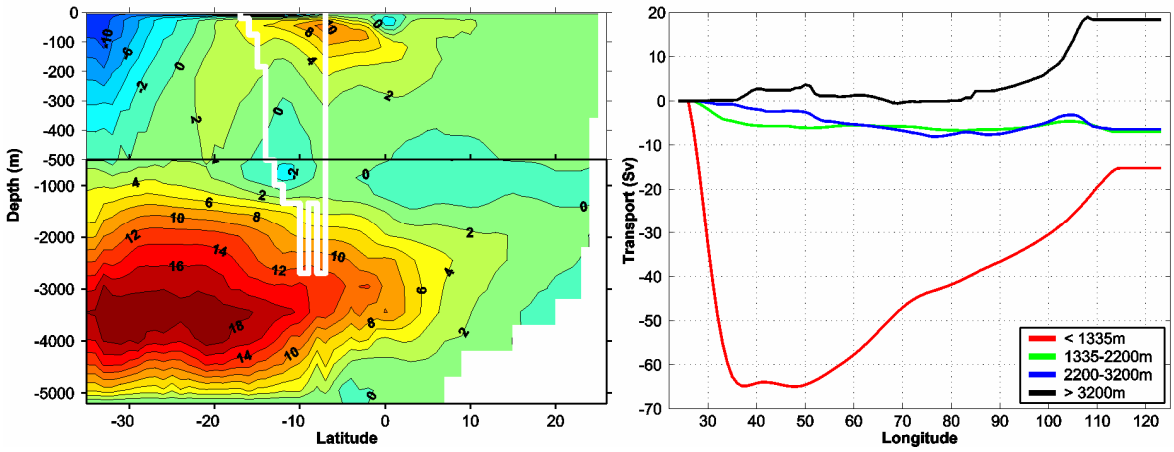

Figure 5.4: The left-hand panel is the time-mean overturning streamfunction for year 1 of the FM solution. Flow is anticlockwise (clockwise) around positive (negative) features, the units are Sv (1 Sv = 10^6 m^3s^{-1}). The white line indicates the location of the Indonesian Throughflow. The right-hand panel shows the cumulative transport across the southern boundary.

[‡] This allows the model dynamics to smooth the flow before it encounters any changes in bathymetry. Previous model runs demonstrate that this improves the compatibility of the high-resolution hydrographic data with the relatively coarse resolution ocean model.

The FM meridional overturning circulation is characterised by an 18 Sv cell at 3500m, which penetrates the basin to about 10°N (figure 5.4). The zonal structure of the transport reveals that the deep inflow is mainly confined to the east, in the Perth Basin (figure 5.4). Due to the nature of the model bathymetry, this is the only location where such a deep inflow is not blocked by topography near 30°S (figure 5.1). In the first year of integration all experiments have a very similar overturning to figure 5.4. It is only after a few years that the different diapycnal mixing regimes cause the model states to diverge.

In all model experiments there is a decrease in the overturning strength over the first few decades (figure 5.5). After 120 years of integration experiment D is near equilibrium, whereas experiments A-C still show a small trend for decreasing MOC at the end of the model run. Experiments A and C show similar evolution of the overturning streamfunction, presumably because the values of K_d in experiment C over much of the water column are close to 2×10^{-5} m^2s^{-1}. Experiment B has the same basin-average K_d as experiment C and demonstrates that the uniform mixing is more efficient at sustaining the deep inflow. This is in agreement with Scott and Marotzke [2002], who found that mixing is most effective at supporting the MOC when it occurs in regions of strong stratification (mainly in the upper water column). Experiment D equilibrates much faster than experiments A-C and shows the largest overturning at year 200.

For completeness a 100-year model integration is carried out using the FM horizontal and vertical mixing (dashed line of figure 5.5). Since horizontal mixing can induce substantial diapycnal mixing across sloping isopycnals, one would anticipate a correspondingly larger overturning circulation. However, after 100 years of integration the impact of using the original FM mixing scheme in experiment A is less than 1 Sv.

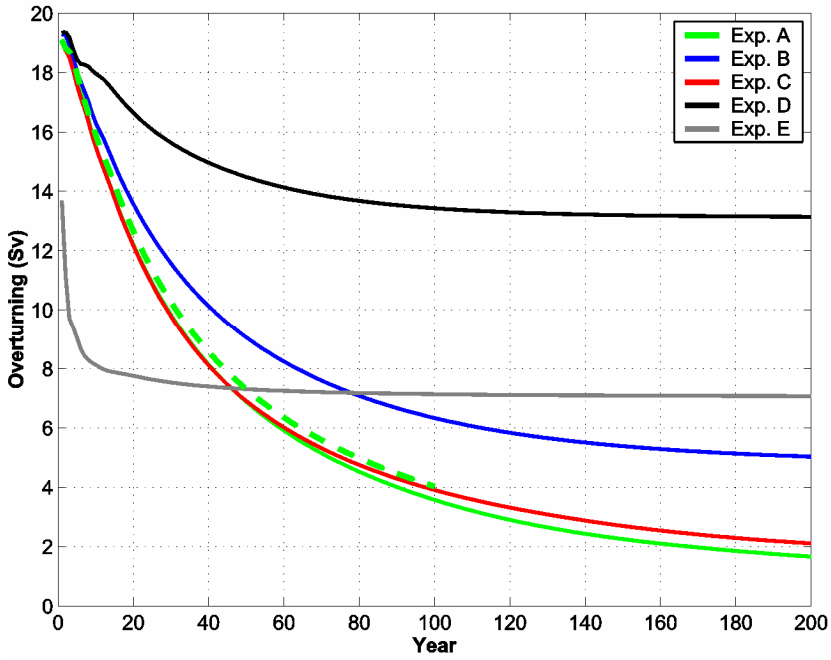

Figure 5.5: Time series of the annual mean overturning streamfunction for 28°S at 3200m for experiments A-D. The green dashed shows a 100 year run of experiment A with horizontal/vertical mixing. The overturning streamfunction for experiment E is computed at 1750m, owing to the shallower overturning cell.

The evolution of the streamfunction at 28°S gives an indication of the evolution of the model state over 200 years of integration. We now focus our attention on the mean overturning streamfunction for year 200 to investigate changes in the zonally integrated circulation throughout the ocean basin. As all diapycnal mixing regimes show an overturning streamfunction very similar to FM after 1 year of integration, this is our reference circulation in all experiments (figure 5.4).

Experiments A and C show similar time evolution of the streamfunction at 3200m and 28°S, but the different K_d fields produce different zonally integrated circulations (figure 5.6). Experiment C has a clockwise overturning cell at about 1000m that penetrates from the southern boundary to beyond 10°N and a slightly stronger deep circulation near 30°S. By year 200, experiment A and C show a similar near-surface circulation to year 1, but a complete collapse of the deep MOC. Experiment B shows a deeper near-surface circulation and a small residual overturning of 4 Sv, which only penetrates to about 22°S. Following the 4 Sv contour flow at 2000m near the southern boundary descends to 4000m as it moves northwards and returns southwards at about 1000m. At year 200 experiment D shows a similar near-surface circulation to experiment B, but a much stronger deep overturning of 12 Sv. This deep overturning has weakened by 30% and is slightly deeper than at the start of the model run.

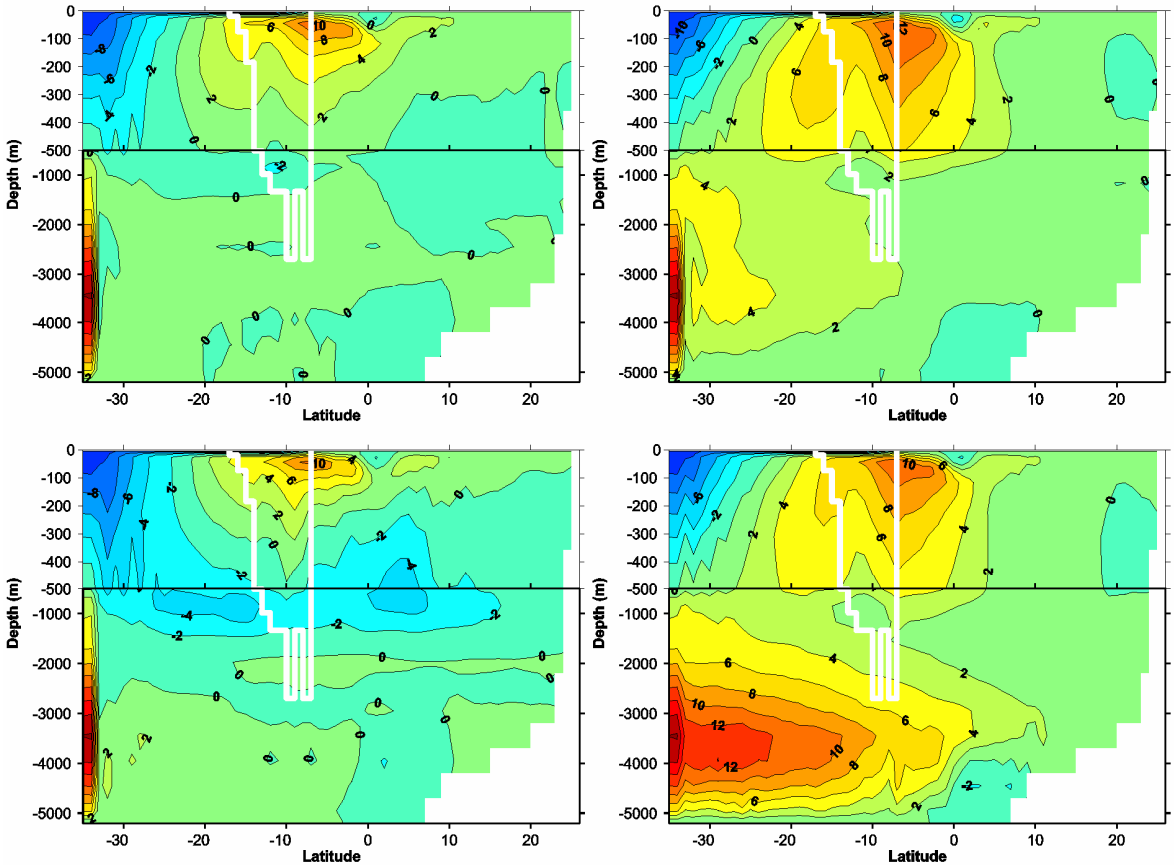

Figure 5.6: The time-mean overturning streamfunction for year 200 of experiment A (upper left); experiment B (upper right); experiment C (lower left); and experiment D (lower right). Flow is anticlockwise (clockwise) around positive (negative) features, the units are Sv (1 Sv = 10^6 m^3s^{-1}). The white line indicates the location of the Indonesian Throughflow.

Using the overturning streamfunction we have established that for most mixing regimes, the overturning circulation in our Indian Ocean model diminishes relatively quickly as the model is integrated forward in time. In order to understand why the circulation changes it is necessary to look in more detail at the model state at the beginning and at the end of the model run. In the following sections we compare the end states of two model runs: experiment C (weak overturning); and experiment D (strong overturning), with the initial model state. Our analysis concentrates on the deep ocean and understanding why the deep overturning circulation changes.

5.5.1 Initial model state

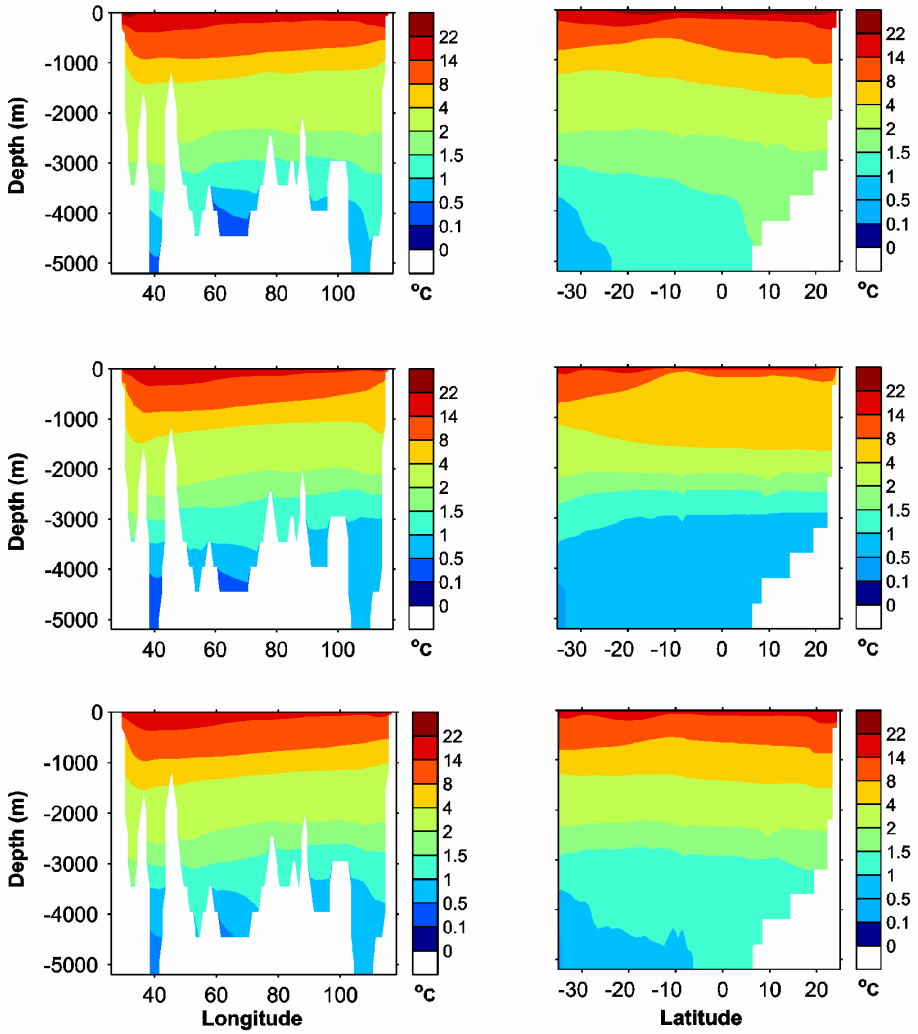

Figure 5.7: The annual-mean distribution of potential temperature for a section at 33°S (left) and a meridional section of the zonal mean value (right). Data shown are: year 1 of experiment C (representative of all model runs, upper panel), year 200 of experiment C (middle panel) and year 200 of experiment D (lower panel).

At the start of the model runs we observe a deep gradient in potential temperature (T) across the Perth Basin (100-110°E), which is associated with the large deep inflow in this part of the basin (figure 5.7). There are also deep zonal T gradients visible at 40°E, between Mozambique Plateau and Madagascar Ridge and about 55-75°E. The first of these gradients is located in a region of northward deep transport and the latter is a region of small southward transport (figure 5.4). The meridional T section (figure 5.7) shows a tongue of cold water from the Southern Ocean below about 3000m. The sloping of the isotherms shows a denser water column in the south and suggests a pressure gradient from the south to the north.

The deep sub-basins of the ocean model show a lot of structure in the temperature and salinity (S) fields (figure 5.8). The cold influence of the southern boundary and the high S in the northernmost basin are particularly striking. Again we observe a strong zonal temperature gradient in the Perth Basin (105-110°E). It is apparent that the Madagascar (50-60°E) and Perth Basins provide the only entrances to the interior deep ocean basins at the southern boundary. The distribution of salinity gives the impression that the Central Indian Basin is filled from the West Australian Basin via a gap in the Ninetyeast Ridge, as suggested by observations [*Warren and Johnson*, 2002].

5.5.2 Experiment C model end state

At the end of experiment C the zonal distribution of deep isotherms have changed substantially (figure 5.7). The most striking changes are the removal of the T gradient across the Perth Basin and at 40°E. In both the zonal and meridional sections there is evidence that the basin has been filled with cold, dense water originating from the south. The coldest water column is north of the southern boundary, suggesting a pressure gradient that would oppose the deep inflow into the basin. The water in the deep sub-basins has been homogenised – there is no longer evidence of any large property gradients and the mean T has dropped substantially (figure 5.8).

After 200 years of model integration the mean potential temperature of the ocean has dropped by 1.1°C and reduced in salinity by 0.01. The largest temperature losses occur in the upper 1000m, with peak values at 33°S near the east and west boundaries. There are some isolated regions of temperature and salinity increase, which occur mainly between 500-2000m. The drift of T/S properties in the model demonstrates that the flow regime in the ocean interior is not balanced with the surface forcings. There seems to be a problem in transferring heat, particularly, but also salt downwards from the sea surface.

5.5.3 Experiment D model end state

Experiment D shows less deviation from the initial conditions than experiment C. After 200 years of model integration T gradient across the Perth Basin is preserved (figure 5.7, 5.8), though it is weaker than at the start of the model run. The basic zonal structure of the deep isotherms is qualitatively similar to the start of the model run. There is evidence of filling of the Indian Ocean sub-basins, but to a lesser extent than previous model runs. The deep sub-basins show some homogenisation of water mass properties, but again some of the structure is preserved.

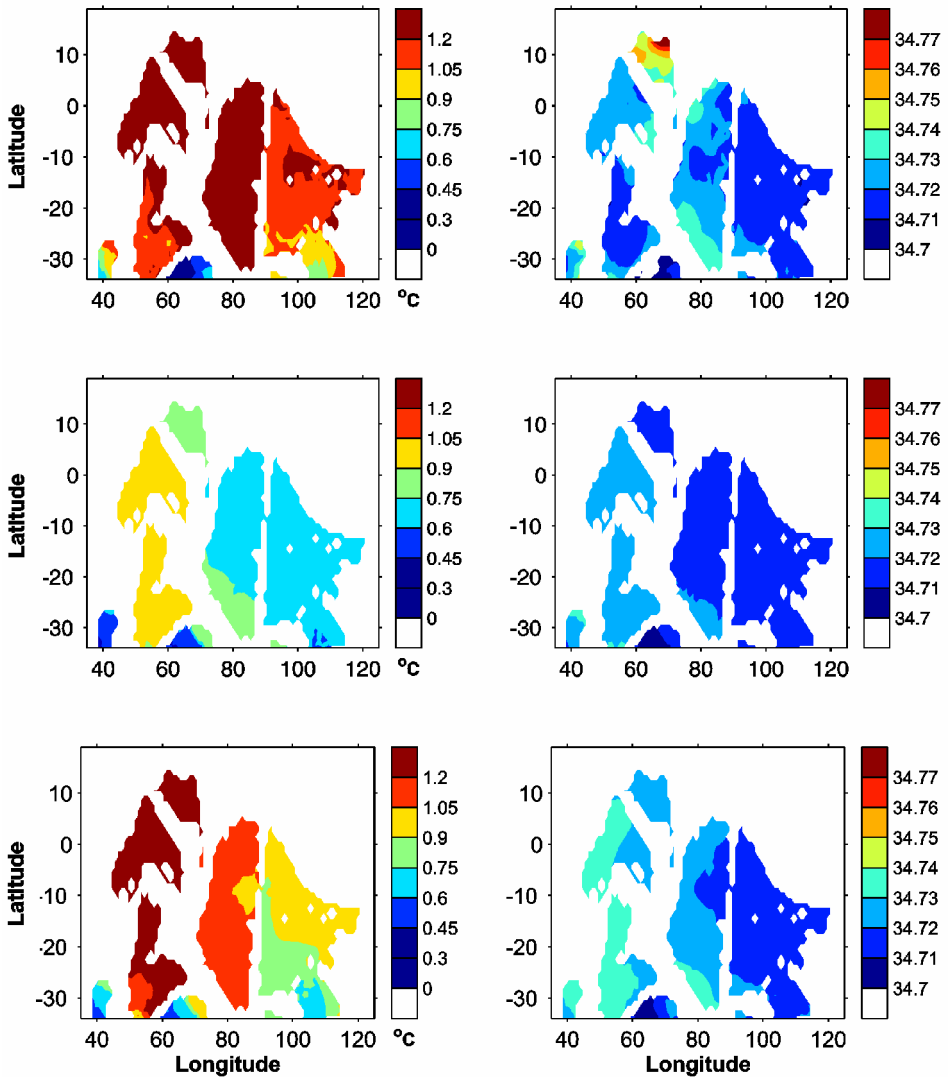

Figure 5.8: Potential temperature (left) and salinity (right) averaged over the deepest three model levels (> 3700m). Data shown are: year 1 of experiment C (representative of all model runs, upper panel), year 200 of experiment C (middle panel) and year 200 of experiment D (lower panel).

The basin mean T has fallen by 0.58°C and salinity has dropped by 0.027. While the drift in T is halved compared to experiment C, the drift in S has more than doubled. This is no-doubt a consequence of more of the relatively fresh deep water from the southern boundary being advected and mixed in the model interior. The largest changes happen in the upper 1000m

5.6 'Ganachaud' configuration results

After a steep decline in the overturning strength over the first decade, experiment E rapidly equilibrates (figure 5.5). The initial decrease in overturning from a larger value than prescribed at the southern boundary suggests that the FM initial conditions may contribute to a strong, but transient initial overturning. After 200 years of model integration the peak deep overturning that in the model interior is 8 Sv, which represents 90% of the 9 Sv prescribed deep inflow. The overturning cell is substantially weaker and shallower than the FM solution and penetrates the basin no further than the equator (figure 5.9). As with the previous model runs, experiment E shows a drift in basin-integrated temperature salinity. The drop in temperature is 0.7°C and the mean salinity is reduced by 0.05. The loss of heat and salt occurs predominantly in the near-surface layers but there are isolated regions of small temperature and salinity increase.

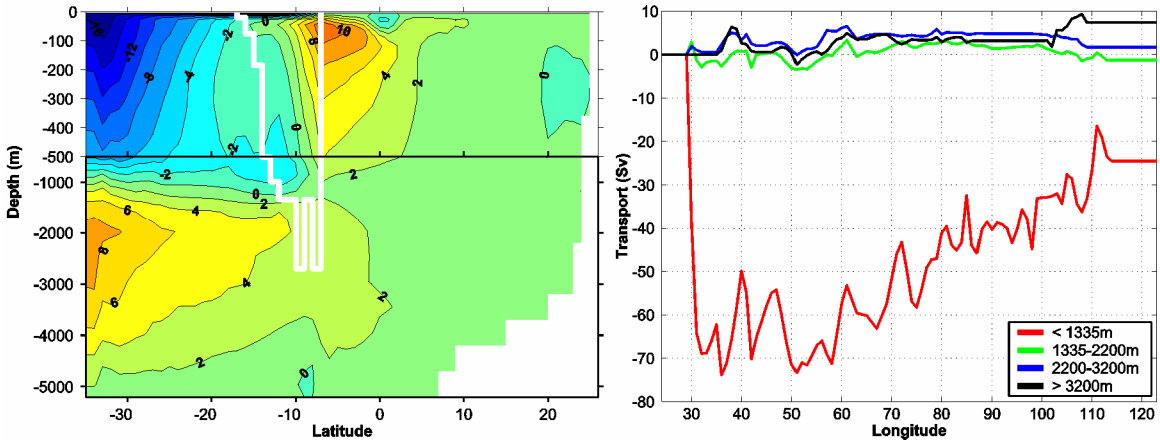

Figure 5.9: The left-hand panel is the time-mean overturning streamfunction for year 200 of the Ganachaud solution. Flow is anticlockwise (clockwise) around positive (negative) features, the units are Sv (1 Sv = 10^6 m^3s^{-1}). The white line indicates the location of the Indonesian Throughflow. The right-hand panel shows the cumulative transport across the southern boundary.

The overturning reported here differs substantially to that estimated by G03. Firstly, the transformation of the flow field at 32°S from isopycnal coordinates to the model grid reduces the deep inflow to 9 Sv, although it is still within the estimated uncertainty of 11 ± 4 Sv. Secondly, the overturning estimated by G03 shows the 11±4 Sv deep inflow penetrates the basin as far north as 8°S. However, the overturning circulation presented here marks a step forward in addressing the disparity between observation-based estimates of the Indian Ocean MOC and GCM studies.

5.7 Discussion

Experiments A-D demonstrate that the distribution of diapycnal mixing has a profound impact on the size of the quasi-steady overturning state. Using the FM uniform K_d of 2×10^{-5} m^2s^{-1} we see a complete collapse of the 18 Sv overturning cell after 200 years of model integration. A similar result is obtained when one implements the observationally-based mixing estimates. Presumably this is because the 'observed' K_d over much of the water column the mixing is close to 2×10^{-5} m^2s^{-1}, despite very large values at depth. This point is elucidated by Scott and Marotzke [2002], who found that diapycnal mixing was most efficient at sustaining a large MOC when it occurred in regions of strong stratification, i.e. the low latitude thermocline. The Scott and Marotzke theory is supported by experiment B, which has larger K_d values in the upper water column than experiment C, but the same basin-integrated value. Experiment D uses diagnosed diapycnal mixing from a 1D advective-diffusive balance and shows a quasi-steady overturning circulation of 12 Sv. This accounts for 70% of the 18 Sv overturning that is prescribed at the southern boundary. Diagnosed K_d is also effective in sustaining a quasi-steady overturning state as inferred from observations (experiment E). In this case 90% (8 Sv) of the 9 Sv prescribed overturning is preserved after 200 years of integration. However, the model shows a much reduced meridional extent to the overturning than suggested by the original box model estimate [*Ganachaud*, 2003a]. The implementation of diagnosed diapycnal mixing is likely to be even more effective in an isopycnal model, where the mixing follows the isopycnal surfaces. The diagnosed diapycnal mixing presented here could be improved by *a priori* mapping the isopycnal surfaces in the model interior and producing several K_d-profiles that are a function of latitude.

5.7.1 Why does the overturning circulation collapse?

The thermal wind equation states that a meridional overturning circulation requires a zonal density gradient to support the vertical shear of northward velocity (Eq. 3.1). At the southern boundary the deep inflow is prescribed, so the model has no 'choice' until it enters the ocean interior. Experiments A and C show large homogenisation if the deep water masses and a removal of the temperature gradient across the Perth Basin after 200 years of integration. At the end of these model runs after the deep inflow cannot be sustained upon entering the model domain because there are not sufficient zonal density gradients to support the vertical shear associated with the overturning in the ocean interior.

The prescribed flow cannot move northward, but mass conservation dictates that the flow must go somewhere. It is possible that the flow could move zonally, if there were a substantial meridional density gradient, but only until it encountered topography. In practice, the easiest solution seems to be for the flow to move vertically upward. Analysis of the *u*- and *w*-velocity components (not shown) shows that most of the deep inflow is directed upwards upon entering the model domain and then flows zonally across the basin to the Agulhas Current, where it is advected out of the model domain. Such a flow pattern requires a pressure gradient to oppose the deep northward flow prescribed at the southern boundary, which could be supplied by the largely homogenous water mass in the Perth Basin (figures 5.7, 5.8). The circulation regimes that show some residual deep overturning all manage to preserve zonal gradients in the ocean interior, to a greater or lesser extent.

Another way of looking at this problem is to consider the how diapycnal mixing is parameterised in the model. The amount of diapycnal mixing (d_{mix}) that occurs at any location is a function of the diapycnal diffusivity (K_d) and the local diapycnal density gradient (approximately $\partial\rho/\partial z$), such that $d_{mix} = K_d\partial\rho/\partial z$. If the basin-wide d_{mix} is not large enough to balance the mass of deep water flowing into the ocean basin, the deep stratification (and $\partial\rho/\partial z$) will increase (figure 5.7, middle panels). Eventually $\partial\rho/\partial z$ (and therefore d_{mix}) becomes large enough to balance the deep inflow. Hence all model experiments reach some form of quasi-steady state.

5.7.2 Heat loss in the upper water column

The loss of heat in the ocean basin and particularly in the upper 1000m is a feature of all model runs. Experiment D demonstrates the least heat loss, despite having the largest overturning circulation. With a greater deep inflow one might anticipate a greater heat loss in the ocean interior. The answer lies in the near-surface K_d values. The higher K_d values mean a more efficient draw-down of heat from the surface layers. The surface forcing is a restoring condition in part, so downward heat export will effectively increase the surface heat flux as the restoring term tries to elevate sea surface temperatures toward the target values. The model runs with the lowest near-surface K_d values exhibit the largest temperature drift over the 200 year integration.

The fact that all model runs show heat loss (and loss of salt, to a lesser extent) suggests that there is a fundamental problem in transferring heat downwards in the GCM. FM noted that when their solution was integrated forward for a few years the heat content in the upper 500m rapidly decreased. The authors suggest that this could be due to

inadequate mixed layer physics and/or inaccurate estimates of the surface heat and freshwater fluxes. The authors also noted a decline in the overturning to about 12 Sv after the first 10 years, and suggest that the uniform K_d, the possibility of misrepresented bathymetry and poor model resolution might make it impossible to sustain the deep circulation. We have demonstrated that given appropriate K_d a large part of the overturning circulation can be sustained indefinitely. However, we also observe a cooling of the upper water column, despite the large near-surface diapycnal mixing values used in some model runs. The implication is that the FM surface fluxes are too weak.

5.8 Conclusions

- We have demonstrated that the quasi-steady deep overturning in the Indian Ocean is very sensitive to the distribution of diapycnal mixing.
- The Ferron and Marotzke (FM) [2003] solution is not sustainable on long time scales, primarily because the prescribed diapycnal mixing is not large enough. Observational estimates of diapycnal mixing are also unable to sustain the FM circulation.
- When on employs a diapycnal mixing diagnosed from a 1D advective-diffusive balance 12 Sv (70%) of the 18 Sv FM overturning is sustainable in quasi-steady state. However, the required mixing values are much larger than the observations suggest.
- We also investigated a southern boundary flow field that is derived from observations – that of Ganachaud [2003a]. We find an 8 Sv quasi-steady overturning state that requires lower values of K_d than FM. The GCM circulation shows lesser meridional extent than Ganachaud [2003a], but the result is a step forward in addressing the disparity between observational and GCM estimates of the Indian Ocean MOC.

Chapter 6: Summary and discussion

6.1 Introduction

In this chapter we summarise the work presented on the Indian Ocean circulation, discuss the wider implications of our findings and suggest some areas for future research. In section 6.2 we discuss the work on the hydrographic observations presented in chapter 3 and put forward a hypothesis which could explain the observed differences in the 1987 and 2002 density structure. The model investigations into decadal variability of the deep circulation presented in chapter 4 are discussed in section 6.3. In section 6.4 we review the work of chapter 5 on the influence of diapycnal diffusivity on quasi-steady overturning states and finish with some concluding remarks in section 6.5.

6.2 The 1987 and 2002 hydrographic observations

In chapter 3 we use hydrographic data at 32ºS from 1987, 1995 and 2002 to investigate changes in the strength of the Indian Ocean subtropical gyre circulation. Relative geostrophic transports are computed for the ocean interior using a zero-velocity surface (ZVS) at 2230dbar and then filtered with a Gaussian (of 8° longitude) to remove the high wave number signal. The estimated relative gyre transports are: 41 ± 5.1 Sv (1 Sv = 10^6 m^3s^{-1}) for 1987, 42 ± 7.0 Sv for 1995 and 58 ± 7.0 Sv for 2002. The 1987 and 1995 values are consistent within the estimated error and the 2002 value represents a 40% increase relative to 1987. The main areas of change in the geostrophic transports are just east of Madagascar Ridge and around Broken Plateau – consistent with differences we observe in the depths of isopycnals in these areas. Maps of contoured velocity suggest that most of the change happened between 1995 and 2002, which is in qualitative agreement with the transport estimates. The different station locations occupied in 1987 and 2002 is an obvious point of criticism in our comparison. However, much of the change in isopycnals (and associated transport) occurs in regions where the two hydrographic sections overlie.

Given that the ocean gyres are fundamentally wind-driven ocean phenomena, one might look to changes in the wind stress fields to try and understand why the relative gyre transports have changed. If a change in the mean winds were responsible for the differences in isopycnals, one would expect such an effect to be most evident in the near-surface region. However, the zonally-averaged velocity profiles show that the larger transport estimated for 2002 is a result of greater meridional velocity shear ($\partial v/\partial z$) at depth (figure 3.8). In the following paragraphs we present a conceptual model of the flow field near 32°S. Using this model, we put forward a hypothesis that could explain the apparent increase in gyre strength between 1987 and 2002 by considering changes in the deep meridional overturning circulation.

6.2.1 Implications for the deep circulation?

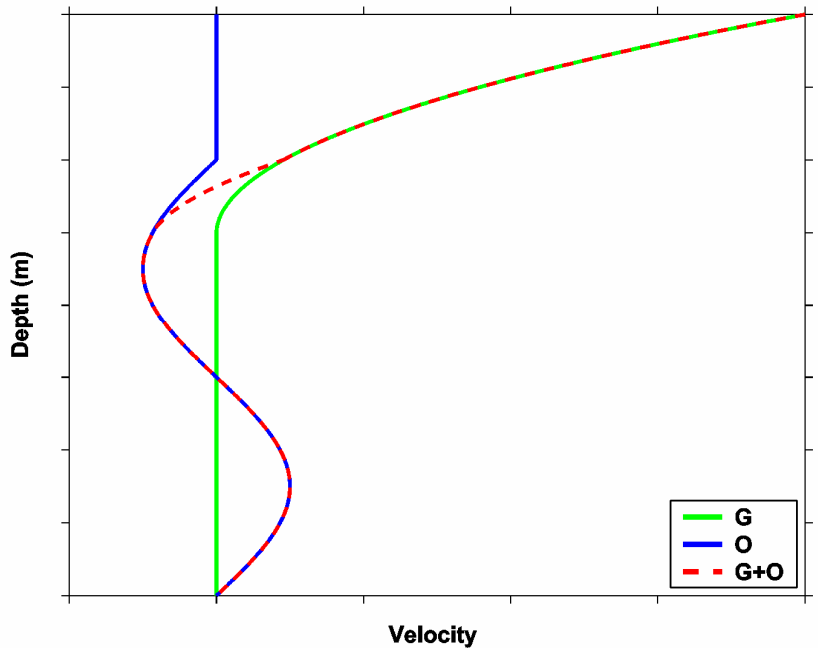

Figure 6.1: Idealised velocity profiles associated with the wind-driven gyre (G); deep meridional overturning circulation (O); and gyre plus overturning (G+O). No information is required about the barotropic flow field in this example.

The basis of our conceptual model is idealised profiles of meridional velocity that are a function of depth (figure 6.1). The profiles are the result of a zonal-integration over the ocean interior – we avoid the boundary currents. Our initial model state is a circulation that is purely wind driven. In this case the velocity profile would look something like the green curve in figure 6.1. We have excluded the western boundary region in our model, so there is no constraint of mass conservation. The absence of a deep overturning circulation

means that there is no current shear below the Ekman pumping layer. We now add an idealised overturning circulation (blue curve, figure 6.1), which is qualitatively similar to many of the model circulations described in chapters 4 and 5. If we make the assumption that the two curves can be linearly combined, we produce the red-dashed curve in figure 6.1.

There are important results from the addition of the overturning profile to the gyre profile:

(i) The addition of the overturning velocity profile causes greater shear at depth in the net velocity field, near the base of the wind-driven layer.

(ii) The presence of the overturning circulation can lead to a greater apparent depth of the gyre circulation (i.e. the depth of minimum velocity shear).

Both of these effects can lead to greater apparent gyre strength when one employs a ZVS at a depth of minimum vertical shear of meridional velocity near the base of the wind-driven layer. The conceptual model suggests that a change in the size or vertical structure of the deep overturning circulation between 1987 and 2002 could account for the observed changes velocity shear below 1000m reported in chapter 3. The implication is that the overturning cell may have increased in magnitude between 1987 and 2002 and/or the depth structure of the overturning may have changed over the same period. The conceptual model also shows that our method for estimating gyre strength from hydrography using a ZVS at a depth of minimum velocity shear (figure 3.5) can overestimate the gyre transport if the return branch of the overturning occurs near the base of the wind-driven layer. This may explain why the depth of minimum vertical shear of meridional velocity in OCCAM is shallower than we observe in the hydrography (the OCCAM data presented in chapter 3 have a weak deep overturning circulation).

6.2.2 Future work

During cruise CD139 a total of 25 autonomous floats were deployed across 32°S in the Indian Ocean [*Bryden et al.*, 2003b] as part of the Agro programme (details at http://www.argo.ucsd.edu). The floats drift at depth of approximately 2000m, surfacing and re-submerging every 10 days to record depth-profiles of temperature and salinity. These profiles and a position fix are transmitted via satellite while the float is at the ocean surface (where it remains for 6 to 12 hours). The information gathered by the floats

presents an excellent opportunity for investigating the seasonal variability in the density structure of the upper water column from an observational standpoint. Work is currently being undertaken by Klaus Getzlaff [*pers. comm.*] to estimate the northward transport associated with the subtropical gyre, using a geostrophic method applied to Argo data. It is hoped that this research will improve our understanding of the mesoscale and seasonal variability of the gyre circulation. More specifically, the work should provide improved error estimates of the geostrophic flow field, which would be particularly useful for inverse studies [e.g. *Ganachaud*, 2003a].

Two model data sets have recently become available that could be used to complement the work presented in chapter 3 and that using Argo observations. The first is an OCCAM 1/4° run with improved surface forcings and more realistic deep water formation [*Marsh et al.*, 2005]. These data could be used to investigate the long term (inter-annual to pentadal) variations in the gyre and deep circulations of the Indian Ocean. The second dataset is from 1/12° OCCAM global ocean model run, which is a fully eddy-resolving model. This latter dataset could be particularly useful for quantifying the impact of mesoscale activity on hydrographic estimates of the geostrophic flow field.

6.3 Decadal variability of deep MOC

In chapter 4 we investigate the influence of lateral boundary conditions near 32°S on the Indian Ocean circulation, using a regional general circulation model (GCM). In the first part of the analysis we establish a time scale for the initial adjustment of the model to the imposed southern boundary conditions. Using the time series of overturning streamfunction at 28°S we note that most of the model adjustment occurs within the first 5-6 years of model integration. This approximate time scale is roughly what one would expect for an adjustment time, based on the observed translation speed of a first-baroclinic Rossby Wave at about 30°S [*Chelton and Schlax*, 1996; *Fu and Chelton*, 2001]. The rapid adjustment of the model may also be related to the complex series of topographic ridges (figure 1.3), which are capable of supporting topographic Rossby waves[*] [e.g *Kantha and Clayson*, 2000]. The limited meridional extent and the continuous boundary of the

[*] Rossby waves are one of the primary mechanisms of ocean adjustment to perturbations in the boundary conditions [e.g. *Gill*, 1982]

continental shelf (from the African continent around to Indonesia) could also contribute to the short adjustment time via Kelvin wave propagation [*Gill*, 1982].

6.3.1 The importance of T, S and v at the southern boundary

The approach used to investigate decadal variability in the deep MOC is to combine hydrographic data with a regional GCM of the Indian Ocean. In chapter 4 we present a method for transforming temperature (T), salinity (S) and meridional velocity (*v*) data onto the model grid that conserves the section integrated quantities. We then test the sensitivity of the model MOC to the southern boundary conditions using T, S and 'reconstructed' *v* from the 1987 and 2002 hydrography. The velocity reconstruction is carried out by computing the baroclinic structure of the hydrographic section using the thermal wind equation (Eq. 3.1) and combining it with barotropic velocities from a global ocean model [*Stammer et al.*, 2002]. The sensitivity of the model to the prescribed density (T and S) and meridional velocity at the southern boundary is tested by systematically replacing southern boundary conditions from a control run with the hydrographically-derived boundary conditions.

We find that the model interior was much more sensitive to prescribed *v* than T and S. This is the opposite of what Ferron and Marotzke [2003] suggest from their work using the same GCM and the MIT adjoint. However, the changes we impose on T and S were relatively small, particularly for the 1987 section. This is because the control conditions use values of T and S from a climatology that incorporates the 1987 section. The use of hydrographic data at the southern boundary introduces short length-scale variability to the T and S fields, but does not alter their large-scale distribution. The hydrographically-derived *v* fields, on the other hand, introduce both short length-scale variability and large changes in the basin integrated transports (figures 4.5, 4.6).

The reconstructed *v*-field for 1987 invokes a vigorous deep overturning in the Indian Ocean of 16-18 Sv, with deep northward flow below 3000m and southward flow between 500 and 1500m near the southern boundary. This zonally integrated circulation is qualitatively consistent with much of the published literature [e.g. *Bryden and Beal*, 2001; *Ganachaud et al.*, 2000; *Robbins and Toole*, 1997; *Talley et al.*, 2003]. The reconstructed *v*-field for 2002 invokes an overturning of 12-14 Sv, with the overturning cell in the opposite sense, stretching from the surface to 4000m. We do not consider this second circulation to be a physical solution and it is the result of strong southward flow at depth near 105°E in the reconstructed *v*-field. This suggests that the approach of combining the

baroclinic flow from hydrography with the ECCO model [*Stammer et al.*, 2002] barotropic flow is flawed. However, it also highlights the differences in baroclinic structure between the 1987 and 2002 hydrographic sections. The model shows a large sensitivity to prescribed velocities at the southern boundary – the *v*-field is critical in determining the decadal time-scale circulation. This result implies that the model is capable of simulating decadal changes in the basin-wide deep circulation using estimates of the velocity field near 32°S.

6.3.2 Evidence for change in the deep circulation

In chapter 4 we attempt to simulate the 1987 and 2002 Indian Ocean circulation, using two current estimates of the flow field near 32°S. The estimates of the flow field near 32°S for 1987 and 2002 are from Ganahaud [2003a] and McDonagh [in prep.], respectively. After transformation of the data onto the model grid the prescribed deep northward flows are 9 Sv for 1987 and 17 Sv for 2002. The larger 2002 deep inflow supports our hypothesis of a stronger deep overturning in 2002 than in 1987 (section 6.2.1).

The 1987 solution invokes only a weak circulation in the ocean interior, despite the 9 Sv deep inflow prescribed at the southern boundary. Only a 4 Sv overturning centred at 2000m depth and of very narrow extent penetrates the model interior. In contrast, the 2002 MOC exhibits 16 Sv overturning cell with a 1500-4500m depth range. This vigorous overturning penetrates the basin beyond the equator. In addition to the differences in zonally-integrated circulations, we see a dramatic re-organisation of the deep currents in the two model runs. For 1987 the largest deep northward flows occurr in the Perth Basin and on into the West Australian Basin. There is also a smaller northward flow which occurred in the Madagascar basin. A small southward flow adjacent to the western wall of the Central Indian Basin acts to reduce the net deep inflow. The deep northward flow for 2002 shows the dominant contribution in the Madagascar Basin. The next largest deep inflow occurs in the Central Indian Basin, showing a complete reversal of the flow direction from the 1987 circulation. We also note contributions to the northward flow in the Perth and West Australian Basins, but these are substantially weaker than in the 1987 circulation.

It is difficult to know how much the change in barotropic signal and different bathymetry near 32°S affects the model solutions. It also remains unclear why certain solutions seem more consistent with the model dynamics than others. The model is not

eddy-permitting and so cannot support the high-wavenumber part of the geostrophic flow present in the hydrography. The fact that the bathymetry is held constant over the first 3 model grid cells serves to 'dynamically smooth' the flow in an attempt to make it more consistent with the model dynamics before it encounters the complex bathymetry. It is tempting to try and smooth the T and S fields before applying the boundary conditions. This is problematic in practice because of the missing values in the section. The Gaussian filter applied to the upper water column in chapter 3 is not suitable for smoothing over large areas of bathymetry. A better alternative if one wanted to pursue smoothing of the velocity field might be to take the time-mean flow field from a model run a few grid cells into the model domain and use that to force the southern boundary in a subsequent model run (effectively smoothing the flow field twice). An alternative would be to extend the model domain further south and duplicate more of the bathymetry. This is perhaps less appealing, due to the change in the Coriolis parameter (*f*) with latitude.

6.3.3 Implications and future work

Perhaps the widest implication of the work presented here is that hydrographic sections can be usefully combined with regional models to study the circulation. Our results suggest that the apparent inconsistency between previous non-GCM and GCM studies are a result of the boundary conditions used, rather than a conflict in the model dynamics. The work presented in chapters 4 and 5 adds to the current literature in demonstrating the robustness of open boundary conditions in GCMs, despite the fact that they are formally ill-posed [e.g. *Bennett*, 1992; *Zhang and Marotzke*, 1999].

The short adjustment time of our Indian Ocean model and the different circulations found in the 1987 and 2002 simulations call into question the validity of the often-used 'steady-state' assumption. Given the complex nature of the Indian Ocean bathymetry, it is perhaps not surprising that the basin is capable of supporting multiple deep flow regimes. What is surprising is the rapid and far reaching influence of the southern boundary conditions. The sensitivity of the interior circulation to the southern boundary velocity field implies that the model could be used to detect decadal changes in the basin-wide deep circulation using estimates of the flow field near 32°S.

The proposed change in circulation between 1987 and 2002 would be more compelling if some of the changes of the deep flows presented here could be verified by observations. Deep current meter moorings, such as those described by Warren et al. [2002] present a potential means of identifying changes in the deep western boundary

currents (DWBCs). Unfortunately the authors were only able to present data over the period 1995-1997 and over this time there is no evidence of a change in the DWBC. A network of similar moorings in the Indian Ocean would present a means of evaluating changes in the deep circulation and validating future model results.

With the advent of increased computing power an obvious improvement to the model work would be to use a higher resolution. This could be used to investigate why some prescribed *v*-fields at the southern boundary are more consistent with the model dynamics than others. An increased horizontal and vertical resolution would improve the representation of bathymetry and accommodate the hydrographic data more easily. The influence of resolution on the impact of the boundary conditions would no doubt be an interesting line of research, particularly if one used an eddy-permitting model. The work of Treguier et al. [2001] suggests that the increased model resolution should not present a problem for the open boundary conditions.

6.4 Diapycnal Diffusivity and Quasi-Steady Overturning States

In Chapter 5 we investigate the influence of the distribution of diapycnal diffusivity on quasi-steady overturning states in a regional model of the Indian Ocean. Most of the work in this chapter uses the model set-up of Ferron and Marotzke [2003] (hereafter FM), who were the first authors to invoke a vigorous deep MOC in a GCM of the Indian Ocean. We replace the horizontal and vertical mixing used by FM with isopycnal mixing and an eddy parameterisation, to improve on the original model configuration. We also address the short integration time of FM by running the model forward for 200 years, so that the model achieves a quasi-steady state.

6.4.1 Collapse of the FM solution

Perhaps the greatest limitation of FM's work was the one-year integration time used in their adjoint model study. We integrate the FM model configuration forward for 200 years to reach a quasi-steady overturning state. By the end of the model run the 18 Sv deep overturning cell present in year 1 has collapsed, leaving a residual circulation of < 2 Sv. We then repeat the model experiment using two alternative distributions of K_d. The first is uniform K_d close to the canonical value of 10^{-4} m^2s^{-1} [*Munk*, 1966; *Munk and Wunsch*, 1998] and the second is a 2-D field, K_d(lat, z), estimated from hydrographic data [e.g. *Naveira-Garabato et al.*, 2004]. In both cases the overturning circulation again

collapses, with the uniform K_d supporting the larger residual circulation (~4 Sv). The mechanism for the decline in the deep overturning is removal of zonal density gradients at depth and homogenisation of the deep ocean. Both of these effects are the result of an imbalance between the diapycnal mixing and the large deep inflow. In a final experiment we attempt to diagnose the K_d field necessary to sustain the FM overturning indefinitely, by considering the mass balance into isopycnal layers at the southern boundary. In this case we are able to preserve 70% of the FM overturning strength in a quasi-steady state, but the K_d values are much larger than suggested by the observations. We conclude that the FM solution cannot be considered a realistic quasi-steady overturning state for the Indian Ocean.

In a second model setup, we apply the technique of diagnosed K_d values to the Ganachaud [2003a] estimate of the flow field at 32°S. In this case all of the 8 Sv overturning applied at the southern boundary is sustained in quasi-steady state. The values of K_d required for the Ganachaud flow field are much less than those required for FM, particularly below 1500m, but still an order of magnitude larger than suggested by the observations for the upper 3000m. This second model setup confirms the usefulness of diagnosed K_d values. It also again raises the issue of relatively large K_d values required in the upper water column to sustain a deep overturning circulation.

FM were perhaps too ambitious in using only 1 year of forward integration in their study – presumably a result of limited computing resources. The work we present in chapter 4 suggests that a minimum time for the forward model (GCM) run should be of the order a decade to give the basin-wide circulation time to respond to changes in the boundary conditions. In order to study the quasi-equilibrium response the forward model would have to be run for longer (for at least 100 years or so). This raises problem of computing power for the adjoint method because it is used iteratively and therefore requires numerous GCM runs.

6.4.2 Refining the technique of diagnosed K_d

While the technique of diagnosing K_d is shown to be effective in our z-level model, there are a number of improvements that could be made if one wanted to fully exploit its potential. Firstly, one could map out the isopycnal surfaces over the ocean interior and adjust the value of K_d as a function depth accordingly (resulting in a 2-D K_d field). Secondly, the approach of diagnosing K_d would more naturally implemented in an isopycnal coordinate model [e.g. *Kantha and Clayson*, 2000]. In such a model the mixing

coefficients would remain on the isopycnal interfaces, rather than being fixed in space. With such improvements one would anticipate less model adjustment to reach a quasi-steady state and better preservation of the initial overturning state.

6.4.3 Observation-based estimates of K_d

One of the problems with the observational estimates of diapycnal diffusivity is the small number of locations that have been sampled. The values must be extrapolated into large areas of ocean where there is no data. Some of the difference between the observation-based estimates and diagnosed estimates of K_d may be due to the methodology of the former. The major assumption that is made in the observational estimates is that the internal wave field activity sampled during each hydrographic section is representative of the time-mean state. One anticipates that the energy available for mixing is related to tidal forcing and to first order may follow the spring-neap cycle. Other time-dependent sources of internal wave energy are eddies and atmospheric momentum transfer (winds). Direct current measurements using LADCPs are an essential ingredient to the observation-based estimates of diapycnal diffusivity presented in chapter 5. Such measurements have only been available since WOCE and as repeat sections are occupied in the future we should gain a better understanding of the time variability of the internal wave field.

A potential candidate for the 'missing mixing' in the upper water column is the transient mixing associated with tropical cyclones. It has been suggested by Emmanuel [2001] that tropical cyclones may play an important role in driving the global MOC by invoking vigorous mixing of waters across the thermocline. Boos et al [2004] conducted an idealised GCM study to show that intense transient diapycnal mixing, with a distribution suggestive of tropical cyclones, can effectively drive a meridional overturning. It would be interesting to carry out a similar model experiment using our Indian Ocean model set-up. Such a mixing could remedy the problems of mixing heat from the surface layers downwards, discussed in chapter 5 and also noted by FM.

6.4.4 Future work

A logical next step in the modelling work would be to evaluate the long-term stability of the model circulation when forced with the McDonagh [in prep.] flow field at the southern boundary. This would be carried out with diagnosed values of K_d so that the required mixing fields could be compared with the observational estimates. The

overturning estimate could then be ranked with the FM and Ganachaud estimates in terms of: its compatibility with the model dynamics and, (ii) the required K_d values.

More work could be done to investigate ways of incorporating the observation-based K_d values in the model. For example, the method we used removes any zonal structure and also removes the largest values. One could explore the limits of the data by choosing a profile with the largest implied K_d and assume it to be representative of the entire Indian Ocean. This would produce a useful upper limit for reference in future model experiments.

One of the issues we have yet to address in our 200-year model runs is that the meridional overturning may not be in steady-state. The '1987' and '2002' configurations from chapter 4 could be used to explore this possibility and to investigate the dynamical adjustment to a change from 1987 to 2002 boundary conditions. The simplest approach would be to run the model forward under the 1987 conditions for some time and then impose the 2002 conditions. A more sophisticated approach would be to combine the two to produce a periodic southern boundary condition with a 15-year cycle and study the long-term response of the MOC.

6.5 Concluding remarks

We have shown that there have been changes in the density structure of the subtropical Indian Ocean gyre between 1987 and 2002. The changes we observe occur at depth and could be indicative of an increase in the size of the deep MOC. This hypothesis is supported by estimates of the flow field across 32°S from Ganachaud [2003a] and McDonagh [in prep.]. The model work suggests that the basin-wide deep circulation of the Indian Ocean is capable of changing on decadal timescales. We have demonstrated that the Indian Ocean model supports different deep flow regimes when forced with the Ganachaud and McDonagh flow field at the southern boundary. The implication is that both the size and zonal structure of the deep inflow across 32°S may have changed between 1987 and 2002.

Our model work suggests that the deep MOC reaches quasi-steady state on century time scales and is determined by the distribution of diapycnal diffusivity (K_d). The distribution of K_d required to support the prescribed deep inflow at the southern boundary can be estimated using a 1-D advective-diffusive balance in isopycnal layers. The two estimates of the flow field near 32°S used in our investigation imply highly non-uniform profiles of K_d in quasi-steady state. Observation-based estimates of K_d also suggest a highly non-uniform distribution of K_d. It is therefore essential for the research community to improve the estimates of K_d and implement a non-uniform K_d distribution in ocean and coupled ocean-atmosphere models that are run to quasi-equilibrium states.

References

Adcroft, A., C. Hill, and J. Marshall, Representation of Topography by Shaved Cells in a Height Coordinate Ocean Model, *Monthly Weather Review, 125* (9), 2293-2315, 1997.

Banks, H.T., Indonesian Throughflow in a coupled climate model and the sensitivity of the heat budget and deep overturning, *Journal of Geophysical Research, 105* (C11), 26135-26150, 2000.

Beal, L.M., and H.L. Bryden, Observations of an Agulhas Undercurrent, *Deep-Sea Research Part I-Oceanographic Research Papers, 44* (9-10), 1715-1724, 1997.

Beal, L.M., and H.L. Bryden, The velocity and vorticity structure of the Agulhas Current at 32 degrees S, *Journal of Geophysical Research-Oceans, 104* (C3), 5151-5176, 1999.

Bennett, A., *Inverse Methods in Physical Oceanography*, 346 pp., Cambridge University Press, 1992.

Bindoff, N.L., and T.J. McDougall, Diagnosing Climate-Change and Ocean Ventilation Using Hydrographic Data, *Journal of Physical Oceanography, 24* (6), 1137-1152, 1994.

Bindoff, N. L., and T. J. McDougall, Decadal changes along an Indian ocean section at 32 degrees S and their interpretation, *Journal of Physical Oceanography, 30*(6), 1207-1222, 2000.

Boos, W.R., J.R. Scott, and K.A. Emanuel, Transient diapycnal mixing and the meridional overturning circulation, *Journal of Physical Oceanography, 34* (1), 334-341, 2004.

Boyer, T.P., and S. Levitus, Quality control and processing of historical oceanographic temperature, salinity, oxygen data, in *NEDSIS*, pp. 64, NOAA, 1994.

Bryden, H. L., and L. M. Beal, Role of the Agulhas Current in Indian Ocean circulation and associated heat and freshwater fluxes, *Deep-Sea Research Part I-Oceanographic Research Papers*, *48*(8), 1821-1845, 2001.

Bryden, H. L., E. L. McDonagh, and B. A. King, Changes in ocean water mass properties: oscillations or trends?, *Science*, *300*(5628), 2086-2088, 2003a.

Bryden, H.L., RRS *Charles Darwin* Cruise 139, 01 Mar - 15 April 2002. Trans-Indian Hydrographic Section across 32S, pp. 122, Southampton Oceanography Centre Cruise Report, Southampton, 2003b.

Bryden, H.L., L.M. Beal, and L.M. Duncan, Structure and Transport of the Agulhas Current and its Temporal Variability, *Journal of Oceanography*, submitted manuscript.

Chelton, D.B., and M.G. Schlax, Global observations of oceanic Rossby waves, *Science*, *272* (5259), 234-238, 1996.

Donohue, K. A., and J. M. Toole, A near-synoptic survey of the Southwest Indian Ocean, *Deep-Sea Research Part II-Topical Studies in Oceanography*, *50*(12-13), 1893-1931, 2003.

Emanuel, K., Contribution of tropical cyclones to meridional heat transport by the oceans, *Journal of Geophysical Research-Atmospheres*, *106* (D14), 14771-14781, 2001.

ETOPO5, Data Announcement 88-MG-02, Digital relief of the Surface of the Earth, NOAA, National Geophysical Data Center, Boulder, Colorado, 1998

Feng, M., G. Meyers, A. Pearce, and S. Wijffels, Annual and interannual variations of the Leeuwin Current at 32 degrees S, *Journal of Geophysical Research-Oceans*, *108*(C11), art. no.-3355, 2003.

Ferron, B., and J. Marotzke, Impact of 4D-variational assimilation of WOCE hydrography on the meridional circulation of the Indian Ocean, *Deep-Sea Research Part II-Topical Studies in Oceanography, 50* (12-13), 2005-2021, 2003.

Fieux, M., and G. Reverdin, Current systems in the Indian Ocean, in *Encyclopedia of ocean sciences. Vol. 1. A-C*, edited by J.H. STEELE, S.A. THORPE, and K.K. TUREKIAN, pp. 621, Academic Press, San Diego, CA, 2001.

Fofonoff, N. P., Physical-Properties of Seawater - a New Salinity Scale and Equation of State for Seawater, *Journal of Geophysical Research-Oceans, 90*(NC2), 3332-3342, 1985.

Fu, L.L., E.J. Christensen, C.A. Yamarone, M. Lefebvre, Y. Menard, M. Dorrer, and P. Escudier, Topex/Poseidon Mission Overview, *Journal of Geophysical Research-Oceans, 99* (C12), 24369-24381, 1994.

Fu, L.-L., and D.B. Chelton, Large-scale ocean circulation, in *Satellite altimetry and earth sciences: a handbook of techniques and applications.*, edited by L.-L. Fu, and A. Cazenave, pp. 463, Academic Press, San Diego, CA, 2001.

Ganachaud, A., C. Wunsch, J. Marotzke, and J. Toole, Meridional overturning and large-scale circulation of the Indian Ocean, *Journal of Geophysical Research-Oceans, 105* (C11), 26117-26134, 2000.

Ganachaud, A., Large-scale mass transports, water mass formation, and diffusivities estimated from World Ocean Circulation Experiment (WOCE) hydrographic data, *Journal of Geophysical Research-Oceans, 108* (C7), art. no.-3213, 2003a.

Ganachaud, A., Error budget of inverse box models: The North Atlantic, *Journal of Atmospheric and Oceanic Technology, 20*(11), 1641-1655, 2003b.

Garternicht, U., and E. Schott, Heat fluxes of the Indian ocean from a global eddy-resolving model, *Journal of Geophysical Research-Oceans, 102* (C9), 21147-21159, 1997.

Gent, P.R., and J.C. McWilliams, Isopycnal Mixing in Ocean Circulation Models, *Journal of Physical Oceanography, 20* (1), 150-155, 1990.

Giering, R., and T. Kaminski, Recipes for adjoint code construction, *Acm Transactions on Mathematical Software, 24* (4), 437-474, 1998.

Gill, A.E., *Atmosphere-Ocean Dynamics*, 662 pp., Academic Press, 1982.

Godfrey, J.S., The effect of the Indonesian throughflow on ocean circulation and heat exchange with the atmosphere: a review, *Journal of Geophysical Research-Oceans, 101* (C5), 12217-12237, 1996.

Godfrey, J.S., and Y. Masumoto, Diagnosing the mean strength of the Indonesian Throughflow in an ocean general circulation model, *Journal of Geophysical Research-Oceans, 104* (C4), 7889-7895, 1999.

Gordon, A.L., Interocean Exchange of Thermocline Water, *Journal of Geophysical Research, 91* (C4), 5037-5046, 1986.

Gordon, A.L., R.F. Weiss, W.M. Smethie, and M.J. Warner, Thermocline and Intermediate Water Communication between the South-Atlantic and Indian Oceans, *Journal of Geophysical Research-Oceans, 97* (C5), 7223-7240, 1992.

Gouretski, V.V., and K.P. Koltermann, WOCE Global Hydrographic Climatology, pp. 55, Bundesamtes für Seeschifffahrt und Hydrographie, 2004.

Griffies, S.M., A. Gnanadesikan, R.C. Pacanowski, V.D. Larichev, J.K. Dukowicz, and R.D. Smith, Isoneutral diffusion in a z-coordinate ocean model, *Journal of Physical Oceanography*, *28* (5), 805-830, 1998.

Griffies, S.M., C. Boning, F.O. Bryan, E.P. Chassingnet, R. Gerdes, H. Hasumi, A. Hirst, A.-M. Treguier, and D. Webb, Developments in ocean climate modelling, *Ocean Modelling*, *2*, 123-192, 2000.

Hall, M. M., and H. L. Bryden, Direct estimates and mechanisms of ocean heat transport, *Deep-Sea Research I*, *29*(3A), 339-359, 1982.

Hasumi, H., and N. Suginohara, Effects of locally enhanced vertical diffusivity over rough bathymetry on the world ocean circulation, *Journal of Geophysical Research-Oceans*, *104* (C10), 23367-23374, 1999.

Jayne, S. R., and R. Tokmakian, Forcing and sampling of ocean general circulation models: Impact of high-frequency motions, *Journal of Physical Oceanography*, *27*(6), 1173-1179, 1997.

Johnson, G.C., D.L. Musgrave, B.A. Warren, A. Ffield, and D.B. Olson, Flow of bottom and deep water in the Amirante Passage and Mascarene Basin, *Journal of Geophysical Research*, *103* (C13), 30973-30984, 1998.

Joos, F., G.-K. Plattner, T.F. Stocker, A. Körtzinger, and D.W.R. Wallace, Trends in marine dissolved oxygen: Implications for ocean circulation changes and the carbon budget, *EOS, Transactions of the American Geophysical Union*, *84*, 197-201, 2003.

Kalnay, E., M. Kanamitsu, R. Kistler, W. Collins, D. Deaven, L. Gandin, M. Iredell, S. Saha, G. White, J. Woollen, Y. Zhu, M. Chelliah, W. Ebisuzaki, W. Higgins, J. Janowiak, K.C. Mo, C. Ropelewski, J. Wang, A. Leetmaa, R. Reynolds, R. Jenne, and D. Joseph, The NCEP/NCAR 40-year reanalysis project, *Bulletin of the American Meteorological Society*, *77* (3), 437-471, 1996.

King, B.A., E. Firing, and T.M. Joyce, *Shipboard Observations during WOCE*, 715 pp., Academic Press, London, 2001.

Lavín, A., H. L. Bryden, and G. Parrilla, Meridional transport and heat flux variations in the subtropical North Atlantic, *The Global Atmosphere and Ocean System, 6*, 269-293, 1998.

Le Dimet, F.X., and O. Talagrand, Variational Algorithms for Analysis and Assimilation of Meteorological Observations - Theoretical Aspects, *Tellus Series a-Dynamic Meteorology and Oceanography*, *38* (2), 97-110, 1986.

Levitus, S., and T.P. Boyer, World Ocean Atlas 1994, Volume 4: Temperature, pp. 117pp., NOAA Atlas NEDSIS 4, 1994.

Levitus, S., R. Burgett, and T.P. Boyer, World Ocean Atlas 1994. Volume 3: Salinity, pp. 99pp., NOAA Atlas NEDSIS 3, 1994.

Lee, T., and J. Marotzke, Inferring meridional mass and heat transports of the Indian Ocean by fitting a general circulation model to climatological data, *Journal of Geophysical Research-Oceans*, *102* (C5), 10585-10602, 1997.

Lee, T., and J. Marotzke, Seasonal cycles of meridional overturning and heat transport of the Indian Ocean, *Journal of Physical Oceanography*, *28* (5), 923-943, 1998.

Ledwell, J.R., E.T. Montgomery, K.L. Polzin, L.C. St Laurent, R.W. Schmitt, and J.M. Toole, Evidence for enhanced mixing over rough topography in the abyssal ocean, *Nature*, *403* (6766), 179-182, 2000.

Longworth, H., J. Marotzke, and T.F. Stocker, Ocean gyres and abrupt change in the thermohaline circulation: A conceptual analysis, *Journal of Climate*, *in press*.

MacDonald, A.M., The global ocean circulation: a hydrographic estimate and regional analysis, *Progress in Oceanography*, *41* (3), 281-382, 1998.

Marotzke, J., R. Giering, K.Q. Zhang, D. Stammer, C. Hill, and T. Lee, Construction of the adjoint MIT ocean general circulation model and application to Atlantic heat transport sensitivity, *Journal of Geophysical Research-Oceans*, *104* (C12), 29529-29547, 1999.

Marsh, R., B.A. de Cuevas, A.C. Coward, H.L. Bryden, and M. Álvarez, Thermohaline circulation at three key sections in the North Atlantic over 1985-2002, *Geophysical Research Letters*, *in press*, 2005.

Marshall, J., A. Adcroft, C. Hill, L. Perelman, and C. Heisey, A finite-volume, incompressible Navier Stokes model for studies of the ocean on parallel computers, *Journal of Geophysical Research-Oceans*, *102* (C3), 5753-5766, 1997a.

Marshall, J., C. Hill, L. Perelman, and A. Adcroft, Hydrostatic, quasi-hydrostatic, and nonhydrostatic ocean modeling, *Journal of Geophysical Research-Oceans*, *102* (C3), 5733-5752, 1997b.

McDonagh, E. L., H. L. Bryden, B. A. King, R. J. Sanders, S. A. Cunningham and R. Marsh, Decadal Changes in the South Indian Ocean Thermocline, *Journal of Climate*, *18* (10), 1575-1590, 2005.

McDonagh, E.L., Using ADCP data to inform geostrophic calculations, *paper in preparation*.

Mesinger, F., and A. Arakawa, Numerical methods used in atmospheric models. Vol 1., in *Global Atmospheric Research Programme (GARP) publication series*, pp. 64, 1976.

Munk, W., Abyssal recipes, *Deep-Sea Research*, *13*, 707-730, 1966.

Munk, W., and C. Wunsch, Abyssal recipes II: energetics of tidal and wind mixing, *Deep-Sea Research Part I-Oceanographic Research Papers*, *45* (12), 1977-2010, 1998.

Naveira-Garabato, A.C., K.L. Polzin, B.A. King, K.J. Heywood, and M. Visbeck, Widespread intense turbulent mixing in the Southern Ocean, *Science*, *303* (5655), 210-213, 2004.

Pond, S., and G. L. Pickard, Introductory Dynamical Oceanography, pp. 329, Elsevier Butterworth-Heinemann, 1983.

Redi, M.H., Oceanic Isopycnal Mixing by Coordinate Rotation, *Journal of Physical Oceanography*, *12* (10), 1154-1158, 1982.

Robbins, P.E., and J.M. Toole, The dissolved silica budget as a constraint on the meridional overturning circulation of the Indian Ocean, *Deep-Sea Research Part I-Oceanographic Research Papers*, *44* (5), 879-906, 1997.

Schmitz, W.J., On the World Ocean Circulation: Volume I. Some global features/North Atlantic circulation., pp. 150, Woods Hole Oceanographic Institution, 1996.

Schott, F.A., and J.P. McCreary, The monsoon circulation of the Indian Ocean, *Progress in Oceanography*, *51* (1), 1-123, 2001.

Schott, F.A., M. Dengler, and R. Schoenefeldt, The shallow overturning circulation of the Indian Ocean, *Progress in Oceanography*, *53*, 57-103, 2002.

Scott, J.R., and J. Marotzke, The location of diapycnal mixing and the meridional overturning circulation, *Journal of Physical Oceanography*, *32* (12), 3578-3595, 2002.

Shi, W., J.M. Morrison, and H.L. Bryden, Water, heat and freshwater flux out of the northern Indian Ocean in September-October 1995, *Deep-Sea Research II*, *49* (7-8), 1231-1252, 2002.

Siedler, G., J. Church, and J. Gould, *Ocean Circulation and Climate*, 715 pp., Academic Press, London, 2001.

Sloyan, B.M., and S.R. Rintoul, The Southern Ocean limb of the global deep overturning circulation, *Journal of Physical Oceanography*, *31* (1), 143-173, 2001.

Sprintall, J., S. Wijffels, T. Chereskin, and N. Bray, The JADE and WOCE I10/IR6 Throughflow sections in the southeast Indian Ocean. Part 2: velocity and transports, *Deep-Sea Research Part II -Topical Studies in Oceanography*, *49* (7-8), 1363-1389, 2002.

Stammer, D., C. Wunsch, R. Giering, Q. Zhang, J. Marotzke, J. Marshall, and C. Hill, The Global Ocean Circulation Estimated from TOPEX/POSEIDON Altimetry and the MIT General Cirulation Model, in *Center for Global Change Science*, pp. 40, Massachussets Institute of Technology, Cambridge, 1997.

Stammer, D., C. Wunsch, R. Giering, C. Eckert, P. Heimbach, J. Marotzke, A. Adcroft, C.N. Hill, and J. Marshall, Global ocean circulation during 1992-1997, estimated from ocean observations and a general circulation model, *Journal of Geophysical Research-Oceans*, *107* (C9), art. no.-3118, 2002.

Stammer, D., C. Wunsch, R. Giering, C. Eckert, P. Heimbach, J. Marotzke, A. Adcroft, C.N. Hill, and J. Marshall, Volume, heat, and freshwater transports of the global ocean circulation 1993-2000, estimated from a general circulation model constrained by World Ocean Circulation Experiment (WOCE) data, *Journal of Geophysical Research-Oceans*, *108* (C1), art. no.-3007, 2003.

Stommel, H.M., The westward intensification of wind-driven ocean currents, *Transactions of the American Geophysical Union*, *29*, 202-206, 1948.

Talley, L. D., and M. O. Baringer, Preliminary results from WOCE hydrographic sections at 80°E and 32°S in the Central Indian Ocean, *Geophysical Research Letters*, *24*, 2789-2792, 1997.

Thacker, W.C., and R.B. Long, Fitting Dynamics to Data, *Journal of Geophysical Research-Oceans*, *93* (C2), 1227-1240, 1988.

Toole, J.M., and B.A. Warren, A Hydrographic Section across the Subtropical South Indian-Ocean, *Deep-Sea Research Part I-Oceanographic Research Papers*, *40* (10), 1973-2019, 1993.

Treguier, A.M., B. Barnier, A.P. de Miranda, J.M. Molines, N. Grima, M. Imbard, G. Madec, C. Messager, T. Reynaud, and S. Michel, An eddy-permitting model of the Atlantic circulation: Evaluating open boundary conditions, *Journal of Geophysical Research-Oceans*, *106* (C10), 22115-22129, 2001.

Trenberth, K.E., and J.M. Caron, Estimates of meridional atmosphere and ocean heat transports, *Journal of Climate*, *14* (16), 3433-3443, 2001.

Veronis, G., The role of models in tracer studies, in *Numerical Models of Ocean Circulation*, pp. 133-146, National Academy of Sciences, Washington, D.C., 1975.

Warren, B.A., and G.C. Johnson, The overflows across the Ninetyeast Ridge, *Deep-Sea Research II, 49* (7-8), 1423-1439, 2002.

Webb, D. J., B. A. de Cuevas, and A. C. Coward, The first main run of the OCCAM global ocean model, *Southampton Oceanography Centre Internal Document, 34*, 1-43, 1998.

Weijer, W., W.P.M. De Ruijter, and H.A. Dijkstra, Stability of the Atlantic overturning circulation: Competition between Bering Strait freshwater flux and Agulhas heat and salt sources, *Journal of Physical Oceanography, 31* (8), 2385-2402, 2001.

Wunsch, C., *The ocean circulation inverse problem*, Cambrige University Press, Cambridge, 1996.

Zhang, K.Q., and J. Marotzke, The importance of open-boundary estimation for an Indian Ocean GCM-data synthesis, *Journal of Marine Research, 57* (2), 305-334, 1999.